Structural and functional characterization of the arrestin-rhodopsin complex

D i s s e r t a t i o n

zur Erlangung des akademischen Grades

d o c t o r r e r u m n a t u r a l i u m

(Dr. rer. nat.)

im Fach Biophysik

eingereicht an der

Lebenswissenschaftlichen Fakultät

der Humboldt-Universität zu Berlin

von

Ciara Lally

Präsidentin der Humboldt-Universität zu Berlin

Prof. Dr.-Ing. Dr. Sabine Kunst

Dekan der Lebenswissenschaftlichen Fakultät

Prof. Dr. Bernhard Grimm

Gutachter/innen: 1. Prof. Dr. Franz Bartl

2. Prof. Dr. Athina Zouni

3. Prof. Dr. Peter Hegemann

Tag der mündlichen Prüfung: 24.07.2017

Acknowledgements

I would like to thank the many people who have contributed to the work in this dissertation, and who have provided support throughout my graduate studies. First and foremost I would like to thank my supervisor, Dr. Martha Sommer, for her guidance both in carrying out research and the writing of this dissertation. The dedication and enthusiasm with which she introduced me to the project, and showed me how to approach scientific problems and present results in a clear and logical way, made my time as a PhD student both productive and enjoyable. I appreciate the encouragement and funding she provided that gave me the opportunities to take part in international conferences, which were stimulating and memorable experiences. As well as being a great mentor, I would also like to thank her for being such a positive role model as a successful woman scientist.

I would like to thank the members of the research committee Prof. Dr. Franz Bartl, Prof. Dr. Hegemann, Prof. Dr. Zouni, Prof. Dr. Dobbek and Prof. Dr. Hermann for their guidance in this dissertation, and the DFG which funded this work.

I would also like to thank the other members of the institute for medical physics and biophysics for making such a pleasant working environment. In particular, I would like to acknowledge Brian Bauer and Anja Koch for their patience and assistance with experiments, and especially the expression and purification of arrestin mutants carried out by Brian Bauer, without which this research would not have been possible. I am grateful to all members of the Retinal-Arrestin-Rhodopsin group – Dr. Martha Sommer, Dr. Martin Heck, Brian Bauer, Julius Naujoks, Vivian Vogt and Florent Beyriere, for their thoughts and advice, and in particular I would like to acknowledge Julius Naujoks for his help in translating the abstract of this dissertation. I would also like to thank our collaborator, Dr. Jana Selent, at University Pompeu Fabra, Barcelona, who carried out the molecular dynamics simulations presented in this dissertation, for her research and insights into the interaction between arrestin and the membrane.

The friendships I made whilst working at the Charité, Berlin, made my time there so enjoyable. I would particularly like to thank Brian Bauer, Julius Naujoks, Martha Sommer, Jacqueline Kalms, Florent Beyriere, Vivian Vogt and Johanna Tiemann for their support both inside and outside the lab, their encouragement with helping me to learn German and feel at home in a different country, and for the many lively memories that have made the past four years so fun.

Lastly, I would like to thank my family for their constant love and support. For my parents who have always encouraged me in my education, and my sister for her friendship, I dedicate this work to them.

Abstract

The protein arrestin is responsible for termination of GPCR signalling. In the rod cell, arrestin binds light-activated phosphorylated rhodopsin in order to block further signal transduction. The binding of arrestin to rhodopsin is a two-step process. Arrestin first interacts with the phosphorylated receptor C-terminus in a pre-complex, which induces conformational changes in arrestin that allow coupling to the helical core of the active receptor in a high-affinity complex. Biochemical studies and crystal structures have provided insights into the conformation of the arrestin-rhodopsin complex. This dissertation describes site-directed fluorescence experiments, which were carried out to further investigate the conformational changes occurring upon arrestin binding to rhodopsin. In particular this involved characterization of a previously unidentified association of arrestin with the membrane, as well as further elucidation of the structure of the pre-complex.

The first section of this dissertation describes the association of arrestin with the membrane. Spin-labelled fatty acids, which spontaneously insert into the membrane and quench fluorescence, were used to determine the proximity of fluorescently-labelled sites on arrestin to different regions in the membrane. Loops on the C-edge of arrestin were found to penetrate the membrane. The C-edge anchor was only engaged after interaction with the phosphorylated receptor, demonstrating that it acts as a functional binding element, and interestingly the orientation and conformation was found to be different in the pre-complex as compared to the high-affinity complex.

The second part of this dissertation describes intramolecular quenching analysis to monitor the orientation of the C-tail, and flexible loops on arrestin when bound in the pre-complex and the high-affinity complex. The presence of the negatively charged molecule IP6, and the inactive phosphorylated aporeceptor (OpsP) displaced just the distal portion of the C-tail. The proximal portion makes several contacts within the N-domain of arrestin, with elements that stabilize the basal conformation of arrestin. Therefore, only when the proximal portion of the C-tail is released, which only occurs upon interaction with the active receptor, are the conformational changes associated with arrestin activation observed, including movement within the central crest loops, and interdomain rotation.

The third part of this dissertation describes investigations of the stoichiometry of the arrestin – rhodopsin complex. Although the interaction of arrestin with a single receptor

has been shown to be functional, higher stoichiometries have also been observed. Titrations with fluorescently-labelled arrestin mutants bound to ROS membranes found that in conditions favouring pre-complex formation, arrestin binding in the high-affinity complex saturated at a one-to-one stoichiometry, as compared to in conditions which abrogated pre-complex formation, where the final stoichiometry of the high-affinity complex saturated at a one-to-two stoichiometry. As pre-complex formation was modulated by the addition of salt, the change in stoichiometry observed was not merely due to a lack of space on the membrane, and the pre-complex plays a role in conferring different binding modes in the arrestin-rhodopsin interaction. Interestingly the membrane anchor was also deployed in conditions favouring a one-to-two arrestin-rhodopsin stoichiometry, thereby ruling out the previously proposed hypothesis that the C-edge could contact a second receptor in the high-affinity complex.

Together the results presented in this dissertation further elucidate the nature of different binding modes of the arrestin-rhodopsin interaction. The conformation of arrestin in the pre-complex is indicated to resemble that of the basal state of arrestin, and involves two sites of contact: interaction with the phosphorylated receptor C-terminus, and association with the membrane. Upon transition to the high-affinity complex, arrestin undergoes a conformational change to a more active conformation: the C-tail is displaced, there is movement within the central flexible loops, and the orientation of the membrane anchor changes. The pre-complex therefore most likely functions to bring arrestin and the receptor into close contact, and in the correct orientation, to allow for fast transition to the high-affinity complex.

Abstract in German

Die Aufgabe des Proteins Arrestin ist die Beendigung der Signalweitergabe über den GPCR Signalweg. In Stäbchenzellen bindet Arrestin an Licht-aktiviertes phosphoriliertes Rhodopsin um die Signalweitergabe zu unterdrücken. Die Bindung von Arrestin an Rhodopsin erfolgt in zwei Schritten. Zunächst wechselwirkt Arrestin mit dem phosphorilierten C-Terminus von Rhodopsin und bildet einen prä-Komplex, dies induziert Konformationsänderungen im Arrestin wodurch die Bildung eines High-affinity Komplex unter Kopplung an den helikalen Kern des aktivierten Rezeptors erfolgen kann. Biochemische Untersuchungen und Kristallstrukturen haben einen Einblick in die Konformation des Komplexes aus Arrestin und Rhodopsin ermöglicht. In dieser Arbeit werden site-directed Fluorezenz Experimente angewandt um die strukturellen Änderungen zu untersuchen, die bei der Bindung von Arrestin an Rhodopsin ablaufen. Insbesondere wird hier eine, bisher nicht beschriebene, Assoziation von Arrestin an die Membran untersucht. Des Weiteren wurden Erkenntnisse über die Struktur des prä-Komplexes gewonnen.

Der erste Teil dieser Arbeit befasst sich mit der Assoziation von Arrestin an die Membran. Spin-markierte Fettsäuren, die sich spontan in die Membran integrieren und Fluoreszenz löschen, wurden verwendet um die Annäherung fluoreszenzmarkierter Stellen des Arrestins an verschiedene Bereiche der Membran zu untersuchen. Es konnte gezeigt werden, dass die Schleifen an der C-Kante von Arrestin in die Membran eindringen. Der Membrananker im selben Bereich hat erst nach erfolgter Interaktion mit dem phosphorilierten Rezeptor in die Membran integriert. Hierbei fiel auf, dass sich Konformation und Orientierung des Ankers zwischen prä-Komplex und High-affinity Komplex unterscheiden.

Der zweite Teil dieser Arbeit beschreibt die Orientierung des C-terminalen Endes sowie verschiedener flexibler Schleifen von Arrestin sowohl in dem prä-Komplex als auch dem High-affinity Komplex unter Verwendung von intramolekularer Fluoreszenzlöschung. In Anwesenheit von IP6, einem negativ geladenen Molekül, sowie dem inaktiven phosphorilierten Aporezeptor (OpsP) wird nur der distale Teil des C-Terminus von Arrestin verdrängt. Der proximale Teil hat an mehreren Stellen Kontakt mit der N-Domäne, in Bereichen, welche die basale Konformation stabilisieren. Wenn dieser proximale Teil sich bei Interaktion mit dem aktivierten Rezeptor löst gibt es Bewegungen innerhalb der Schleifen am zentralen Kamm und eine Rotation der

Domänen gegeneinander. Diese Änderung der Konformation ist mit der Aktivierung von Arrestin verknüpft.

Im dritten Teil dieser Arbeit wird die Stöchiometrie des Arrestin-Rhodopsin-Komplexes untersucht. Es wurde gezeigt, dass ein einzelner Rezeptor mit Arrestin eine funktionale Einheit bilden kann, es gibt auch Untersuchungen bei denen eine höherer Stöchiometrie beobachtet wurde. Titrationen mit fluoreszenzmarkiertem Arrestin und ROS-Membranen haben gezeigt, dass Arrestin unter Bedingungen, die die Bildung des prä-Komplexes begünstigen, einen High-affinity Komplex im stöchiometrischen Verhältnis 1 : 1 mit einem Rezeptormolekül bildet. Unter Bedingungen, die eine Ausbildung des prä-Komplexes verhindern, bilden Arrestin und Rezeptormoleküle einen High-affinity Komplex im stöchiometrischen Verhältnis 1:2. Es wird gezeigt, dass der Membrananker bei Bedingungen mit einer ein Arrestin zu zwei Rhodopsin Stöchiometrie ausgefahren ist; daher ist die bisherige Hypothese, dass der Kontakt zu dem zweiten Rezeptor über die C-Kante des Arrestins vermittelt wird, auszuschließen.

In ihrer Gesamtheit ermöglichen die, in dieser Arbeit präsentierten, Ergebnisse ein tiefer gehendes Verständnis der unterschiedlichen Bindungsmodi innerhalb der Wechselwirkung zwischen Arrestin und Rhodopsin. Die Konformation vom Arrestin im prä-Komplex scheint die Konformation im Basalzustand nachzubilden unter Beteiligung zweier Kontaktstellen: Interaktion mit dem phosphorilierten C-Terminus des Rezeptors und Assoziation mit der Membran. Beim Übergang in den High-affinity Komplex durchläuft Arrestin eine Konformationsänderung in eine aktivere Konformation: der C-Terminus wird verdrängt, es erfolgt eine Neuausrichtung der zentralen flexiblen Schleifen und die Orientierung des Membranankers ändert sich. Die Aufgabe des prä-Komplexes ist somit Arrestin und den Rezeptor zusammen zu bringen sowie die korrekte Orientierung sicherzustellen um einen schnellen Übergang in den High-affinity Komplex zu ermöglichen.

Contents

List of figures

List of tables

Abbreviations

Å = angstroms

A (amino acid) = Alanine

A = absorbance

A_s = absorbance of reference

A_u = absorbance of unknown sample

AFM = Atomic force microscopy

Arr = arrestin

ATP = adenosine triphosphate

ATR = All-*trans*-retinal

B = monobromobimane

B2AR = β2 adrenergic receptor

C (atom) = Carbon

C (amino acid) = Cysteine

χ^2 = chi-squared (statistical robustness of the fit)

Cl = chlorine

cps = fluorescence count per second

D = Aspartate

DEER = double electron-electron resonance

°C = degrees Celcius

DMSO = dimethyl sulfoxide

DNA = deoxyribose nucleic acid

5-doxyl stearic acid = 2-(3-Carboxypropyl)-4,4-dimethyl-2-tridecyl-3-oxazolidinyloxy

E = Glutamate

EDTA = Ethylenediaminetetraacetic acid

EM = electron microscopy

EPR = electron paramagnemtic resonance

F (amino acid) = Phenylalanine

F = fluorescence

F_s = fluorescence of sample

F_u = fluorescence of unknown sample

F_w = fluorescence of fluorophore in presence of quencher

F_0 = fluorescence of fluorophore in absence of quencher

FTIR = Fourier transform infrared spectroscopy

g = relative centrifugal force

g (weight) = grams

γ = fraction of fluorophores unquenched in the ground state

γDQ = fraction of dynamically quenched fluorophores

γF = fraction of unquenched fluorophores

λmax = wavelength of maximum absorbance

ga = gauge

GPCR = G protein coupled receptor

GRK = GPCR receptor kinase

h = hour

H (atom) = Hydrogen

H8 – helix 8

HDX = hydrogen deuterinium exchange

HOMO = highest occupied molecular orbital

I = isoleucine

Icl – intracellular loop

IP6 = inositol hexaphosphate

IPTG = Isopropyl β-D-1-thiogalactopyranoside

IRF = instrument response function

K = Lysine

Kd = dissociation constant

K_{nr} = non-radiative decay

L = leucine

logI(t) = log of intensity decay

LUMO = lowest unoccupied molecular orbital

M (amino acid) = methionine

M = molar

Meta = metarhodopsin

Meta I = metarhodopsin I

Meta II = metarhodopsin II

Meta III = metarhodopsin III

Mg = magnesium

µg = micrograms

µl = microliters

µM = micromolar

µm = micrometers

mL = milliliters

mM = millimolar

mm = millimeters

N = Asparagine

Na = Sodium

NBD = N,N'-Diemthyl-N-(Iodoacetyl)-N'-(7-Nitrobenz-2-Oxa-1,3-Diazol-4-yl)Ethylenediamine)

nm = nanometers

NMR = nuclear magnetic resonance

N-tempoyl palmitamide = 4-Palmitamido-2,2,6,6-tetramethylpiperidine-1-oxyl

Ops = opsin

Ops* = active opsin

OpsP = phosphorylated opsin

Ops*P = phosphorylated active opsin

P = Proline

PCR = polymerase chain reaction

PDB = protein databank

PDE = phosphodiesterase

pH = potential of hydrogen

PMSF = phenylmethylsulfonyl fluoride

PP2A = protein phosphatase 2A

Q = Glutamine

ϕ = quantum yield

ϕ_s = quantum yield of reference

ϕ_u = quantum yield of unknown sample

R = Arginine

Γ = emissive rate of the fluorophore

Rh = inactive rhodopsin

Rh* = active rhodopsin

RhP = inactive phosohorylated rhodopsin

Rh*P = active, phosphorylated rhodopsin

RPE = retinal pigment epithelium

ROS = rod outer segment

S (amino acid) = serine

s = second

SDPC = 1-stearoyl-2-docosahexaenoyl-sn-glycero-3-phosphocholine

SDS-PAGE = sodium dodecyl sulfate polyacrylamide gel electrophoresis

SLFA = spin-labelled fatty acids

T (amino acid) = threonine

τ = fluorescence lifetime

τ_w = lifetime of fluorophore in presence of quencher

τ_0 = lifetime of fluorophore in absence of quencher

t = time

TM – transmembrane helix

TRIS = 2-Amino-2-(hydroxymethyl)propane-1,3-dio

TrIQ = tryptophan induced quenching

V = valine

V2Rpp = vasopressin receptor phosphorylated C-terminus

W (amino acid) = Tryptophan

W = Watts

x = unspecified amino acid

Y = Tyrosine

1. Introduction

1.1 G protein coupled receptors

G protein coupled receptors (GPCRs) are a ubiquitously expressed class of membrane proteins. There are over 700 different types of receptors in the family, which all have the same general structure and activation mechanism (Lefkowitz 2004). GPCRs interact with environmental and physiological ligands, including odorants, light, hormones and neurotransmitters, which can be activating (agonists) or deactivating (inverse agonists and antagonists). GPCRs are major drug targets, and almost half of currently marketed pharmaceuticals target a GPCR. Agonist binding results in conformational changes in the receptor, leading to G protein binding and activation, which then elicits further downstream effects in the cell (Pierce 2002). Phosphorylation of the receptor, and the subsequent binding of arrestin, results in termination of the signal (Gurevich and Gurevich 2004).

1.2 Rhodopsin

Rhodopsin is the GPCR present in retinal rod cells, which detects light at the single photon level. In its basal state rhodopsin is bound to its inverse agonist, 11-*cis*-retinal, via a protonated Schiff-base linkage to the protein. Light absorption isomerises 11-*cis*-retinal to the agonist all-*trans*-retinal (ATR), which induces activating conformational changes in the receptor. The binding partners of rhodopsin are the G protein transducin, the receptor kinase GRK1, and arrestin-1 (kühn 1980b, 1980a, 1978; Kuhn, Hall, and Wilden 1984). The interaction between rhodopsin and arrestin-1 is the focus of this dissertation.

1.2.1 The rod cell

The rod cell is adapted for highly efficient detection of light and transduction of the signal. It is composed of an outer and inner segment, which are connected by a narrow cilium (Figure 1.1). The large outer segment is composed of hundreds of flattened membranous discs surrounded by a plasma membrane (Molday 1998). Half of the volume of the rod outer segment discs is composed of rhodopsin, and Atomic Force Microscopy (AFM) revealed that there were up to 50,000 rhodopsin molecules per μm^2 in the rod outer

segment (Liang et al. 2003; Fotiadis et al. 2003), making up more than 80% of all proteins in this compartment (Daemen 1973). AFM and cryoelectron tomography studies suggest that rhodopsin molecules are highly organized within the disc membrane, arranged in ordered "track" structures, each containing two rows of rhodopsin dimers (Gunkel et al. 2015; Liang et al. 2003).

The smaller inner segment contains the nucleus, mitochondria, and other organelles and cellular machinery necessary to support cellular metabolism and protein synthesis, and leads to the synaptic terminal. Arrestin and transducin translocate in opposite directions between the outer and inner segments depending on light intensity. In dim light arrestin is sequestered in the rod inner segment, whereas in bright light conditions, when there is a sufficient population of light-activated rhodopsin, it translocates to the rod outer segment (Broekhuyse et al. 1985). Transducin, on the other hand, moves towards the rod outer segment in dim light for activation by light-activated rhodopsin, and translocates to the inner segment in bright light to prevent excess signalling (Brann and Cohen 1987; Philp, Chang, and Long 1987).

The retinal pigment epithelium (RPE) lies in close proximity to the rod outer segment and contains the enzymes involved in the retinoid cycle, which catalyses the conversion of all-*trans*-retinal (ATR) back to 11-*cis*-retinal. Briefly, ATR released from light-activated rhodopsin (Rh*) is reduced to all-*trans*-retinol, which is transported to the RPE. In the RPE a series of enzymatic reactions occur, where esterification of all-*trans*-retinol leads to the formation of retinyl esters, from which hydrolysis and isomerisation reactions form 11-*cis*-retinol. Subsequent oxidation leads to 11-*cis*-retinal, which is released back into the rod outer segment for binding to rhodopsin (McBee et al. 2001; Kiser et al. 2012).

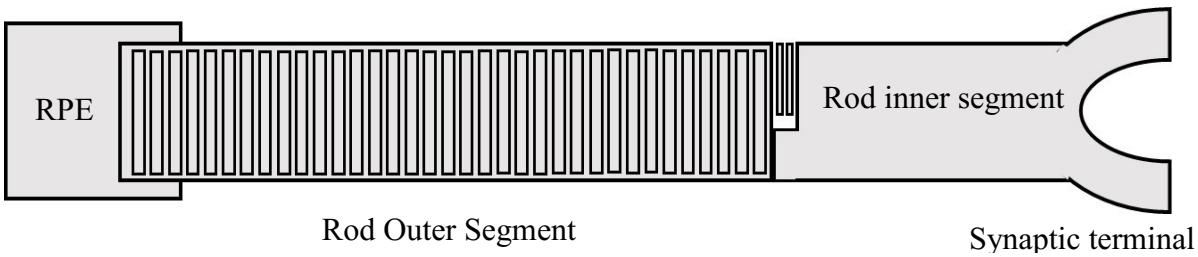

Figure 1.1 Schematic of the rod cell
The rod cell is composed of outer and inner segments: the rod outer segment contains rhodopsin and components of the visual signal transduction cascade. The rod inner segment contains the cellular organelles and machinery, and leads to the synaptic terminal. The tip of the rod cell is in close contact with cells of the retinal pigment epithelium, which contain enzymes responsible for the retinoid cycle that catalyse the conversion of all-trans-retinol back to 11-cis-retinal for regeneration of rhodopsin.

1.2.2 Visual signal transduction

Visual signal transduction (see figure 1.2) is a cycle involving **activation** (binding and activation of transducin), **deactivation** (receptor phosphorylation and arrestin binding), and **recovery** (dephosphorylation and regeneration of rhodopsin):

1. Activation – The initial step occurs when rhodopsin absorbs a photon of light. A binding crevice opens on the cytoplasmic side of Rh*, where transducin binds. Transducin is a heterotrimeric G protein, consisting of an α, β and γ subunit. The α subunit has a guanine nucleotide binding site, which upon binding to active rhodopsin exchanges GDP for GTP. This step results in dissociation of transducin into two components: Gα-GTP, and βγ. Gα-GTP interacts with and activates the enzyme phosphodiesterase (PDE), which results in the hydrolysis of cGMP to GMP. Low cellular concentrations of cGMP lead to a change in permeability of cGMP-gated channels in the synaptic terminal, resulting in hyperpolarisation of the cell and an action potential (Leskov et al. 2000) (Arshavsky, Lamb, and Pugh 2002).
2. Deactivation – Rh* signalling is terminated in a two-step process. First, GRK1 binds and phosphorylates Rh*, after which arrestin binds. As arrestin binds in the same cytoplasmic crevice as transducin, it occludes any further binding of transducin to the active receptor (Kuhn, Hall, and Wilden 1984; Wilden, Hall, and Kuhn 1986). The arrestin - rhodopsin interaction will be described in detail in section 1.4
3. Recovery – Several minutes after light-activation of rhodopsin, the retinal Schiff base hydrolyses and all-*trans*-retinal leaves the ligand binding pocket of the receptor, resulting in the phosphorylated aporeceptor, opsin. The retinoid cycle converts all-*trans*-retinal back to 11-*cis*-retinal, which enters the retinal-binding pocket of opsin and reforms the Schiff base, thereby resulting in the regeneration of rhodopsin (Lamb and Pugh 2004; Philp, Chang, and Long 1987; Kiser, Golczak, and Palczewski 2014). After regeneration of rhodopsin and dissociation of arrestin, the receptor is dephosphorylated by the protein phosphatase 2A (PP2A) (Palczewski et al. 1989; Lee et al. 2010).

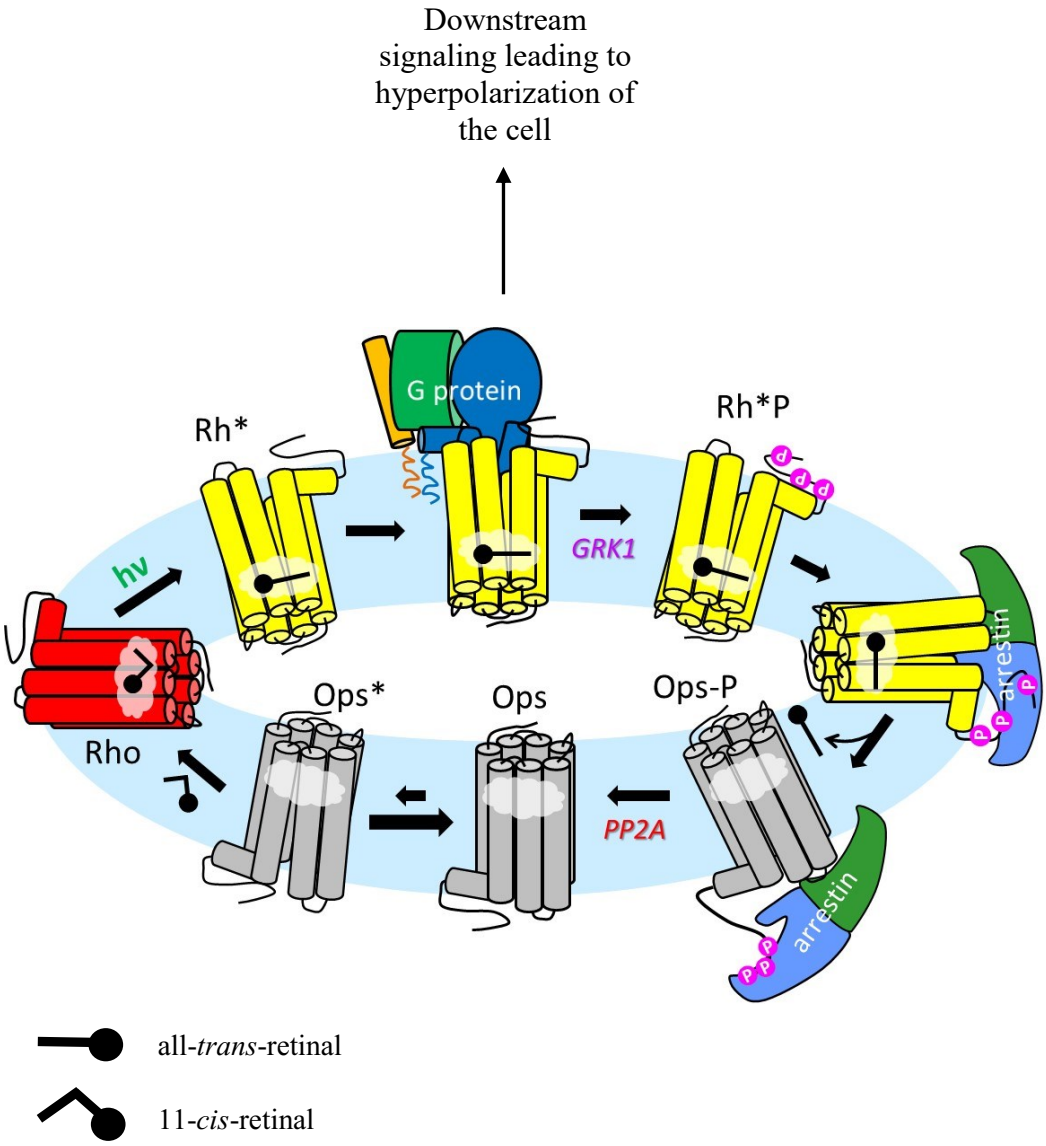

Figure 1.2 Schematic of signal transduction.
After light-activation, rhodopsin (Rh) binds and activates the G protein transducin, which dissociates and induces downstream effects resulting in hyperpolarisation of the cell. Deactivation of the system requires first phosphorylation of rhodopsin by rhodopsin kinase (GRK1), which allows for arrestin to bind. Release of all-trans-retinal (ATR), and dephosphorylation of the receptor by protein phosphatase 2A (PP2A), leads to arrestin dissociation. The resulting aporeceptor, opsin, exists in a conformational equilibrium between OpsP and Ops*P (see section 1.2.4 for more details). 11-cis-retinal re-enters the retinal binding pocket of Ops*, regenerating rhodopsin (Rho). Figure provided by Dr. Martha Sommer.*

1.2.3 Structure of Rhodopsin

Rhodopsin consists of 348 amino acids, and is structured as 7 transmembrane helices connected by three extracellular loops and three cytoplasmic loops, as well as helix 8

which lies parallel to the membrane on the cytosolic side. Rhodopsin is bound by its inverse agonist, 11-*cis*-retinal in its basal state, which is covalently linked to Lys296 through a protonated Schiff base linkage. Upon light-activation, 11-*cis*-retinal isomerises to all-*trans*-retinal and the Schiff base deprotonates, resulting in protein structural changes and an active conformation (Hofmann et al. 2009; Palczewski et al. 2000).

Figure 1.3 Structure of the retinoid ligands

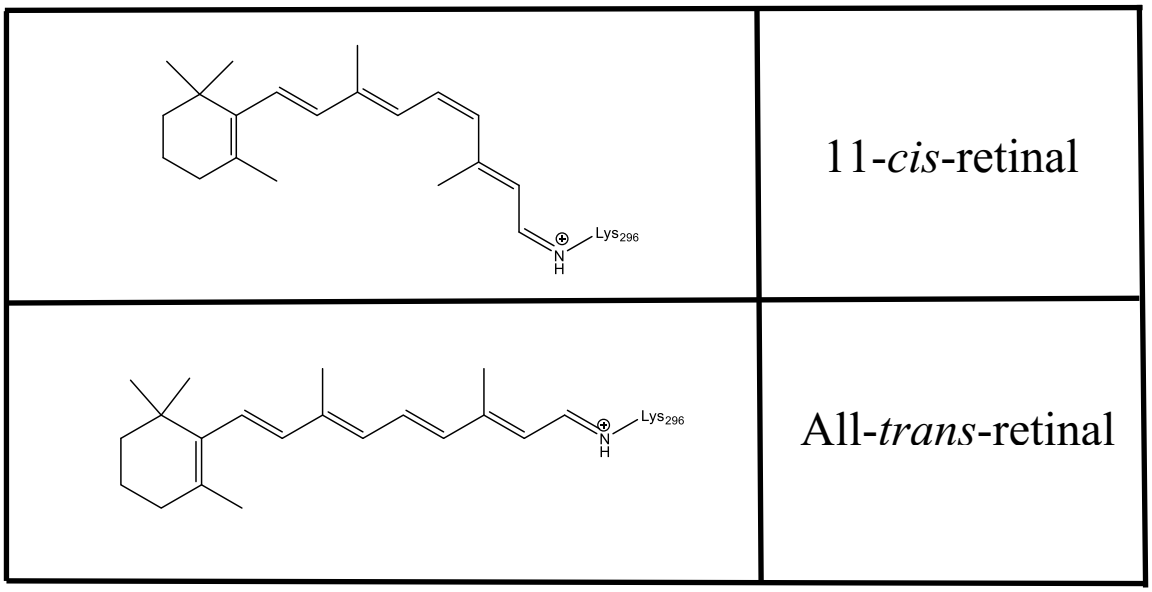

The basal structure of rhodopsin (shown in figure 1.4), is stabilised by two highly conserved motifs. The first is the E(D)RY motif on transmembrane helix 3 (TM3), which tethers TM3 and TM6 by forming an ionic lock. The second is the NPxxY(x)F motif on TM7 – Helix 8 (H8), which tethers TM7 and H8 and links TM7 to TM1 and TM2. Upon light-activation these interactions are broken. In particular the breaking of the TM3-TM6 ionic lock allows for movement of TM6, which undergoes an outward movement on the cytoplasmic side, opening a crevice which allows for binding of transducin and arrestin (Nygaard et al. 2009; Hofmann et al. 2009).

The rhodopsin C-terminus contains seven phosphorylation sites: 3 serine and 4 threonine residues. At least three of these sites are required to be phosphorylated for high-affinity arrestin binding (Gurevich and Benovic 1993, 1995; Mendez et al. 2000). The arrestin binding site has been shown to involve interactions with residues on intracellular loop 2, which lies adjacent to the E(D)RY motif, as well as intracellular loop 3, which is located

near the cytosolic side of TM3 and TM5 (Raman, Osawa, and Weiss 1999; Shi et al. 1998; Krupnick et al. 1994; Krupnick, Gurevich, and Benovic 1997). Additionally, intracellular loop 1, and the neighbouring TM7 and H8 have also been determined as an interaction site for loops on arrestin (Raman, Osawa, and Weiss 1999; Szczepek et al. 2014; Kang et al. 2015).

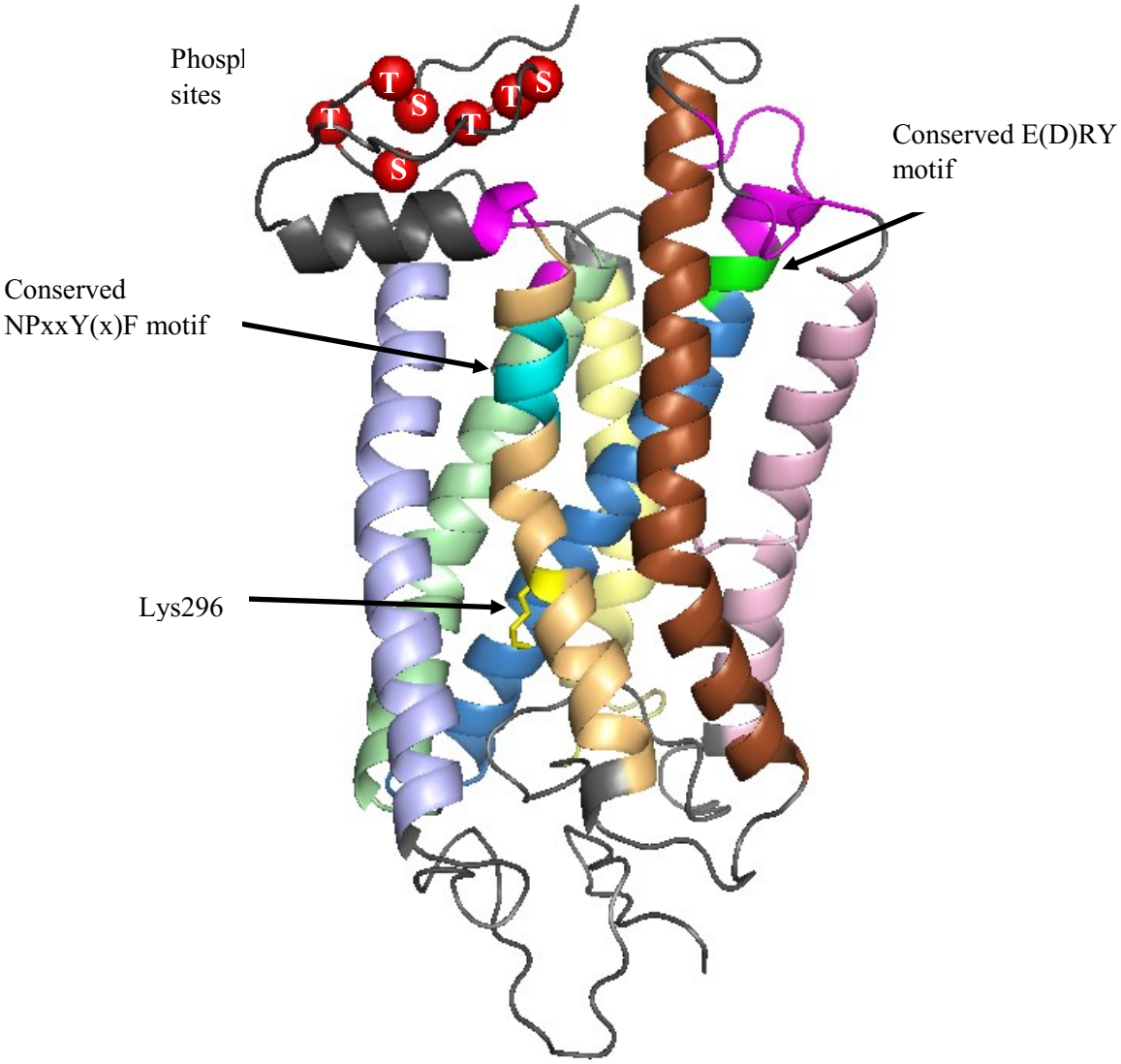

Figure 1.4 Structure of basal rhodopsin
Helices are coloured: light blue =TM1, pale green = TM2, blue = TM3, pale yellow = TM4, light pink = TM5, brown = TM6, light orange = TM7, dark grey = H8. Sites involved in arrestin binding are shown in magenta, and are centred around intracellular loop (ICL) 1 near TM7-H8, lying adjacent to the conserved NPxxY(x)F motif, shown in cyan, and ICL2 and ICL3 near TM5 and TM3, which lies adjacent to the conserved ERY motif, coloured in green. The red spheres indicate the Cα of serine and threonine residues on the C-terminus which are phosphorylated by GRK1 for arrestin binding. Lys296, to which the retinal is covalently bound, is shown in yellow. PDB reference, 1U19.

1.2.4 Photo-activation cycle of rhodopsin

The light-induced activation of rhodopsin occurs through a series of intermediate energy barriers (shown in figure 1.5). The first step after retinal isomerization results in the formation of Metarhodopsin-I (Meta-I), through spectroscopically distinguishable, short-lived intermediates termed Batho and Lumi. Meta-I formation occurs on a fast, microsecond, timescale and corresponds to conformational changes localized to the retinal binding pocket. From Meta-I, a series of further sequential sub-states occur, termed Metarhodopsin-IIa, Metarhodopsin-IIb, and Metarhodopsin-IIbH*, which are spectroscopically identical, and exist in an equilibrium, which favours Metarhodopsin-IIbH*. These sub-states correspond to more global changes in the conformation of the receptor. The initial sub-state (Metarhodopsin-IIa) corresponds to deprotonation of the Schiff base. Subsequent breakage of constraints that hold the receptor in its basal conformation, lead to the outward movement of TM6, which defines the second sub-state (Metarhodopsin-IIb). The final sub-state (Metarhodopsin-IIbH*) corresponds to the uptake of a proton to residue E134 on the conserved E(D)RY motif on TM3 (see figure 1.4). It is this active conformation of the receptor that is able to bind transducin (Hofmann et al. 2009). An alternative pathway leads to the formation of Meta-III from Meta-I. To date, there is little known about the exact nature of this pathway, but the Meta-III conformation differs from Meta-II in that it has a reprotonated Schiff base that exists in the *syn* configuration, as opposed to the *anti* configuration that exists in the other Meta intermediates (Vogel et al. 2003).

The decay of Meta-II occurs within minutes: the retinylidene Schiff base is hydrolysed and all-*trans*-retinal is released, leaving the aporeceptor opsin. This exists in an equilibrium between an inactive state (Ops), and a conformation more similar to the active receptor (Ops*). In the native membrane the conformational equilibrium is heavily shifted in favour of the inactive Ops (Vogel and Siebert 2001). However, the retinal ligands are only able to bind Ops*, through a retinal channel that is present in the active receptor conformation. The retinal channel is formed by the opening of two “holes”, through rearrangement of bulky residues between TM7 and TM1 (Hole A), and TM5 and TM6 (Hole B), which connect the retinal binding pocket with the lipid bilayer (Hofmann et al. 2006; Park et al. 2008; Scheerer et al. 2008). Binding of 11-*cis*-retinal stabilizes the inactive receptor conformation, and the two holes are snapped shut, thereby trapping the inverse agonist in the binding pocket until light-activation (Piechnick et al. 2012). All-*trans*-retinal, on the other hand, enters and leaves in a fast equilibrium. Therefore

conditions which shift the conformational equilibrium of opsin towards Ops*, such as interaction with either transducin or arrestin, or activating mutations, allow for all-*trans*-retinal to re-enter the ligand binding pocket (Sommer, Hofmann, and Heck 2012; Jastrzebska et al. 2013; Schafer et al. 2016).

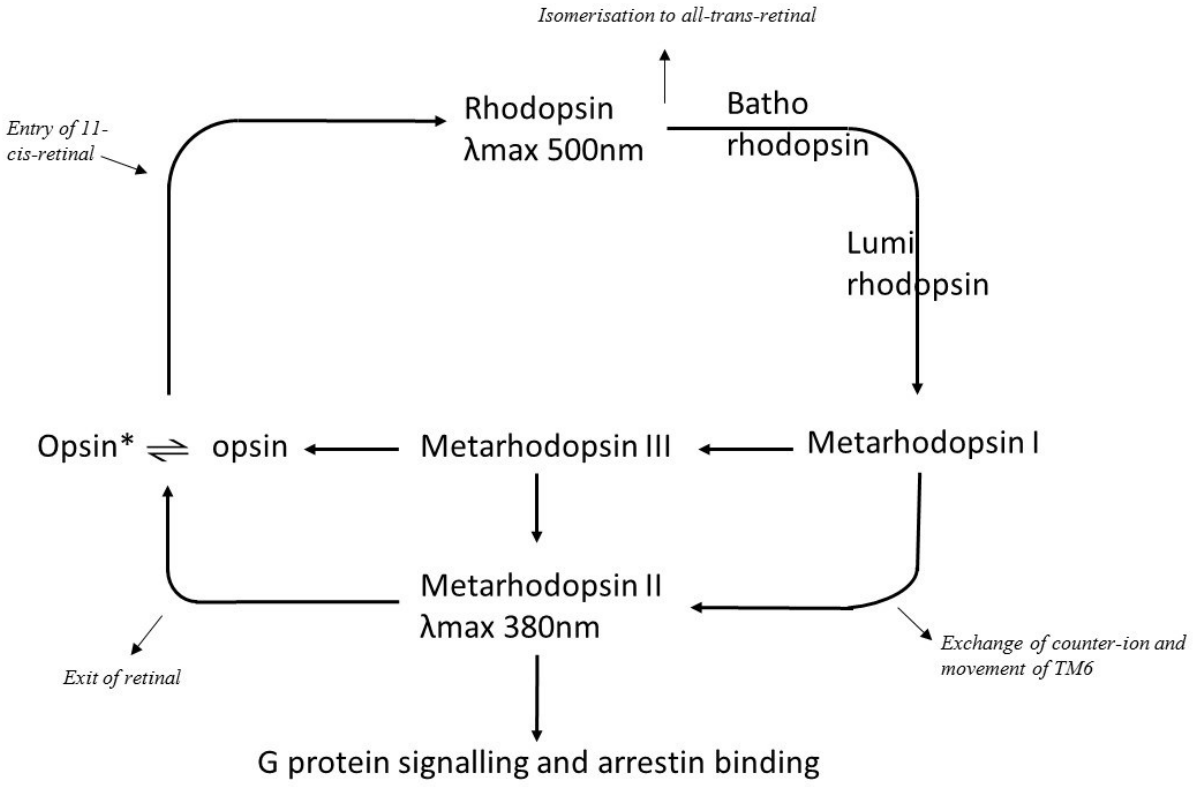

Figure 1.5 Photo-activation cycle of rhodopsin.
After absorption of a photon of light, rhodopsin is activated through a series of intermediates to metarhodopsin II, which binds and activates transducin, and binds arrestin. Exit of the agonist all-trans-retinal, and rebinding of the inverse agonist 11-cis-retinal regenerates rhodopsin. See main text for details.

1.3 Arrestin

The arrestin family is comprised of just four different variants which all share the same basic structure. Arrestin-1 and arrestin-4 are expressed in rod and cone cells, respectively, and regulate the visual opsins. Arrestin-2 and arrestin-3, also called β-arrestin-1 and β-arrestin-2, are ubiquitously expressed and interact with hundreds of different GPCRs (Lohse and Hoffmann 2014). The β-arrestins are conformationally flexible in order to confer the necessary receptor-binding promiscuity. The main function of arrestin is to block G protein binding and thereby terminate G protein-mediated signalling. However, the β-arrestins also mediate their own signalling by binding to other signalling molecules including transcription factors, signalling kinases and phosphatases. The β-arrestins additionally mediate receptor internalization and trafficking by binding components of the cellular internalization machinery such as clathrin and AP2 (Xiao et al. 2007; Lohse and Hofmann 2015; Reiter et al. 2012).

1.3.1 Arrestin-1

The first crystal structure of native bovine arrestin-1 obtained from rod outer segments was solved in 1998 (Granzin et al. 1998). A higher resolution structure of recombinant arrestin-1 was published soon after (Hirsch et al. 1999). Arrestin-1 crystallized in a tetrameric form, with 2 monomers displaying an “open” conformation, and 2 monomers displaying a “closed” conformation. The differences between these conformations are localized to flexible loops that form the oligomerization interfaces, namely the finger loop, the 160-loop, and the 344-loop (figure 1.6). Arrestin self-associates in a concentration-dependent manner, with tetramers and dimers forming at higher concentrations, and the monomeric form prevalent at lower concentrations (Vishnivetskiy et al. 1999; Imamoto et al. 2003; Hanson et al. 2007). Interestingly, the tetramer that forms in solution differs from the crystallographic tetramer (Hanson et al. 2007; Hanson et al. 2008). The physiologically relevant tetramer is believed to associate with microtubules in the inner segment when arrestin is sequestered there in dim light conditions (Hanson et al. 2007). Translocation of arrestin to the outer segment in bright light conditions lowers the concentration, which promotes dissolution of the oligomer. This phenomenon favours receptor binding, as key-receptor binding elements are occluded within the oligomerization interface, and only the monomer can interact with the receptor (Hanson et al. 2008).

The basic structure of arrestin consists of two near-symmetric cup-like domains placed end-to-end, called the N- and C-domain. Each domain is composed of a 4 stranded β-sheet packed upon a 3 stranded β-sheet. Additionally there is a small α-helix in the N-domain, and the C-domain is connected via a linker region to the long flexible C-tail. This C-tail interacts extensively with the N-domain, although the distal portion remains unresolved in the crystal structure (Granzin et al. 1998) (Hirsch et al. 1999; Vishnivetskiy et al. 1999).

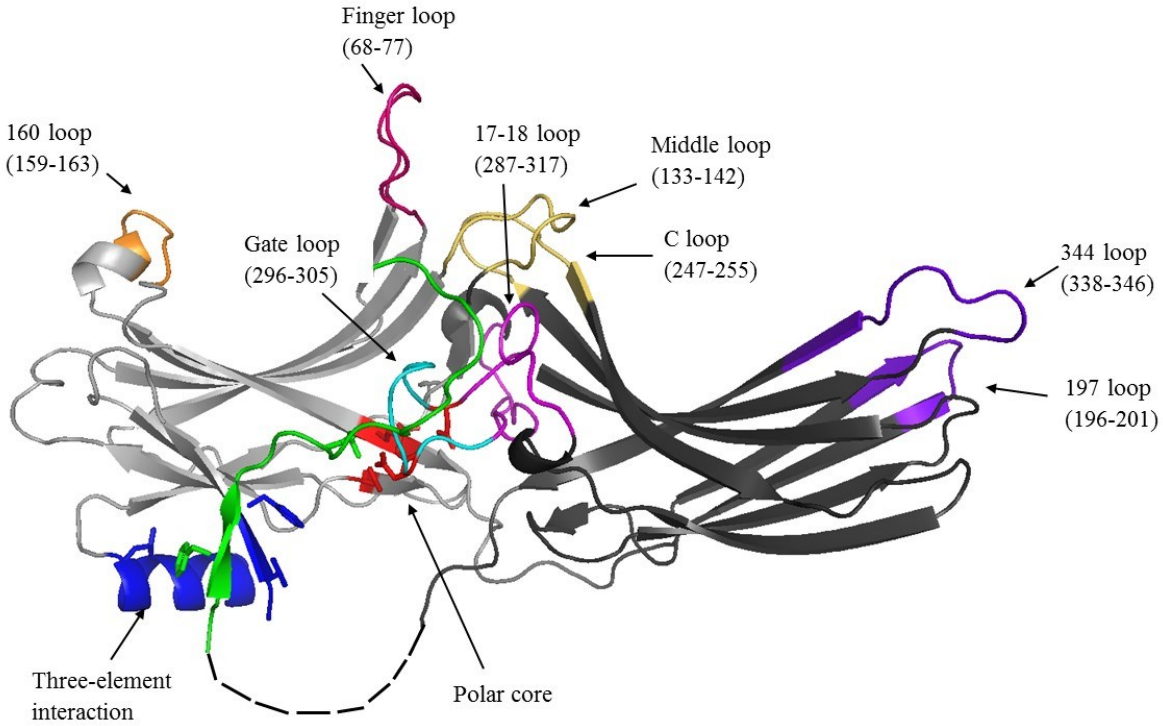

Figure 1.6 Structure of visual arrestin-1
The N-domain is coloured in light grey, and the C-domain in dark grey. The dashed line indicates a portion of the C terminus that remains unresolved in the crystal structure. Regions important in the stabilization of arrestin, or involved in the arrestin – receptor complex are labelled, and discussed below (PDB reference: 1CF1, α monomer).

Description of important regions in arrestin

The labelled loops in figure 1.6 are described below. These regions of arrestin are involved either in the stabilization of basal arrestin, or at the binding interface of the arrestin-rhodopsin complex. The activation of arrestin and the structure of the complex will be explained in more detail in the following sections.

The C-tail, shown in green, is comprised of the terminal 32 residues on arrestin-1: 372-404. It is flexible, and unstructured, with the distal portion remaining unresolved in crystal structures. It is connected by a flexible linker to the C-domain, and it interacts at several sites on the N-domain, including the polar core and three element interaction (Hirsch et al. 1999). The C-tail acts as an auto-regulatory element, which constrains arrestin in a basal conformation, and is displaced upon interaction with the receptor (Smith et al. 1994; Pulvermüller et al. 1997).

The polar core, shown in red, is a cluster of charged residues buried between the N- and C- domain, including residues D30, R175, K176, D296, D303 and R382. Of these residues R382 is on the C-tail, and sites D303 and D296 are on the gate loop (296-305), shown in cyan. The cluster is stabilised by salt bridges, as shown in figure 1.7, which stabilise the basal conformation of arrestin. Displacement of the C-tail results in disruption of the polar core, and movement of the gate loop (Hirsch et al. 1999; Kim et al. 2013; Shukla et al. 2013).

The three element interaction, shown in blue, is a hydrophobic interaction between residues on β-strand-I (9-14) and α-helix-I (103-111) on the N-domain, and β-strand-XX (373-380) on the C-tail (shown in green), see figure 1.7. Along with the polar core, this interaction helps to stabilise the inactive arrestin conformation (Hirsch et al. 1999; Vishnivetskiy et al. 1999).

The Finger loop, shown in dark pink, is comprised of residues 68-77. It is a flexible loop which is folded down in the β-conformer of the arrestin structure, and extended in the α-conformer (Hirsch et al. 1999). Numerous studies have highlighted this loop as an interaction site with the active receptor (Sommer, Hofmann, and Heck 2012; Hanson et al. 2006; Szczepek et al. 2014; Kang et al. 2015).

Central crest loops, include the finger loop, described above, as well as the C-loop (residues 247-255) and the middle loop (133-142), shown in gold, and the 17-18 loop (residues 287-317), shown in magenta, which also includes the gate loop, described above, which is shown in cyan. These loops lie at the interdomain interface and form several interactions between the two domains in the basal arrestin conformation. Upon arrestin activation, they undergo a reorientation, and interact with sites on the active receptor in the complex (Kim et al. 2013; Shukla et al. 2013).

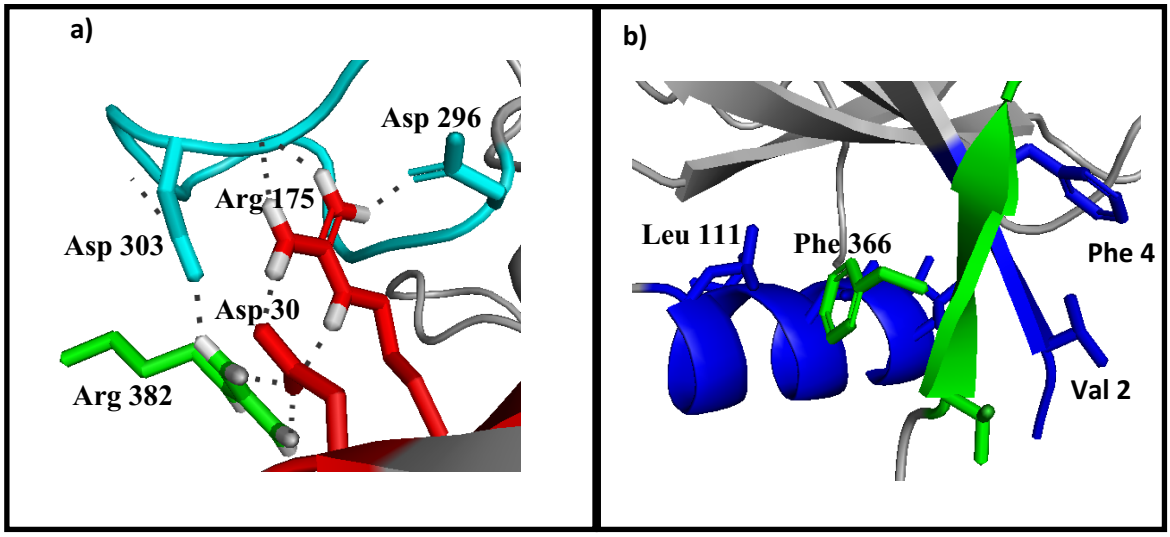

Figure 1.7 The polar core and the three element interaction
a) *the polar core. Residues from the N-domain are shown in red, from the C-tail in green, and the gate loop in cyan. Stabilising salt bridges between the negatively and positively charged amino acids comprising the polar core are shown as black dashes.* ***b)*** *The three element interaction: Hydrophobic interactions are formed between the N-domain: α-helix -I and β-sheet-I, shown in blue, and the C-tail shown in green.*

The C-edge loops, are shown in purple, and consist of the 344-loop (residues 338-346) and the 197-loop (residues 196-201). They are on the distal C-edge of arrestin, and results presented in section 3.1 of this dissertation describe their interaction with the membrane upon arrestin binding to rhodopsin.

The 160-loop, shown in orange, consists of residues 159-163. These residues are on the distal N-edge of arrestin. The flexible loop contains many charged residues, with three acidic residues (E160, E161, and D162) lying adjacent to the basic K163 residue. This loop has been suggested as a putative site of interaction with rhodopsin (Shukla et al. 2014; Kang et al. 2015).

1.3.2 Activation mechanism of arrestin

1.3.2.1 Initial model of arrestin activation

Early insights into the activation mechanism of arrestin proposed that it was a two-step process, requiring both a phosphorylation and an activation sensor. Arrestin binding was found to be highly specific for the active phosphorylated receptor (Rh*P), with a lower level of binding observed with both the unphosphorylated active receptor (Rh*) and the phosphorylated inactive receptor (RhP), and virtually no binding to the inactive non-

phosphorylated receptor (Rh) (Kuhn, Hall, and Wilden 1984; Gurevich and Benovic 1993).

Initial experiments identified three regions which were involved in arrestin activation:

1. The first region identified was the C-tail. Truncation of the terminal 37 residues of arrestin, and the subsequent discovery of p44, a natural splice variant of arrestin lacking the C-tail (Smith et al. 1994), displayed phosphorylation independent binding to the receptor. Further proteolysis experiments found that in the presence of the phosphorylated receptor C-terminus, the C-tail of arrestin was displaced. Moreover, this effect could be mirrored by the presence of IP6, which contains several phosphate groups, or heparin, a large polyanion molecule, thereby suggesting a large negative charge would lead to C-tail displacement (Palczewski, Buczylko, et al. 1991) (Gurevich et al. 1994; Zhuang et al. 2010). This provided initial evidence to support the idea that the C-tail of arrestin acted as an autoinhibitory structure.
2. The second region which resulted in a loss of binding specificity when mutated was the polar core, in particular the salt bridge between R175 – D296 (see figure 1.7) (Vishnivetskiy et al. 1999). Mutations that neutralised or reversed the charge of either of these residues resulted in increased binding to Rh* and Rh*P, as compared to wild type arrestin, whereas a charge reversal of both sites, which retained the salt bridge, restored the binding specificity (Gurevich and Benovic 1995) (Gurevich and Benovic 1997; Raman et al. 2003).
3. The third region identified was the three element interaction. Mutations which removed the hydrophobic residues involved in the interaction, resulted in increased binding to RhP and Rh*. Lying adjacent to β-strand-1 in the three element interaction, are two lysine residues, K14 and K15. Charge reversal mutations of these residues led to a dramatically decreased binding to Rh*P and RhP, leading to the proposal that they act as the initial phosphate sensor (Vishnivetskiy et al. 2000).

Further mutagenesis studies showed that shortening the hinge region between the two domains abrogated binding, but substitution of individual residues had no effect (Vishnivetskiy et al. 2002). This, combined with the large diameter of arrestin as compared to the cytoplasmic side of rhodopsin, and the high energy barrier of interaction (Schleicher, Kühn, and Hofmann 1989), led to the proposal that C-tail displacement and

subsequent disruption of the polar core and three element interaction led to a large-scale conformational change. The two domains were thought to move relative to each other in a “clam-shell” movement, bringing the edge of both domains into contact with the cytoplasmic side of the receptor.

1.3.2.2 Recent perspectives on the arrestin activation mechanism

Various experimental techniques have been utilised in order to follow the conformational changes occurring in arrestin upon binding to rhodopsin, and have repudiated the idea of the large clam-shell movement of arrestin. Double electron-electron resonance (DEER) experiments, which measured intramolecular distances of doubly spin-labelled arrestin mutants in the unbound and Rh*P-bound states, found no evidence to support the large scale movement of the two domains relative to each other (Kim et al. 2012). Instead smaller movement was seen to be localised to some loops on arrestin, namely the finger loop and the middle loop, as well as to a smaller extent on the distal edges of arrestin: the 160-loop and 344-loop. Similarly FTIR experiments detected no large scale changes in the conformational structure of arrestin upon binding to Rh*P, although a loss in β-sheet structure suggested that binding was correlated with an increased flexibility in the arrestin structure (Beyriere et al. 2015). Therefore, the initial hypothesis of arrestin activation had to be modified.

Further insights into the conformational changes occurring in the arrestin structure upon activation came from the crystallisation of pre-active arrestin p44, which lacks the terminal 35 residues constituting the arrestin C-tail (Kim et al. 2013) and the structure of active arrestin-2 bound to a peptide analogue of the vasopressin phosphorylated receptor C-terminus (V2Rpp) (Shukla et al. 2013).

1.3.2.3 Conformational changes associated with arrestin activation

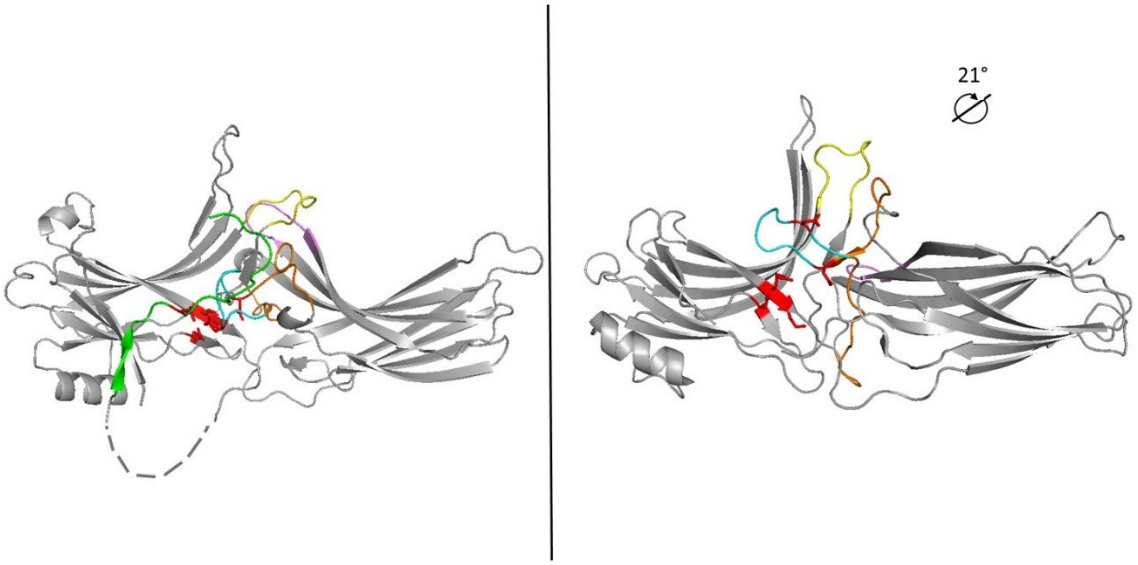

Figure 1.8 Structure of basal arrestin and p44
Left: *Basal arrestin, PDB code: 1CF1, α conformer.* ***Right:*** *p44, PDB code: 4J2Q. The C-tail present only in the basal arrestin structure is shown in green. Loops which undergo conformational changes between the two structures are coloured: cyan = gate loop, orange = 17/18 loop, yellow = middle loop, violet = C loop, and the polar core is shown in red. The 21° interdomain rotation that is observed in the p44 structure is indicated.*

The structures both obtained similar results for the orientation of loops in the active arrestin structure. The loops undergoing rearrangements as compared to the basal structure of arrestin are described below.

Displacement of the C-tail and movement of the gate loop

In the structure of arrestin – V2Rpp the C-tail was displaced and this resulted in disruption of the polar core and the three element interaction, which was also observed in the p44 structure which lacks the C-tail. The gate loop, containing the residues D296 and D302 which comprise part of the polar core, was observed to move towards the N-domain as compared to the basal structure of arrestin, and this movement resulted in an exposed cleft of positively charged residues (K14, K15, K171, K175 and K300), which act as a potential binding site for the phosphorylated receptor C-terminus (Kim et al. 2013). Indeed, the phosphorylated residues on V2Rpp were shown to contact the residues on arrestin-2 equivalent to K14 and K15 on the concave surface of the N-domain (Shukla et al. 2013). The movement of the gate loop seen in the p44 structure was confirmed with fluorescence quenching experiments with arrestin bound to the active phosphorylated

receptor Rh*P (Kim et al. 2013). A fluorophore at site I299 on the gate loop was quenched by a tryptophan substituted at site L173 in the N-domain when arrestin was bound to Rh*P but not in the unbound state. These observations confirm that the two sites are distant in basal arrestin and become close upon arrestin activation, and are consistent with the gate loop movement seen in both structures.

Extension of the finger loop and movement of the central crest loops

Both structures also suggested that the finger loop was extended in the active arrestin structure (Kim et al. 2013; Shukla et al. 2013). Fluorescence studies which indicated that this loop enters into a hydrophobic environment (Sommer, Smith, and Farrens 2005), and Electron Paramagnetic Resonance (EPR) studies which showed that it becomes immobilised (Hanson et al. 2006) upon interaction with Rh*P, suggest that the extension of the loop observed allows for binding to the active receptor. Furthermore, the β-sheet at the base of the finger loop is extended in the p44 conformation as compared to basal arrestin, which could serve to stabilise the interaction between the finger loop and the active receptor. The 17-18 loop winds around the two β-sandwiches of the N- and C-domains of arrestin, and is involved in stabilising the interdomain interface in basal arrestin. In the p44 structure, movement of this loop disrupts several interactions at the interdomain interface, which results in the 21° rotation of the two domains relative to each other. In particular the hydrogen bond network YKS(N)D(A) connecting the finger loop, middle loop and C-loop in basal arrestin is disrupted. A short β-strand forms adjacent to the 17-18 loop, which forms a new hydrogen bond network, TMQGL, with the middle loop (which moves closer to the finger loop) and the base of the finger loop. This new hydrogen bond network helps to stabilise the finger loop in its extended conformation. The C-loop, on the other hand, moves towards the C-domain, away from the finger loop, to allow space for binding to the receptor (Kim et al. 2013) (see figure 1.9).

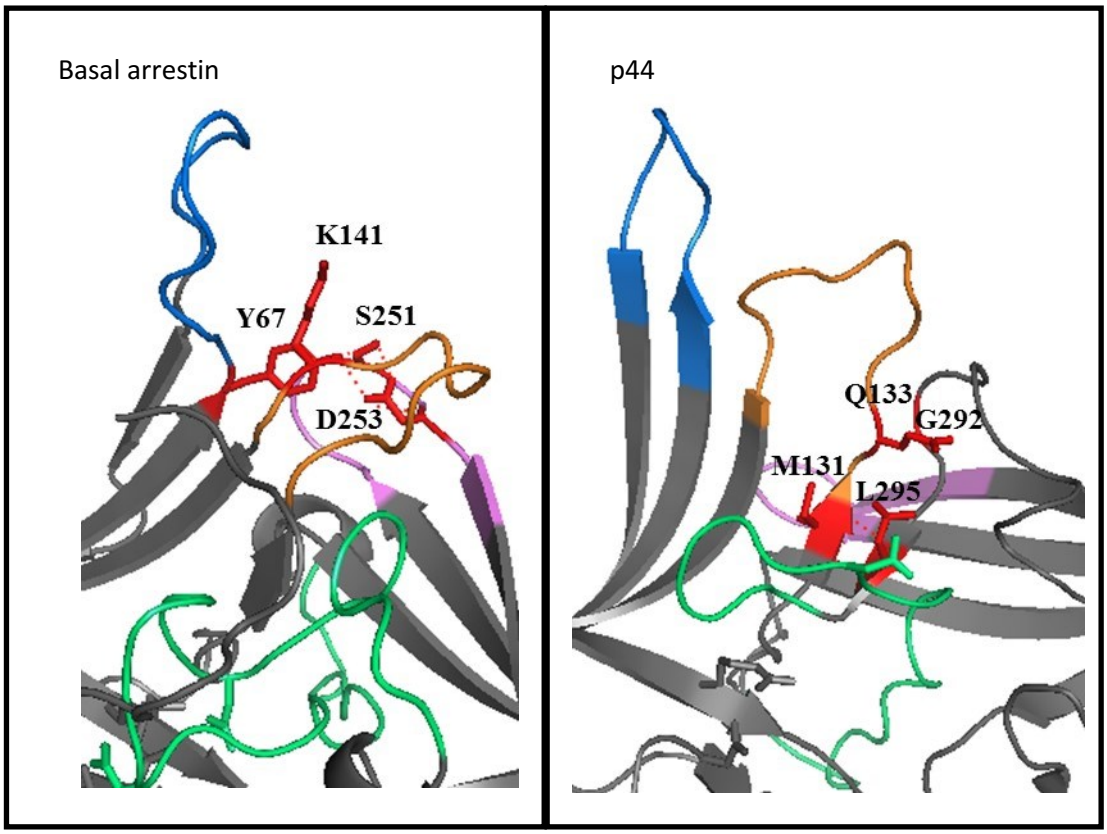

Figure 1.9 Hydrogen bond networks within the central crest loops left: basal arrestin (1CF1, chain a) and right: p44 (4J2Q, chain a)
green: 17-18 loop, orange: middle loop, pink: C loop, blue: finger loop. Side chains comprising the H network are shown in red. In basal arrestin this network is YKS(N)D(A). In p44, this network is broken, and a new H-bond network forms, which is T(M)QGL.

1.4 Structure of the arrestin – rhodopsin complex

The finger loop of arrestin was suggested as a putative binding site in the arrestin-rhodopsin complex, due to the conformational rearrangement which resulted in the loop adopting an extended conformation in activated arrestin (Kim et al. 2013; Shukla et al. 2013), as well as its sequence similarity to the binding site of the Gα-subunit of transducin. A peptide of the finger loop was co-crystallised with Ops* and the resulting structure showed that it could bind in the crevice adjacent to the ERY motif on the cytoplasmic side of the receptor, and made additional contacts to the TM7-H8 helical bundle (Szczepek et al. 2014). The loop was observed to adopt a reverse-turn structure upon binding to the receptor.

Further insights into the nature of the complex came from an Electron Microscopy (EM) structure (Shukla et al. 2014). The structure obtained was of a mutated β2-Adrenergic

receptor (β2AR), in complex with β-arrestin 1, along with a FAB30 antibody to stabilise the complex. Negative EM staining revealed two conformations of arrestin. The first involved interaction of arrestin with the helical core of the receptor, whereas the second conformation showed arrestin "hanging off" from the receptor, at a 90° angle to the membrane, in an interaction with the edge of one of the arrestin-domains. This suggested that binding of arrestin to the receptor is flexible, and there are possibly different binding modes of interaction. Hydrogen-Deuterium exchange (HDX) was carried out in order to confirm the visualisation of interacting loops on arrestin with the receptor, and demonstrated that the finger loop, middle loop, and C loop were all in a more buried environment upon complex formation.

1.4.1 Crystal structure of the complex

The most detailed perspective of arrestin binding to rhodopsin came from the crystal structure of the complex (Kang et al. 2015). The structure was derived from a constitutively active mutant opsin fused via a 15-amino acid linker to a constitutively active mutant arrestin. Crystallization was facilitated by fusion of T4 lysozyme to the N-terminus of opsin.

The crystal structure of the Ops*/arrestin-1 fusion complex identified four main areas at the arrestin-receptor interaction interface.

1. The finger loop on arrestin, which had been previously identified as involved in binding to the active receptor (Sommer, Smith, and Farrens 2005; Hanson et al. 2006) (Szczepek et al. 2014) was confirmed to interact with the cytoplasmic side of TM7, H8 and ICL1. The cytoplasmic face of the helices is positively charged, whereas the finger loop contains three negatively charged residues: (E70, D71 and D73). Therefore, the interaction is stabilised not only by shape, but by electrostatic interaction. Interestingly, the loop adopted an alpha helical conformation, as opposed to the reverse-turn structure observed in structure of the finger loop peptide (Szczepek et al. 2014). This could be attributed to differences between peptide and protein binding, or an artefact of activating mutations introduced into arrestin and rhodopsin in the ops*/arrestin-1 fusion complex. However, it could also be as a result of flexibility in the finger loop, resulting in different binding orientations.

2. The second interaction site was found to involve the central crest loops of arrestin. The middle loop and C-loop are in close contact in the basal structure of arrestin, but upon activation of arrestin move away from each other (Kim et al. 2013; Shukla et al. 2013). This results in a crevice forming between the two loops, which is able to accommodate ICL2 of rhodopsin, which adopts an α-helical conformation upon interaction. The nearby 17-18 loop on arrestin also forms contacts with the cytoplasmic side of TM5, which lies adjacent to ICL2.
3. The third interaction site was with the β-strand which forms at the base of the finger loop, containing residues 79-86. In the crystal structure this is observed to interact with TM5, TM6 and ICL3. The 160-loop on the N-edge was also found to make contacts with the cytoplasmic face of TM6.
4. The final interaction site was between residues 11-18 on the N-terminal edge of arrestin and the C-terminus of the receptor. This was not resolved in the crystal structure, and therefore the interaction was not directly observed. However, modelling studies and DEER experiments, as well as the orientation of arrestin with the receptor in the complex, led to this region being proposed by Kang et al as a final binding interface between arrestin and rhodopsin.

The identification of interfaces of interaction observed in the ops*/arrestin-1 fusion complex crystal structure were supported by biochemical studies. Mutations introduced into the finger loop and central crest loops reduced arrestin binding to the active rhodopsin, and cross-linking experiments between arrestin and active rhodopsin also supported the close contact of residues at each of the identified interaction sites. Moreover HDX exchange experiments, which were shown to occur at a slower rate in complexed arrestin as compared to basal arrestin, indicated that the arrestin structure is stabilised by complex formation. In particular, the shielding of the finger loop from HDX exchange in the complex confirmed burial of this loop in the interaction, a result also previously observed with fluorescence and EPR studies (Sommer, Smith, and Farrens 2005; Hanson et al. 2006).

The complex obtained showed asymmetric binding of arrestin to the active receptor, with the C-domain of arrestin orientated in a manner that suggests interaction with the membrane. There was no membrane present in the structure, and the distal C-edge of arrestin was not fully resolved in the structure, and therefore this could not be confirmed. However, the C-edge of arrestin contains a cluster of hydrophobic residues, which have been shown to dramatically reduce binding to active rhodopsin upon mutation to alanine

(Ostermaier et al. 2014). Furthermore, fluorescence labels at site 344 on the C-edge of arrestin show that the site moves into a hydrophobic environment, in a concentration-dependent manner, upon interaction of arrestin with the receptor (Sommer, Hofmann, and Heck 2012). This possibility, and the nature of an interaction between the C-edge of arrestin and the membrane, will be explored further in this dissertation.

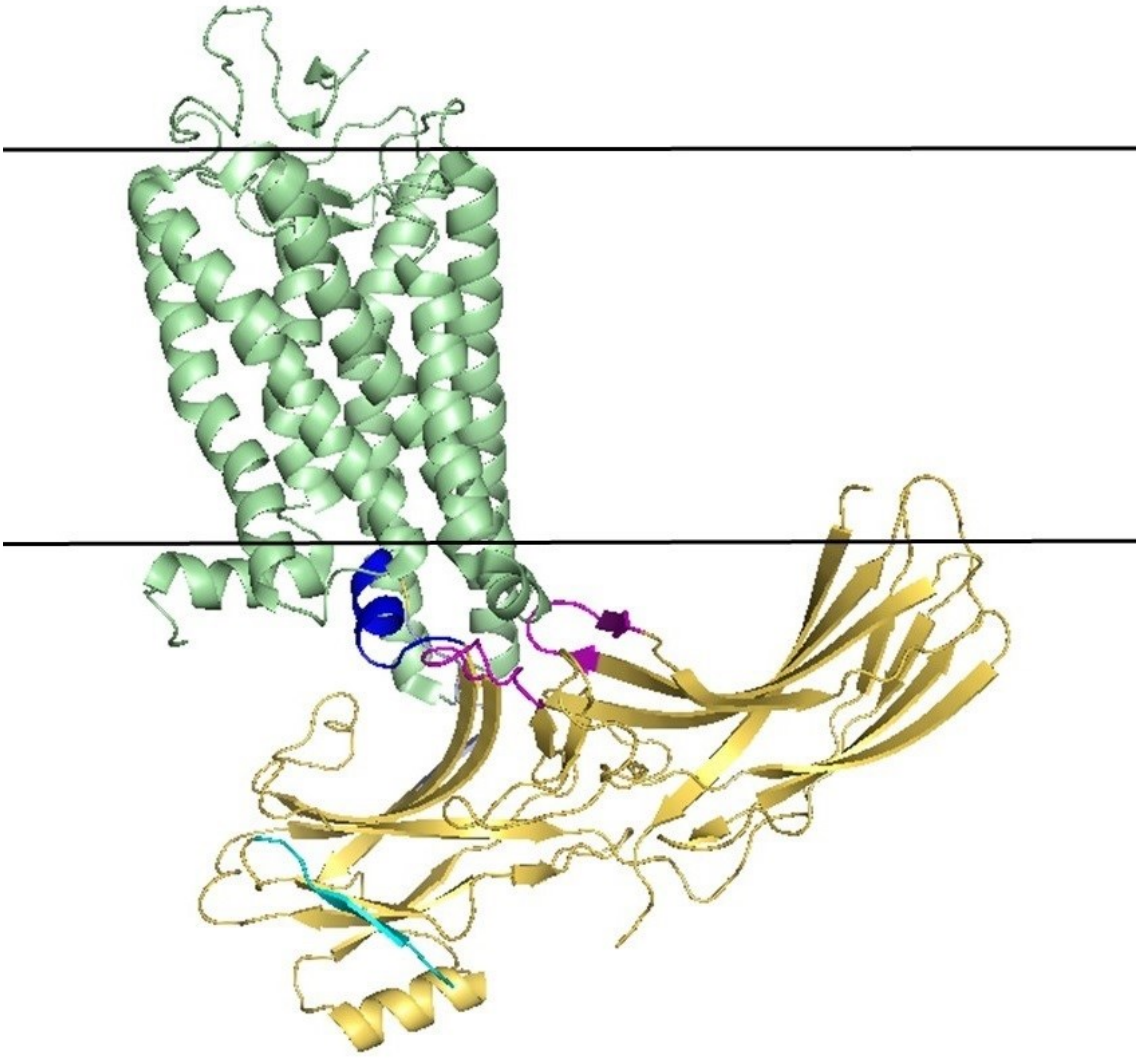

Figure 1.10 Structure of the ops*/arrestin-1 fusion complex
Rhodopsin is shown in light green, and arrestin in shown in yellow. Main interaction sites are with the arrestin finger loop (shown in blue), and the arrestin middle and C-loop (shown in magenta), and the β-sheet at the base of the finger loop (shown in light blue). The distal N-edge of arrestin, which was proposed to interact with the unresolved receptor C-terminus is shown in cyan. PDB code: 4ZWJ.

1.5 Binding modes of arrestin

The crystal structure of the arrestin-1/ops* complex has provided insight into one binding mode of arrestin with active opsin. However, this does not rule out the possibility of further binding modes. The negative stain EM structure obtained (Shukla et al. 2014) contained two visualisations of the arrestin-receptor complex. In one structure arrestin is interacting with the helical core of the receptor, and could correspond to the high-affinity complex. However, in the second structure arrestin is contacting the receptor through one of its edges, lying at a 90° angle to the membrane. This could reflect a different binding mode of the complex, and could be a representation of the pre-complex, as described below.

1.5.1 The pre-complex

As well as binding the light-activated phosphorylated receptor (Rh*P), arrestin is also able to interact with the inactive phosphorylated receptor (RhP) in a lower affinity interaction, characterised by a Kd of 80μM in 100mM NaCl (Zhuang et al. 2013), and a Kd of around 1μM in the absence of salt (Sommer, Hofmann and Heck 2012). This interaction between arrestin and the phosphorylated receptor C-terminus, is thought to represent an intermediate step in arrestin binding to Rh*P (see scheme 1). Arrestin binding to Rh*P was initially proposed to be a two-step process through the determination of kinetic binding constants of both arrestin and p44 binding to Rh*P. As p44 is in an active conformation, it was pre-complexed in the dark to RhP, whereas arrestin remained unbound. Upon light-activation, the rate of p44 binding was faster than that of arrestin, and was concentration independent. The authors therefore proposed that binding of arrestin to Rh*P involved an initial first step, which brought the proteins into contact through the phosphorylated receptor C-terminus, and primed arrestin for the second binding step, which involved a conformational rearrangement resulting in tight binding (Schröder, Pulvermüller, and Hofmann 2002).

$$RhP + Arr \rightleftharpoons [Rh^*P \sim Arr]_{pre\text{-}complex} \rightleftharpoons [R^*P - Arr]_{high\text{-}affinity\ complex}$$

Scheme 1
Arrestin binding to rhodopsin is a two-step process. First arrestin engages the phosphorylated receptor C terminus in a pre-complex interaction, before transition to high-affinity binding.

To date little is known about the structure of the pre-complex. Proteolysis (Palczewski, Pulvermüller, et al. 1991; Palczewski, Buczylko, et al. 1991) and nuclear magnetic resonance (NMR) (Zhuang et al. 2013) experiments have determined that interaction between arrestin and the phosphorylated receptor C-terminus results in flexibility in the C-tail region of arrestin. The interaction was also found to display much higher sensitivity to salt than the high-affinity complex, implying that the interaction is mainly electrostatic (Gurevich and Benovic 1993; Sommer, Hofmann, and Heck 2012). Studies comparing sites on arrestin in the presence of RhP and Rh*P determined that the conformation of arrestin in the pre-complex is distinct from that in the high-affinity complex. Fluorescence experiments indicated that the finger loop, the C-edge loops and the C-loop are all orientated in different environments in the pre-complex as compared to the high-affinity complex, as fluorophores attached at sites on these loops all demonstrate an increase in fluorescence upon binding to Rh*P as compared to RhP (Sommer, Hofmann, and Heck 2012). Additionally, EPR experiments found that the central crest loops and C-edge loops, as well as sites on the concave surface of the N-domain, demonstrated a decreased mobility in the pre-complex as compared to basal arrestin (Hanson et al. 2006). Upon light-activation, there was a further change in mobility in the central crest loops, with the middle loop becoming more mobile, and the finger loop almost immobilized. These studies highlight that the structure of arrestin in the pre-complex and the high-affinity complex are different. However, the orientation of these loops in the pre-complex remain to be elucidated, and will be further investigated in this dissertation.

1.5.2 Stoichiometry of the complex

The crystal structure of the ops*/arrestin-1 fusion complex showed one arrestin bound to one receptor (Kang et al. 2015). This stoichiometry has been determined to be functional, as binding assays carried out with monomeric rhodopsin reconstituted into nanodiscs, found that arrestin was able to bind with a similar affinity as to native membranes (Bayburt et al. 2011). Furthermore, arrestin binding and stabilisation of the active receptor state, metarhodopsin II, was also found to saturate at a one-to-one stoichiometry of arrestin to receptor (Pulvermüller et al. 1997; Schleicher, Kühn, and Hofmann 1989).

However other binding stoichiometries cannot be ruled out. The idea of a one-to-two stoichiometry was initially proposed due to the large diameter of arrestin as compared to rhodopsin (Modzelewska et al. 2006). Initial evidence for a one-to-two binding

stoichiometry came from arrestin binding studies with ROS membranes containing different proportions of light-activated receptors. The study observed that at higher photo-activation densities overall binding stoichiometry plateaued at one arrestin per two receptors, as compared to at lower photo-activation densities, where the binding stoichiometry plateaued at one-to-one (Sommer, Hofmann, and Heck 2011). Further experiments monitored fluorescence changes occurring at sites on the finger loop and the 344-loop, in combination with centrifugal pull-down assays which determined the amount of arrestin bound. The fluorophore on the finger loop reported the amount of arrestin bound to Rh*P, but showed minimal fluorescence change in the presence of the aporeceptor even though arrestin was bound. However, the fluorescence changes occurring with the fluorophore on the 344-loop reported the amount of arrestin bound to both Rh*P and the aporeceptor. Therefore, a model was proposed that suggested the finger loop of arrestin always interacted with the active receptor crevice in a high affinity interaction. However, the 344-loop of arrestin was more flexible, interacting either with the membrane, in the case of a one-to-one binding stoichiometry, or contacting a neighbouring receptor in a low affinity interaction, in the case of a one-to-two binding stoichiometry (Sommer, Hofmann, and Heck 2012). The validity of the model will be investigated in this dissertation, along with factors influencing the final stoichiometry of the high-affinity complex.

1.6 Aims of the project

This dissertation further elucidates the interaction between arrestin and rhodopsin. The crystal structure obtained of the ops*/arrestin-1 fusion complex (Kang et al. 2015) provided clear insights into the nature of the complex, but left some unresolved questions. The structure obtained was in the absence of membrane, and the C-edge loops of arrestin were unresolved. However, the orientation of arrestin in the complex indicated that an interaction between the C-domain of arrestin and the membrane was possible. This dissertation addresses this possibility using site-directed fluorescence in combination with spin-labelled fatty acids which spontaneously insert into the membrane. As the spin labels quench fluorescence, the proximity between fluorophores individually attached to different sites on arrestin and different regions of the membrane are able to be monitored, and a binding interaction between arrestin and the membrane can be characterized.

Moreover, even though the ops*/arrestin-1 fusion complex structure fits well to biochemical studies, which proposed the finger loop was involved in the arrestin-rhodopsin binding interface (Szczepek et al. 2014), and that no large-scale conformational rearrangement occurred upon formation of the complex (Beyriere et al. 2015; Kim et al. 2012), there is evidence to suggest that other binding modes are possible. Arrestin interacts initially with the phosphorylated receptor C-terminus, in an interaction termed the pre-complex, before transition to tight binding in the high-affinity complex (Schröder, Pulvermüller, and Hofmann 2002). However, there is little information about the structure of this complex. This dissertation presents new insights into the structure of the pre-complex as compared to the high-affinity complex, using intramolecular quenching, which monitors conformational changes occurring in arrestin upon interaction with the different receptor species. The implications of pre-complex formation on the final binding stoichiometry will also be addressed. Through modulating the pre-complex interaction using salt, and observing the effect on the stoichiometry of the complex, it can be determined whether there is a link between pre-complex formation and the final binding stoichiometry of the high-affinity complex observed after light-activation (Sommer, Hofmann, and Heck 2011, 2012).

2. Methods and Techniques

2.1 Fluorescence Spectroscopy

Site directed fluorescence spectroscopy is a useful tool for observing intramolecular conformational changes occurring in proteins, and interactions of proteins with binding partners (e.g. ligands, peptides, proteins and membranes). Experiments reported in this dissertation utilised this technique to monitor arrestin-rhodopsin interactions, and to follow the conformational changes occurring in arrestin between the basal and bound conformations. The technique involved substituting a single site in arrestin with cysteine and then modifying that cysteine with a sulfhydryl-reactive fluorophore, either monobromobimane, or N,N'-Diemthyl-N-(Iodoacetyl)-N'-(7-Nitrobenz-2-Oxa-1,3-Diazol-4-yl)Ethylenediamine) (NBD) (purchased from Invitrogen), shown in figure 2.1. Specificity of labelling was ensured by first removing all native reactive cysteines from arrestin (C63A, C128A, C143A). As these fluorophores are small (<1 kilodalton) they do not significantly affect the structure of arrestin, when placed at a surface exposed site. Moreover, the fluorophores chosen are solvent sensitive, which means their spectra characteristics (lifetime, intensity, and wavelength of emission) are dependent on the relative polarity of their environment, and therefore are able to provide information about structural changes occurring at the site to which they are attached.

Figure 2.1 Fluorophores used for arrestin-labelling

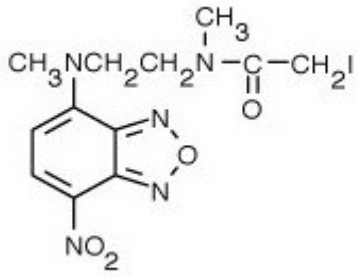

N,N´-Dimethyl-N-(iodoacetyl)-N´-(7-Nitrobenz-2-oxa-1,3-diazol-4-yl)ethylenediamine (NBD)

λmax excitation = 500nm

λmax emission = 550nm

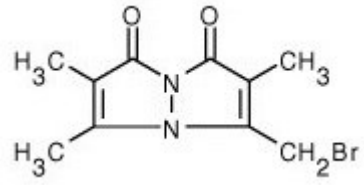

Monobromobimane

λmax excitation = 390nm

λmax emission = 490nm

In this dissertation, fluorescence spectroscopy was implemented to address several different questions. Interaction of different sites on arrestin with the membrane were observed using fluorescently-labelled arrestin in conjunction with spin-labelled fatty acids, which act as quenching agents and are able to spontaneously insert into the membrane. In addition, mutation of selected sites on arrestin to tryptophan, which quenches fluorophore emission when located in a close proximity (<10Å), allowed conformational changes occurring in arrestin upon interaction with different forms of the receptor to be monitored, through intramolecular quenching. Finally, through attaching fluorophores on the arrestin-rhodopsin binding site, binding of arrestin to rhodopsin at varying concentrations allowed for determination of the binding stoichiometry of the interaction. The theoretical basis of these processes are described below, with information taken from the book Principles of Fluorescence Spectroscopy (Lakowicz 2010).

2.1.1 Overview of the physics of fluorescence

Fluorescence spectroscopy relies on the principle of electron excitation by a photon of light, and the subsequent release of energy as the electron returns to the ground state energy level. The wavelength of light is related to energy by the formula $E = h\nu$, where E = energy, h = Planck constant, and ν is the frequency of light. When a molecule absorbs a photon of light, the resulting energy can be enough to excite an electron into a higher energy orbital. When the electron returns to its ground state energy level, the energy difference is emitted. This process is shown in figure 2.2. The ground state (S_0) can be defined as the highest occupied molecular orbital (HOMO), and the excited state (S_1) the lowest unoccupied molecular orbital (LUMO). In the case of fluorophores, the energy difference between the LUMO and the ground state is sufficiently high that the emitted energy is released as a photon of visible light, which can be detected.

The S_1 and S_0 states are made up of different vibrational levels, and therefore the excited electron loses energy through very fast vibrational relaxation processes before emitting a photon of light to return to the ground state. As a lower energy corresponds to a longer wavelength of light, this explains why the emission wavelength of the fluorophore is longer than the exciting wavelength.

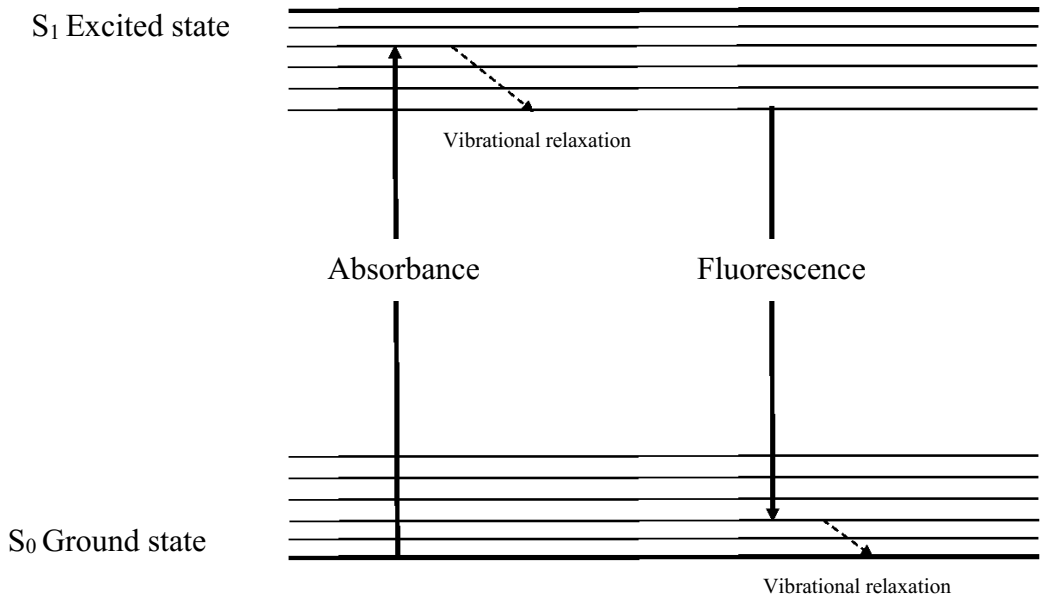

Figure 2.2 Jablonski diagram
The basic Jablonski diagram depicts the principles of absorbance and fluorescence. Upon absorption of a photon of light, the electron is excited to a higher energy orbital, termed the S_1 excited state. The electron loses energy very quickly, on the picosecond timescale, through vibrational relaxation and interconversion, until it occupies the lowest vibrational orbital in the S_1 state. The electron then returns to the ground state, on a nanosecond timescale, and emits energy released as a photon of light, which is detected as fluorescence. Figure adapted from Principles of Fluorescence Spectroscopy (Lakowicz 2010)

2.1.2 Quantum yield and fluorescence lifetime

The quantum yield of a fluorophore determines the proportion of photons emitted compared to photons absorbed by the molecule

The quantum yield is given by the equation:

$$\phi = \frac{\Gamma}{\Gamma + \mathrm{Knr}}$$

Where ϕ = quantum yield, Γ = emissive rate of the fluorophore, and K_{nr} = rate of non-radiative decay to the ground state (Lakowicz 2010).

All quantum yields are less than 1, as a fluorophore will never emit all of the energy absorbed as fluorescence, as explained above. However, the closer the quantum yield is to 1, the brighter it will be.

The lifetime of a fluorophore, is the amount of time that the molecule spends in the excited state, before returning to the ground state. This is given by the equation:

$$\tau = \frac{1}{\Gamma + Knr}$$

where τ = lifetime, Γ = emissive rate of the fluorophore, and K_{nr} = rate of non-radiative decay to the ground state (Lakowicz 2010).

In reality, individual molecules of the same fluorophore type will emit fluoresced photons at different times, and τ describes the average value for the population. For many fluorophores covalently attached to proteins, as with monobromobimane-labelled arrestin used in this dissertation, there is more than one lifetime. This is due to the heterogeneous environment of the fluorophore, caused by protein mobility. Therefore, it is useful to measure both the lifetime and the proportion of fluorophores in the sample with each lifetime.

2.1.3 Solvent relaxation effect

Not all fluorophores in the excited state will emit energy as fluorescence. Instead other processes can occur which cause transition to the ground state in a non-radiative way. These include collision with small solvent molecules, energy transfer to nearby molecules, or complex formation. Therefore, the observed fluorescence of a fluorophore is highly dependent on its environment, which is a useful tool for determining conformational changes in the protein at the site to which the fluorophore is attached.

One very simple tool is the change in intensity observed when the fluorophore is in a hydrophobic environment as compared to a hydrophilic environment. When the molecule is in a hydrophilic environment, more energy will be lost from the excited state of the fluorophore due to collisions. In general the dipole moment of the molecule in the excited state is larger than in the ground state. As the rotational movement of small molecules such as water, are rapid, there is time for the solvent molecules to rearrange around the dipole moment of the excited state, before the molecule fluoresces, and the resulting collisions result in a loss of energy from the excited state. Therefore a loss of fluorescence intensity, as well as a red-shift of the emission spectrum, is observed when the fluorophore is present in an aqueous environment. When the fluorophore is embedded in

a hydrophobic environment (e.g. protein interior or lipid phase of membrane), it is protected from these solvent effects.

2.1.4 Quenching

Molecular quenching is a process by which fluorescence intensity is reduced through physical interaction of the fluorophore and another molecule, i.e. the quencher. Quenching can either be dynamic; whereby the quencher collides with the fluorophore during the lifetime of the excited state, resulting in return to ground state without emission of a photon, or static; which results from the quencher forming a complex with the fluorophore in the ground state, to create a non-fluorescent complex, as shown in figure 2.3

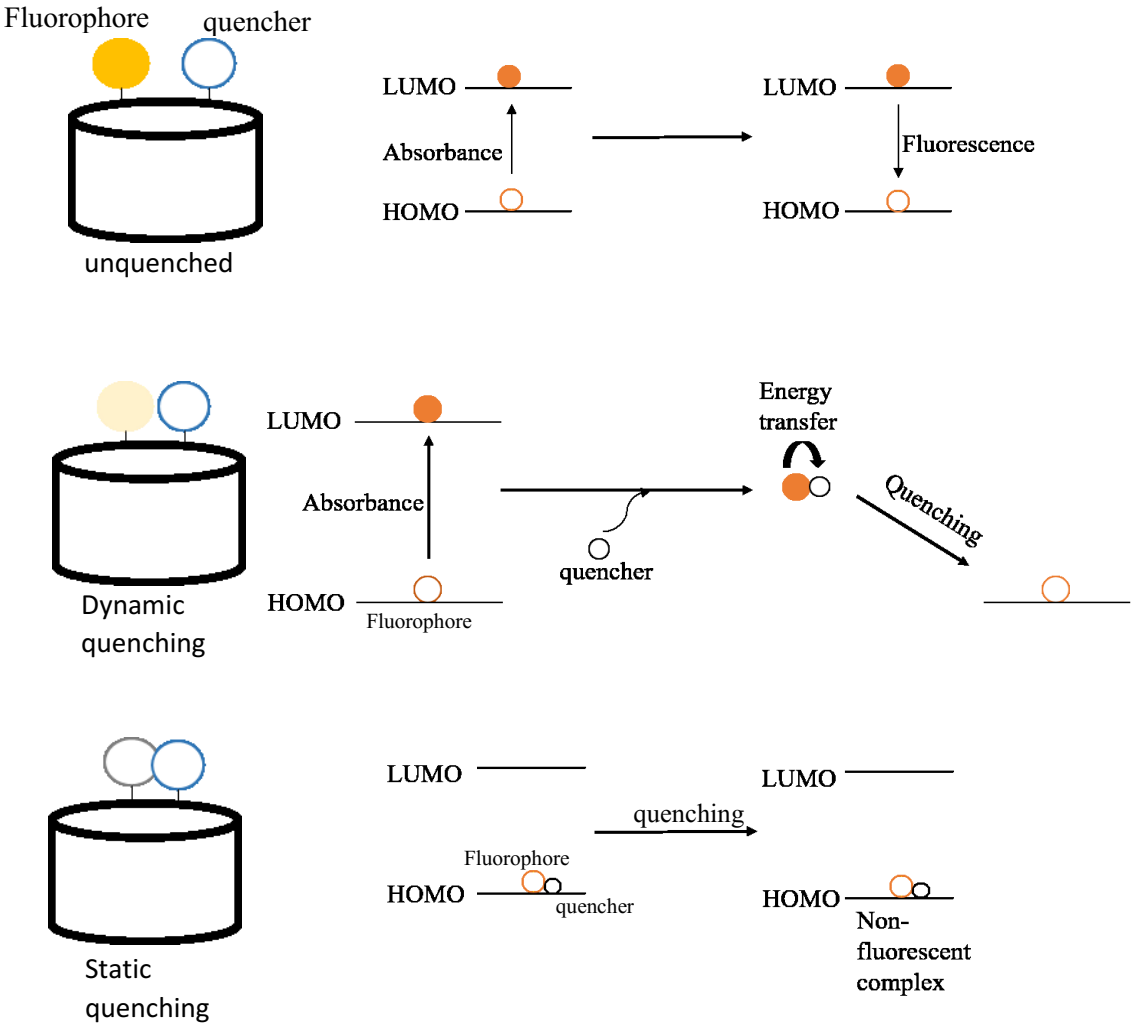

Figure 2.3 Mechanisms of quenching
Top: *when the fluorophore (yellow circle) and quencher (blue circle) are far apart, there is no effect on fluorescence.*
Middle: *When the fluorophore and quencher are in close proxinity the quencher can collide with the excited fluorophore resulting in a decreased fluorescence intensity and lifetime.*

Bottom: *Static quenching forms a non-fluorescent complex in the ground state, and no fluorescence is observed for the complexed molecule (grey circle).*
Figure adapted from (Mansoor, Dewitt et al. 2010)

Quenching is a useful tool in protein interactions in order to identify regions either on the same protein, or on interacting proteins, that are in contact. If there is no change in fluorescence intensity in the absence and presence of the quencher, the two regions of the protein must be distant from each other. If there is a decrease in fluorescence, however, then either dynamic or static quenching must be occurring. Steady-state fluorescence spectroscopy only provides information about the intensity of the fluorescence, and therefore can only distinguish whether a sample is quenched or unquenched. In order to determine whether the quenching is dynamic or static, time-resolved spectroscopy is required, which also calculates the fluorescent lifetime of the sample. With static quenching a non-fluorescent complex forms, resulting in a decrease in overall fluorescence but no change in the fluorescence lifetime. This is because static quenching has no effect on any excited molecule. With dynamic quenching, however, the quencher interacts with the excited molecule. This decreases both the intensity and the lifetime of the fluorophore, and therefore the two fluorescence quenching mechanisms can be distinguished from each other (Mansoor, Dewitt et al. 2010).

2.1.4.1 Mechanisms of dynamic quenching

Dynamic quenching occurs by three main processes. These processes are not mutually exclusive, and it is likely that a combination of more than one are responsible for the quenching effect. The mechanisms are shown in more detail below:

1. **Intersystem crossing** where the contact with the quencher causes the fluorophore to become a triplet state. Triplet states are lower in energy than the excited single state, and are much longer-lived. Therefore, loss of energy to the ground state occurs by non-radiative decay (Knr), with energy lost through collisions (see figure 2.4).

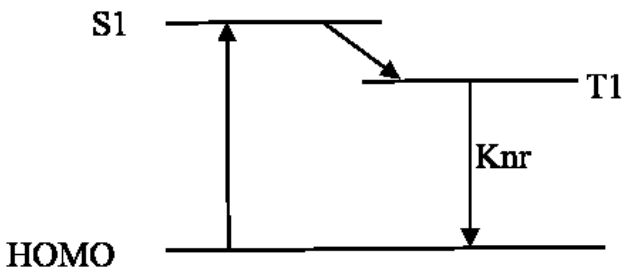

Figure 2.4 Intersystem crossing
Dynamic quenching occurs by the fluorophore becoming a triplet state.
figure adapted from (Lakowicz 2010)

2. **Electron exchange** involves the excited state fluorophore transferring the excited electron to the LUMO of the quencher. The quencher then transfers back an electron to the fluorophore, in the ground state. This mechanism results in no fluorescence, but the quencher remains in an excited state (figure adapted from (Lakowicz 2010))

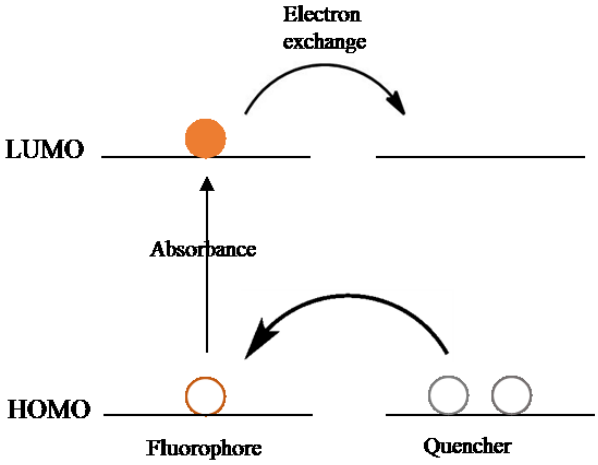

Figure 2.5 Electron exchange
Dynamic quenching involving transfer of electrons between the fluorophore and the quencher.
Figure adapted from (Lakowicz 2010)

3. **Photo-induced electron transfer** this is similar to electron exchange, but only involves 1 electron transfer, and therefore results in both molecules having a charge, through which they form an ionic complex. In photo-induced electron transfer the electron donor can be either the fluorophore or the quencher (Lakowicz 2010).

2.1.4.2 Examples of quenching agents

Tryptophan induced quenching (TrIQ)

Tryptophan, and to a lesser extent tyrosine, are able to quench fluorescence due to their large electronegative rings, and therefore are useful for studying protein interactions (Mansoor, Dewitt et al. 2010). In this study, double mutations of arrestin were carried out such that a fluorophore was attached at one site, and a tryptophan introduced into a secondary site. This then allowed for conformational changes in arrestin to be monitored when bound to different forms of the receptor, as the distance between the two mutated sites was followed.

Iodide quenching

Another method of quenching useful with fluorophore-labelled proteins is iodide quenching. Small halide ions are able to act as collisional quenchers, by spin-orbit coupling to the triplet state of the excited fluorophore. When these ions collide with the activated fluorophore, they result in a decreased lifetime of the excited state, and the intensity of fluorescence in lowered. By measuring the fluorescence spectra of a fluorescently labelled protein in a halide solution, the environment of the fluorophore can be determined. When it is solvent exposed there will be more opportunity for collisions between the ions in the solution and the fluorophore, and therefore more quenching will be observed, than when the fluorophore is buried in the interior of the protein or the binding pocket.

Spin-labelled fatty acids

Attachment of a fluorescence quencher group to fatty acids allows for proximity of fluorescent probes with the membrane to be determined. Experiments described in this dissertation monitored membrane association of fluorescently-labelled arrestin by measuring the degree of quenching occurring between the fluorophore and a nitroxide spin-label quenching group, placed at varying positions on the acyl chain of the fatty acid. The fluorophore quenching mechanism by the spin label is not completely understood, and it is possible that multiple mechanisms are involved. As the spin labels are paramagnetic, it can be expected that they are able to quench fluorescence in a similar way to Oxygen, through intersystem crossing (described in section 2.1.4.1). In this mechanism of quenching the excited fluorophore becomes a triplet state, which has a lower energy and is longer lived than the singlet state, making it more likely that return

to the ground state occurs through non-radiative decay. Nitroxide spin labels have also been observed to quench fluorescence through electron transfer (as described in section 2.1.4.1). In this mechanism electron transfer between the fluorophore and the quencher results in the quencher remaining in the excited state, and as no direct transition occurs from the excited state to the ground state of the fluorophore, quenching occurs.

2.2 Methods

2.2.1 Preparation of Rod Outer Segment Membranes

Bovine eyes were obtained from either W.L. Lawson Company (USA) or Teterow slaughter house, Germany, and retina were mechanically extracted and stored in 40% sucrose solution at -80°C. Rod outer segment membranes (ROS) were then separated from the rest of the cells using a sucrose gradient, using a protocol previously described in Sommer et al 2012 and was carried out under dim red light conditions. 100 retina were thawed and shaken for 4 minutes in 45% (weight to volume) sucrose solution in ROS buffer (70mM potassium phosphate, 1mM $MgCl_2$, 0.1mM EDTA, 1mM DTT, 0.5mM PMSF, pH 7), and centrifuged in a fixed angle rotor for 5 minutes at 2500g. The supernatant was filtered through gauze and diluted 1:1 with ROS buffer, slowly so as to avoid osmotic shock, and then centrifuged for 7 minutes at 6000g. Three sucrose solutions in ROS buffer were prepared and the density tested using a hydrometer: 25.5% (1.105g/ml), 27.125% (1.115g/ml), 32.25% (1.135g/ml). The pellets were suspended in 25.5% sucrose solution, and then layered on top of four gradients consisting of 27.125% sucrose solution underlaid with 32.25% sucrose solution. The gradients were centrifuged using a swinging bucket rotor, with slow start and stop settings, at 83,000g for 30 minutes. ROS membranes were then collected from the sucrose gradient interface using a syringe fitted with an 18ga needle. The ROS membranes were then diluted 1:1 in ROS buffer, mixed and centrifuged for 30 minutes at 48000g. The pellets were then resuspended in ROS buffer and stored at -80°C.

2.2.2 Phosphorylation of Rhodopsin

ROS membranes were phosphorylated under illuminated conditions, using the native rhodopsin kinase present in the membranes. First, the ROS membranes were homogenized using a 50mL glass douncer, in 100mM potassium phosphate buffer, pH 7.4. 8mM ATP and 2mM $MgCl_2$ were added, and the tubes were placed on a rocking platform and illuminated using a standard desk lamp. After 2 hours 50mM hydroxylamine was added, and incubated at room temperature for 10 minutes to convert all light-activated rhodopsin to opsin. Membranes were washed four times in 100mM potassium phosphate buffer pH7.4, followed by one wash in 50mM Hepes buffer pH7. Washing

involved centrifugation for 30 minutes at 48000g, followed by resuspension of the pellets in buffer and homogenization in the douncer. After the final wash pellets were resuspended in 50mM Hepes buffer, pH7, and aliquoted into small fractions and snap frozen in liquid nitrogen, for storage at -80°C.

2.2.3 Regeneration of Opsin to Rhodopsin

Regeneration of the washed phosphorylated opsin (OpsP) to rhodopsin (RhP) was achieved by incubating with a 3-fold molar excess of 11-*cis*-retinal for one hour. The reaction was terminated by the addition of 20mM *o-tert-butyl*-Hydroxylamine. The concentration of rhodopsin was determined by measuring the difference in absorbance at 500nm (extinction coefficient 0.0408 $\mu M^{-1}cm^{-1}$) after photo-bleaching, in the presence of 100mM hydroxylamine. Photo-bleaching was carried out in the presence of >495nm filter for 15s. The loss in absorbance at 500nm corresponds to the change in absorbance of the ligand as it isomerises from 11-*cis*-retinal (λmax 500nm) to all-*trans*-retinal (λmax 380nm).

2.2.4 Extra-Meta-II assay

This assay quantifies the fraction of receptors significantly phosphorylated (2-3 phosphates) (Gurevich and Benovic 1993, Gurevich and Benovic 1995, Mendez, Burns et al. 2000) to allow for arrestin binding, and is described in (Parkes and Liebman 1984). Arrestin binding is monitored through its ability to stabilize the active Meta-II receptor species. The assay is carried out in conditions which favour Meta-I (2°C, 50mM Hepes buffer pH 8). Formation of Meta-II (λmax 380nm) from Meta-I (λmax 480nm) after photo-bleaching with a short flash (>495nm) can be determined through following the increase in absorbance at 380nm. The amount of Meta-II stabilized in the presence of arrestin is compared to the amount stabilized in the presence of a high-affinity transducin peptide which binds the receptor in a phosphorylation independent manner. ROS membranes containing rhodopsin to which >95% was bound by arrestin were used for further experiments.

2.2.5 Preparation of arrestin mutants

Arrestin mutants were created using a recombinant bovine arrestin-1 construct lacking the native cysteine and tryptophan residues (C63A, C128S, C143A, W194F), which is cloned in the pET15b vector. Mutations were made by PCR, with primers ordered from Sigma Aldrich and sequenced by LGC genomics. The plasmid DNA was expressed in *Escherichia coli* XL1-Blue supercompetant cells (Stratagene 200518) and isolated with miniprep kits from ThermoFischer Scientific. *E.coli* BL21 (DE3) competent cells (New England BioLabs) were transformed with plasmid DNA and incubated overnight at 30° on ampicillin-containing medium. A single colony was selected and used to inoculate 5ml LB medium with ampicillin (100µg/ml), which was incubated for 8h at 28°C, with shaking. 1ml from this culture was used to inoculate 150ml LB medium with ampicillin. This culture was incubated overnight at 28°C in a shaking incubator, and then split between four flasks with 2L LB medium with ampicillin, and 30µM IPTG was added once the cell density reached an optical density of 0.6 at 600nm. This culture was incubated for 16h at 28°C, and then cells were harvested by centrifugation at 5000g for 15 minutes. The cells were lysed by resuspension in lysis buffer (10 mM Tris-HCl, 2 mM EDTA, 100 mM NaCl pH 7.5 + 5 mM DTT), and DNAse II was added, before microfluidising. The suspension was centrifuged for 30 minutes at 27000g, and the supernatant was mixed with ammonium sulphate (0.32g/ml) for protein precipitation. Centrifugation at 27000g for 30 minutes precipitated the protein and the pellet was resuspended in 10 mM Tris-HCl, 2 mM EDTA pH 7.0 + 5 mM DTT. A subsequent centrifugation step at 27000g for 30 minutes removed the insoluble protein, and the supernatant was filtered through a 0.8µm cellulose filter and loaded to 3 x 5ml HiTrap Heparin columns (GE healthcare), diluted 1:3 with 10 mM Tris-HCl, 2 mM EDTA, 100 mM NaCl pH 7 + 5 mM DTT. Arrestin was eluted by a NaCl gradient (0.1 – 0-5 M). Fractions containing arrestin were identified by SDS-PAGE, pooled, and loaded onto a 5 ml HiTrap SP column linked to a 5 ml HiTrap Q column, diluted 1:10 with 10 mM Tris-HCl, 2 mM EDTA pH 8.5 + 5 mM DTT buffer. Arrestin was eluted with a two-step NaCl gradient: 0 – 0.1 M and 0.1 M – 0.5 M NaCl. The arrestin-containing fractions were identified by SDS-PAGE and pooled. The pooled arrestin was concentrated and exchanged into 50mM Hepes, 130mM NaCl, pH7 using spin columns (Amicon-Ultra 0.5). The concentration was determined by absorbance at 280nm (Extinction coefficient of $0.02076 \mu M^{-1} cm^{-.1}$). Arrestin was then aliquoted, snap frozen, and stored at -80°C.

2.2.6 Labelling of arrestin mutants

Arrestin mutants were labelled with thiol-reactive fluorophores for site-directed fluorescence. The fluorophores used were monobromobimane or N,N'-Diemthyl-N-(Iodoacetyl)-N'-(7-Nitrobenz-2-Oxa-1,3-Diazol-4-yl)Ethylenediamine) (NBD). The fluorophores were dissolved in DMSO, and the concentration was determined by diluting an aliquot by 1:1000 in ethanol. Monobromobimane has a λmax at 380nm (extinction coefficient of $0.005\mu M^{-1}cm^{-1}$) and NBD has a λmax of 500nm (extinction coefficient of $0.025\mu M^{-1}cm^{-1}$).

Arrestin mutants were thawed and diluted to 50μM in 50mM Hepes, 130mM NaCl pH 7. Monobromobimane or NBD were added at a 50-fold molar excess, and the sample was gently shaken on a platform, in the dark, for 3h. The excess fluorophore was removed through washing three times using an Amicon-Ultra 0.5 spin column, with 50mM Hepes, 130mM NaCl, pH7, followed by size exclusion using G-15 sephadex in microcolumns (Sigma Aldrich).

Note on nomenclature: for each single cysteine arrestin mutant, labelling with bimane is denoted by B, and when labelled with NBD is denoted with NBD, for example the arrestin mutant I72C, when labelled with bimane becomes I72B and when labelled with NBD becomes I72NBD.

2.2.7 Preparation of ROS membranes enriched with spin labelled fatty acids

ROS membranes were enriched with the following fatty acids:

1. 2-(3-Carboxypropyl)-4,4-dimethyl-2-tridecyl-3-oxazolidinyloxy (5-doxyl-stearic acid) (Sigma-Aldrich)

2. Methyl palmitate (Sigma-Aldrich)

3. Stearic acid (Sigma-Aldrich)

4. 4-Palmitamido-2,2,6,6-tetramethylpiperidine-1-oxyl (N-tempoyl palmitamide) (Avanti polar lipids)

The fatty acids were dissolved in ethanol to a stock concentration of 10mM. Membranes containing phosphorylated rhodopsin (RhP) were diluted to a concentration of 5μM in 2ml 50mM Hepes, pH 7. Fatty acids were added gradually to the membranes at 30°C, with a volume of 2μl every 2 minutes, to a final fatty acid concentration of 250μM, followed by incubation for 1h at 30°C whilst gently shaking, adapted from the protocol

by (Watts, Volotovski et al. 1979). This method allows for incorporation of fatty acids into the membrane, without forming micelles. As a control the same volume of ethanol was also added to ROS membranes.

2.2.8 Centrifugal Pull-down Analysis

This assay measures arrestin binding to ROS membranes, using centrifugal force to pellet the membranes, along with any associated arrestin.

Determination of arrestin binding to ROS membranes enriched with spin-labelled fatty acids

In order to determine that all monobromobimane-labelled arrestin was bound to the receptor in the fluorescence quenching assays with ROS membranes enriched with spin-labelled fatty acids, samples were prepared with the concentrations used in the fluorescence measurements (1μM arrestin + 4μM ROS membranes) enriched with each of the fatty acids, under dim red light. Samples measuring binding to the active receptor were photo-bleached (>495nm) for 15s. Samples were centrifuged for 10 minutes at 16000g. The supernatant was removed, and the pellets resuspended in loading buffer containing 2% SDS, and SDS-PAGE was carried out. Gels were stained with Coomassie Brilliant Blue.

Centrifugal pull-down assay titrations

Titrations determining the amount of arrestin bound at varying concentrations of the receptor or arrestin were also carried out. These titrations used arrestin labelled with NBD for analysis by UV-VIS spectrometry.

Both receptor and arrestin titrations were carried out, with final concentrations of 0, 0.5, 1, 2, 4, 6, 10 and 12μM, against a final concentration of 4μM arrestin or receptor, respectively. All samples were prepared under dim red light, and those samples monitoring binding to the light-activated receptor, were photo-bleached (>495) for 15s. Samples were centrifuged for 10 minutes at 16000g. The supernatant was carefully removed and a UV-VIS absorbance spectrum was taken. The NBD signal (λmax 500nm, extinction coefficient of $0.025\mu M^{-1}cm^{-1}$) was recorded. The concentration of NBD-labelled arrestin in the supernatant was subtracted from the total concentration of NBD-labelled arrestin in the sample to provide the concentration of arrestin pulled down by the ROS membranes.

Analysis of centrifugal pull-down titrations

Titration results were analysed using Sigmaplot graph fitting software.
Graphs were produced with the concentration of the variable (titrator) on the x axis, against the concentration of arrestin pulled down on the y axis.

Mathematical analysis of centrifugal pull down titration curves

The data were fit to a curve derived from the definition of the dissociation constant (Kd):

$$Kd = \frac{[A][R]}{[AR]}$$

The total amount of arrestin (A_{tot}) and receptor (R_{tot}) are given by:

$A_{tot} = [A] + [AR]$ and $R_{tot} = [R] + [AR]$

Fitting these equations into the Kd equation, and rearranging gives the equation:

$$[AR] = k.\frac{(p-\sqrt{(p^2-4q)})}{2}$$

Where $p = Kd + [A_{tot}] + [R_{tot}]$, $q = [A_{tot}].[R_{tot}]$ and k = scalar factor to scale the experimental data to concentration units.

For each graph the Kd and stoichiometry were obtained from the fit.
For arrestin titrations the independent variable was $[A_{tot}]$, with the Kd and $[R_{tot}]$ being dependent variables. The dependent $[R_{tot}]$ was indicative of the concentration of arrestin bound, and therefore of the final binding stoichiometry.
For receptor titrations the independent variable was $[R_{tot}]$, with the Kd and $[A_{tot}]$ being the dependent variable. In this case, the concentration $[A_{tot}]$ was indicative of the concentration of arrestin bound, and therefore of the final binding stoichiometry.

2.2.9 Steady-state fluorescence

Steady-state fluorescence was measured on a SPEX Fluorolog 1680 instrument in front face mode. Excitation slits were set at 0.3mm to minimize bleaching of rhodopsin, and emission slits were set at 4mm. For monobromobimane-labelled arrestin mutants excitation was at 400nm and emission was measured from 420nm – 600nm, (2nm step size, 0.5s integration per point). For NBD-labelled arrestin mutants excitation was at 500nm and emission was measured from 520nm – 700nm (2nm step size, 0.5s integration per point). For measurements with light-activated rhodopsin, samples were illuminated for 10s with 150W fibre optic light source (>495nm)

Analysis of steady-state fluorescence data

Sigmaplot graph fitting software was used to analyse the data. Background fluorescence was subtracted, and graphs were plotted of fluorescence count (cps) against wavelength. For analysis of titration experiments the integrated fluorescence of each of the curves was calculated, and plotted against the concentration of the titrator.

Analysis of quenching efficiency of spin-labelled fatty acids

The integrated fluorescence of each mutant in the presence of the spin labelled fatty acid was compared to the integrated fluorescence of each mutant in the presence of the corresponding fatty acid lacking the spin-label: for N-tempoyl palmitamide this control was methyl palmitate and for 5-doxyl stearate this control was stearic acid.

2.2.10 Time-resolved fluorescence spectroscopy

Time-resolved fluorescence experiments were carried out using a Fluotime 300 spectrometer from Picoquant. The laser used was 375nm, pulsed diode laser, and emission was measured at 480nm. The intensity of fluorescence was measured, and a graph of the intensity decay (log I(t) against time (t) was produced, using the software FluoFit from Picoquant. The data collected was deconvoluted to a decay curve, using the instrument response function (IRF), which was determined with a solution of Ludox. The IRF is a deviation from a "perfect" system which would have an infinitely small excitation pulse-width, and infinitely accurate detectors and electronics. The lifetimes were fit using χ^2 analysis to determine the best fit. As each of the samples reported more than one lifetime, the calculated average amplitude weighted lifetime was used. The amplitude weighted lifetime value reports the lifetime a single fluorophore with the same steady-state intensity as the sample would have, and therefore is proportional to the steady-state fluorescence (Sillen and Engelborghs 1998). It is calculated with the formula:

amplitude weighted lifetime = $\sum \alpha_i \tau_i$

where α = fraction of fluorophores with each lifetime, τ.

Quantum yield calculation

Quantum yield, which is a measure of the number of photons emitted from a fluorophore as compared to the number absorbed, can be determined by comparing the fluorescence to a standard which fluoresces in a similar region to the molecule in question. The ratio

of the absorbance and fluorescence of the standard can then be compared to the molecule in question, as related by the equation:

$$\phi u \propto \phi s \left(\frac{AsFu}{AuFs}\right)$$

Where ϕ_u is the quantum yield of the unknown sample, ϕ_s is the quantum yield of the reference, A_s and A_u are the absorbance of the reference and unknown sample respectively, and F_u and F_s are the fluorescence intensities of the unknown sample and reference respectively.

In this work the quantum yields were determined by using quinine sulphate, which absorbs at 340nm, and has a quantum yield of 0.55 (Eaton 1988).

The time-resolved fluorescence measurements were carried out in low salt (50mM Hepes, pH 7) buffer. However, under these conditions there is some aggregation of arrestin, which leads to error due to scattering when measuring the absorbance of the sample. Therefore, the quantum yield of each of the mutants was initially measured in isotonic buffer (50mM Hepes, 130mM NaCl, pH 7). Salt titrations monitoring fluorescence intensity, then allowed for determination of the quantum yield of each of the mutants in low salt buffer by multiplying the quantum yield of the mutant in isotonic buffer by the observed fluorescence change. The quantum yield in the presence of 2.5mM IP6 was similarly determined by titration curves at different concentrations of IP6.

Calculation of quenching efficiency

Quenching was calculated by comparing the amplitude weighted lifetimes and the quantum yield of the fluorophore in the presence and absence of the quencher, tryptophan. The following equations were used to calculate quenching (Mansoor, Dewitt et al. 2010):

Equation 1 calculates the fraction of fluorophores present which are uncomplexed in the ground state, and are free to fluoresce. Fw corresponds to the quantum yield of the fluorophore in the presence of the quencher, and F0 is the quantum yield in the absence of the quencher. τ is the lifetime of the fluorophore, with τw with quencher and τ0 without the quencher.

1. $\gamma = \frac{Fw}{F0} \cdot \frac{\tau 0}{\tau w}$

Fluorophores which are statically quenched form a non-fluorescent complex in the ground state, and therefore the fraction of statically quenched fluorophores is given by **equation 2**:

2. $1 - \gamma$

The fraction of uncomplexed fluorophores calculated in equation 1 represent two populations: the fluorophores that are unquenched (γF), and the fluorophores that are dynamically quenched (γDQ). By using equation 1 therefore, the fraction of both of these populations can be calculated.
The fraction of fluorophores which emit light without being quenched is given by **equation 3**:

3. $\gamma F = \frac{\tau w}{\tau 0} . \gamma$

The fraction of fluorophores which are dynamically quenched, is then calculated by **equation 4**:

4. $\gamma DQ = (1 - \frac{\tau w}{\tau 0}) . \gamma$

3. Results

3.1 The C-edge of arrestin functions as a membrane anchor

3.1.1 Introduction

The initial proposal that the C-domain could interact with the membrane came from experiments which monitored fluorescence changes on the finger loop and the 344-loop of arrestin, when bound to different functional forms of rhodopsin (Sommer, Hofmann et al. 2012). The fluorescence of a monobromobimane fluorophore attached at site 72 (I72B) on the finger loop was directly proportional to the amount of arrestin bound to the light-activated phosphorylated receptor (Rh*P), but showed a minimal fluorescence change when bound to OpsP, even though pull-down experiments showed comparable binding to both forms of the receptor. Conversely the fluorescence of the monobromobimane fluorophore attached to site 344 (S344B) on the C-edge, was directly proportional to the amount of arrestin bound, in both the presence and absence of the ligand. The pull down analysis for both mutants indicated a binding stoichiometry of one arrestin to 1.4 Rh*P, suggesting a mixture of one-to-one and one-to-two stoichiometries. The authors therefore proposed a model to explain arrestin binding to either one or two receptors. In the case of a one-to-two stoichiometry the finger loop was proposed to insert into the active binding crevice of Rh*P, with the 344-loop contacting a neighbouring receptor. In the case of a one-to-one stoichiometry, the finger loop engages Rh*P with the 344-loop inserting into the membrane (see figure 3.1.1).

Figure 3.1.1 Model showing the interaction of arrestin with light-activated rhodopsin (Meta-II) in a one-to-one and a one-to-two stoichiometry.
The finger loop is highlighted in magenta and the 344-loop in orange. Figure taken from Sommer, Hofmann and Heck (2014) Handbook Exp Pharma

Further support for the idea that the C-domain of arrestin could interact with the membrane arose from the crystal structure of the Ops*/arrestin-1 complex (Kang, Zhou

et al. 2015). The crystal structure obtained was of constitutively active mutant human rhodopsin in complex with constitutively active mouse arrestin-1, fused via a 15 residue linker. The structure shows an asymmetric orientation of arrestin in complex with rhodopsin. The N-domain interacts extensively with the active receptor, and the finger loop is buried within the active receptor crevice. Due to the interdomain rotation present in the active arrestin, the C-domain is tilted, and the authors speculated that in this orientation interaction with the membrane is possible. As there was no membrane present in the crystal structure, this could not be confirmed. However, the C-edge of arrestin contains a patch of highly conserved hydrophobic residues (L342, L339, F197, F198), and mutation of these sites to alanine has been found to decrease binding of arrestin to Rh*P (Ostermaier, Peterhans et al. 2014). Given the large distance of these residues to the receptor binding site, it is possible that the membrane serves as an additional binding site in the arrestin-receptor complex.

In this section, experiments are presented to probe the role of the arrestin C-edge in membrane interaction. The approach was based on the quenching of fluorophores attached to specific sites on arrestin by spin-labels present in the membrane. Proximity of different sites on arrestin to the membrane were measured for both the dark-state pre-complex with phosphorylated rhodopsin (RhP), and for the high-affinity complex with light-activated phosphorylated Meta II (Rh*P). Fluorescence data was compared to molecular dynamics simulations, which were performed by Dr Jana Selent (University Pompeu Fabra, Barcelona). These results have been published in: Lally CCM, Bauer B, Selent J, Sommer ME. (2017) *C-edge Loops of Arrestin Function as a Membrane Anchor* Nature Communications **8:**14258.

Fluorophore-labelling of arrestin mutants

Arrestin was labelled with the fluorophore monobromobimane, at 16 different sites which had been individually mutated to cysteine in an arrestin construct lacking native cysteines (see methods 2.2.6) (figure 3.1.2).

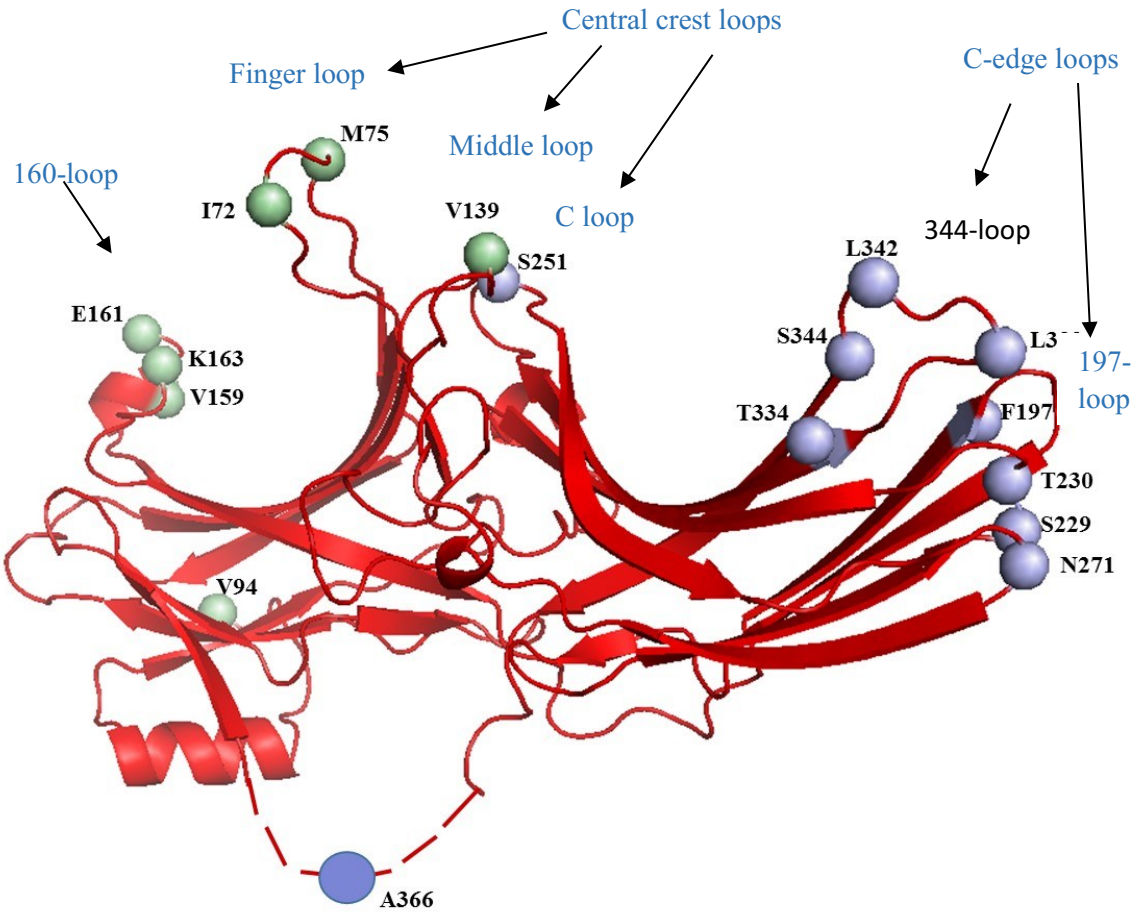

Figure 3.1.2 Sites on arrestin-1 labelled with monobromobimane

Arrestin 1CF1, chain A, The Cα of each of the sites on arrestin that were labelled with monobromobimane are shown as spheres. Green spheres show the Cα of residues in the N-domain, and blue spheres in the C-domain.

Enrichment of ROS membranes with spin-labelled fatty acids

The proximity of each labelled site to the membrane was probed by enriching native ROS membranes containing phosphorylated rhodopsin with spin-labelled fatty acids. Fatty acids insert spontaneously into the membrane, and spin labels are known to quench monobromobimane fluorescence when in collisional distance ((Lakowicz 2010), although this is a new approach for investigating arrestin binding. Different spin-labelled fatty acids were employed, which contain the spin label at varying positions on the acyl chain, in order to assess proximity of each site on arrestin to different areas of the membrane. 4-palmitamido-TEMPO reports proximity to the membrane surface (phospholipid head-group region), 5-doxyl-stearic acid reports insertion into the hydrophobic region of the membrane (near carbon 5 on the acyl chain), and 10-doxyl-nonodecane reports deep insertion into the membrane (near carbon 10 on the acyl chain).

Initial experiments with ROS membranes enriched with 10-nonodecane showed no quenching, indicating that no sites on arrestin inserted this deep into the membrane. Further experiments focussed on 4-palmitamide TEMPO (N-tempoyl palmitamide) and 5-doxyl stearic acid, which induced significant quenching for many bimane-labelled arrestin mutants. Quenching efficiency was calculated by comparing the fluorescence signal of arrestin in the presence of ROS membranes enriched with spin-labelled fatty acids with ROS membranes enriched with the corresponding fatty acids containing no spin label. For N-tempoyl palmitamide this control fatty acid was methyl palmitate, and for 5-doxyl stearic acid this control was stearic acid (see table 3.1.1). Control membranes which contained no fatty acid were also employed. In this case, ethanol was added at an equal volume to make them comparable to fatty acid-enriched membranes.

Table 3.1.1 Structures of spin-labelled fatty acids and control fatty acids containing no spin label

Spin Labelled Fatty Acids (SLFAs)		
Name	**Structure**	**Range of quenching**
4-palmitamido-TEMPO (N-tempoyl palmitamide)	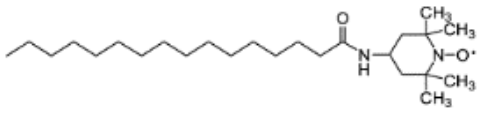	Membrane surface
5-Doxyl-Stearic acid	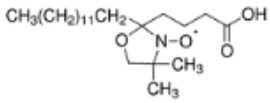	Hydrophobic portion, around carbon-5 on the acyl chain)
10-Doxyl Nonodecane	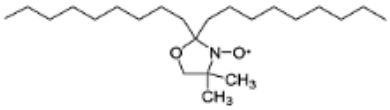	Hydrophobic portion, around carbon-10 on the acyl chain
Methyl palmitate	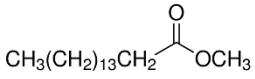	Control fatty acid, no spin label present
Stearic acid	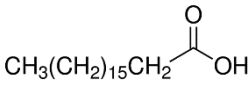	Control fatty acid, no spin label present

3.1.2 Quenching of fluorescently-labelled arrestin by spin-label fatty acids

Measurements were carried out to monitor arrestin interaction with dark-state phosphorylated rhodopsin (RhP) in the pre-complex, as well as after photo-activation with active phosphorylated rhodopsin (Rh*P) in the high-affinity complex. Therefore, for each arrestin mutant, a total of 11 measurements were performed for each data set:

1. Unbound arrestin

Arrestin + RhP (before photo-activation)

2. ROS membranes + ethanol (no fatty acid present)
3. ROS membranes + methyl palmitate
4. ROS membranes + N-tempoyl palmitamide
5. ROS membranes + stearic acid
6. ROS membranes + 5-doxyl stearic acid

Arrestin + Rh*P (after photo-activation)

7. ROS membranes + ethanol (no fatty acid present)
8. ROS membranes + methyl palmitate
9. ROS membranes + N tempoyl palmitamide
10. ROS membranes + stearic acid
11. ROS membranes + 5-doxyl stearic acid

Experimental conditions were chosen such that the amount of arrestin bound to dark state rhodopsin (pre-complex binding) was comparable to light-activated rhodopsin (high-affinity binding). Pre-complex binding is a primarily electrostatic interaction, where arrestin binds to the phosphorylated receptor C-terminus. ROS membranes were prepared to yield high levels of rhodopsin phosphorylation (see methods section 2.2.2 and 2.2.4), and all of the receptors were confirmed to be sufficiently phosphorylated for arrestin binding. By reducing the salt concentration at which the experiments were carried out, electrostatic binding of arrestin to dark-state rhodopsin was maximised. The affinity, as determined by the dissociation constant (Kd), of arrestin to Rh*P has been calculated to be in the nanomolar range (Pulvermüller, Maretzki et al. 1997, Bayburt, Vishnivetskiy et al. 2011), compared to just 80μM for arrestin binding to RhP in the presence of 100mM NaCl (Zhuang, Chen et al. 2013). However, the Kd of arrestin binding to highly phosphorylated RhP in buffer with minimal salt has been reported to be 1μM (Sommer,

Hofmann et al. 2012). Therefore, by using an excess of receptor and minimal salt in the fluorescence experiments, comparable levels of arrestin binding to dark-state RhP and light-activated Rh*P were obtained (See supplementary figure 3.1.1, at the end of the chapter). Importantly, this allowed for direct comparison between quenching efficiencies between the pre-complex and the high-affinity complex, as there was minimal background signal from unbound arrestin.

Example spectra for some of the mutants are presented in figure 3.1.3, and the calculated quenching efficiencies for all replicates, along with any wavelength shifts observed are presented in supplementary table 3.1.1 (presented at the end of the chapter).

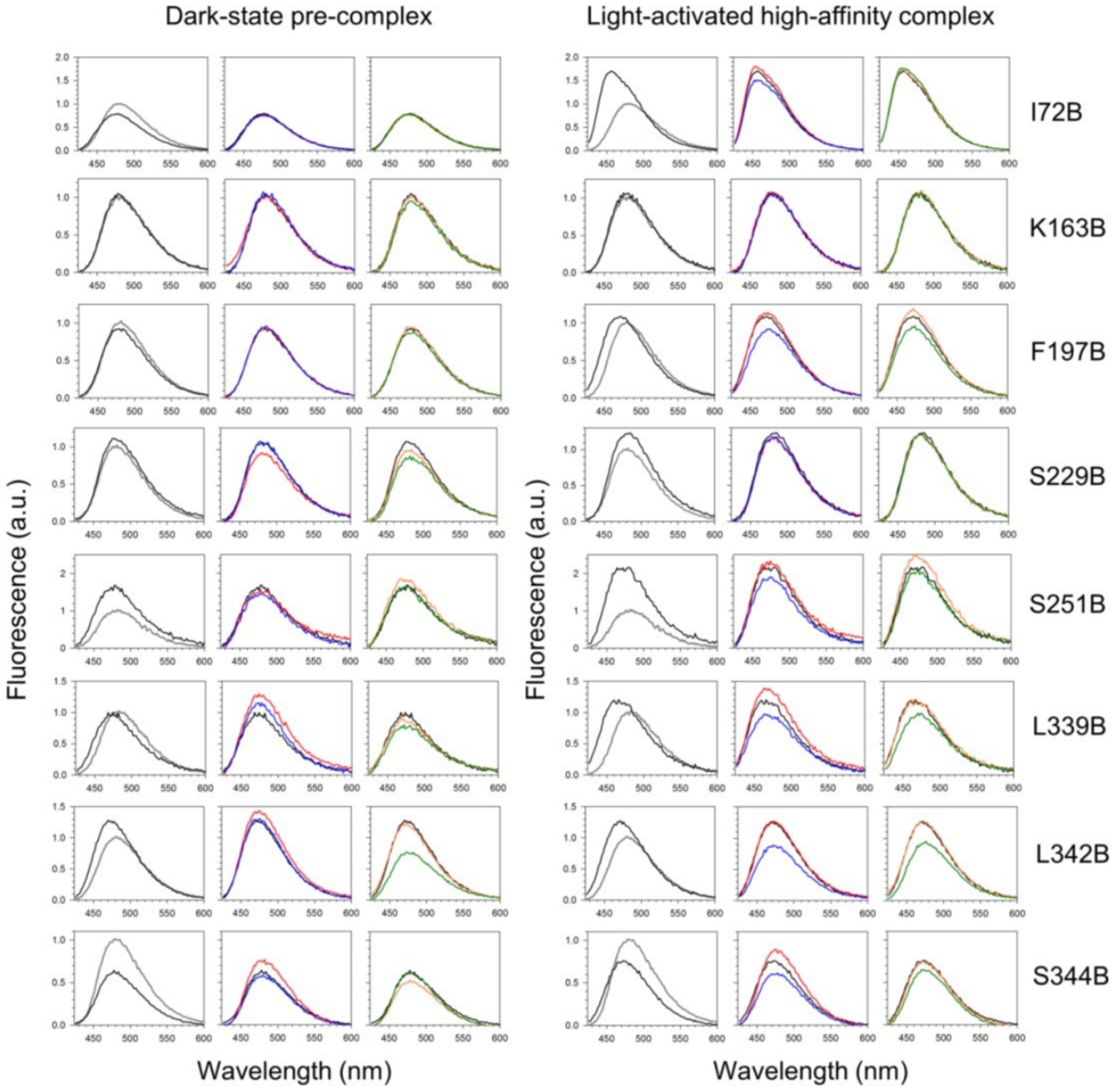

Figure 3.1.3 Example fluorescence spectra for bimane-labelled arrestin mutants with enriched ROS membranes ***grey*** *= arrestin only,* ***black*** *= arrestin + ROS membranes containing RhP (left) or Rh*P (right).* ***Blue*** *= arrestin + ROS membranes enriched with N-tempoyl palmitamide,* ***red*** *= arrestin + ROS membranes enriched with methyl palmitate,* ***green*** *=*

arrestin + ROS membranes enriched with 5-doxyl stearic acid, ***orange*** *= arrestin + ROS membranes enriched with stearic acid. Spectra are normalised such that the fluorescence intensity of unbound arrestin is 1.* Figure taken from Lally CCM, Bauer B, Selent J, Sommer ME. (2017) *C-edge Loops of Arrestin Function as a Membrane Anchor* Nature Communications **8:**14258.

The observed quenching efficiencies are shown in figure 3.1.4. The Cα of each site to which the bimane fluorophore was attached is represented as a sphere, whose colour corresponds to the quenching efficiency.

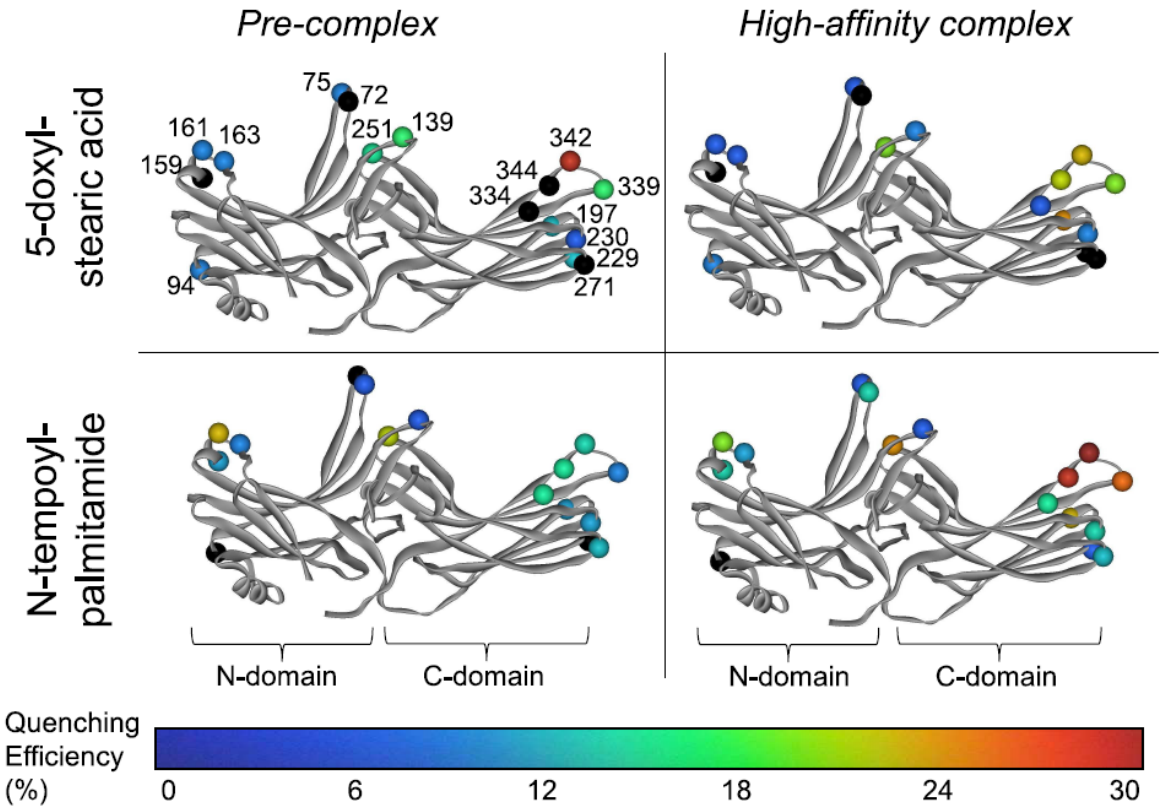

Figure 3.1.4 Colour map depicting quenching efficiencies of different sites on arrestin

All mutants tested are shown on the structure of arrestin (PDB 1CF1, α chain), as spheres at the Cα residue of the amino acid to which a monobromobimane label was attached. The amount of quenching observed by ***top:*** *5-doxyl stearic acid and* ***bottom:*** *N-tempoyl palmitamide is depicted using the colour map: blue signifies no quenching, and red signifies quenching up to 30%. Black spheres signify negative quenching (see main text).*
Figure taken from Lally CCM, Bauer B, Selent J, Sommer ME. (2017) *C-edge Loops of Arrestin Function as a Membrane Anchor* Nature Communications **8:**14258

C-edge loops of arrestin function as membrane anchor

Most of the quenching observed is localised to the C-edge loops of arrestin. Interestingly, the pattern of quenching differs between the pre-complex and the high-affinity complex, indicating that association of the C-edge with the membrane changes orientation

depending on the activation state of the receptor (see figure 3.1.4, and supplementary table 3.1.1).

In the pre-complex the fluorophores at sites L342 and L339 were accessible to 5-doxyl stearic acid, (quenching efficiency of 30% and 15% respectively), suggesting insertion into the hydrocarbon core of the membrane. The fluorophore at site L342 was also quenched to a lesser degree by N-tempoyl palmitamide (11%) suggesting that it is positioned somewhere between the two spin labels. The other sites on the 344-loop: 344 and 334 were quenched by the N-tempoyl palmitamide only (17% and 13% respectively), suggesting that they are making contact with the phospholipid head-group region of the membrane. None of the other loops on the C-edge were observed to contact the membrane in the pre-complex.

Upon light-activation a change in orientation of the C-edge with respect to the membrane was observed. Monobromobimane fluorophores at sites 342, 339 and 344 all became accessible to quenching by both the N-tempoyl palmitamide (quenching efficiency of 31%, 27%, 30% respectively) and 5-doxyl stearic acid (22%, 18%, 19% respectively), implying that they are located just inside the membrane interior. The sites 342 and 339 are located closer to the membrane surface in the high-affinity complex as compared to the pre-complex, whereas site 344 moves further into the interior. Additionally site 197 was quenched in the high-affinity complex, by both N-tempoyl palmitamide (23%) and 5-doxyl stearic acid (23%), placing it just inside the hydrophobic portion of the membrane.

In addition to the observed decrease in fluorescence intensity due to quenching, some of the mutants displayed a wavelength shift when bound to the ROS membranes, in particular at sites 72, 197, 339, 342 and 344. Wavelength shifts are associated with movement of the fluorophore into a more hydrophobic environment (see section 2.1 for more details). For the sites on the C-edge of arrestin, these wavelength shifts correspond to quenching by 5-doxyl stearic acid, indicating insertion in the hydrophobic portion of the membrane. For site 72 on the finger loop, however, the wavelength shift most likely corresponds to insertion into the hydrophobic binding pocket of the receptor. Indeed, an EPR study that measured the mobility of spin labels attached to arrestin (Hanson, Francis et al. 2006) supports this finding. The spin label at site 72 had a lower mobility when bound to RhP in the pre-complex as compared to the unbound state, and was almost completely immobilised in the high-affinity complex. In contrast, the spin label at site

344 had a lower mobility when bound to RhP in the pre-complex, and no further change in mobility was observed upon light-induced transition to the high-affinity complex. These results are consistent with site 344 being embedded in the fluid ROS membrane, whereas the loss of mobility observed at site 72 is consistent with binding to the receptor crevice.

Some negative values were determined for quenching with 5-doxyl stearic acid, particularly at sites 271 and 159, and in the pre-complex at sites 344 and 334, resulting from a higher fluorescence intensity in the presence of 5-doxyl stearic acid as compared to stearic acid. A possible explanation for this could be due to the carboxyl head group of stearic acid, located in the polar region of the membrane. Carboxyl groups are known to quench fluorescence, and negative quenching could arise from unequal abilities of the carboxyl group of 5-doxyl stearic acid and stearic acid to quench bimane fluorescence. Notably, all sites which displayed negative quenching by 5-doxyl stearic acid were quenched by N-tempoyl palmitamide, for which the spin label is located at the membrane surface. This correlation suggests close proximity of these sites to the carboxyl group.

Association of the central crest loops and 160-loop with the membrane

Some residues on the N-domain of arrestin also display quenching, particularly in the finger loop, which binds in the crevice of the active receptor and the middle loop, which undergoes a movement upon activation of arrestin (see Introduction section 1.3.3). In the high-affinity complex, quenching by N-tempoyl-palmitamide is observed for site 72. From the crystal structure of the ops*/arrestin-1 complex (Kang, Zhou et al. 2015), this residue is located at the base of the finger loop, and therefore is likely to be close to the membrane when the finger loop is bound to the receptor. Site 75, which is located at the tip of the finger loop, and according to available crystal structures is buried deep within the receptor crevice (Szczepek, Beyriere et al. 2014, Kang, Zhou et al. 2015) displays no quenching from N-tempoyl-palmitamide. Sites 139 and 251 on the middle loop and C loop respectively, show interesting quenching patterns. Site 251 is quenched by N-tempoyl palmitamide in both the pre-complex (20%) and the high-affinity complex (23%). In the crystal structure this loop is seen to be near to the membrane surface, close to the cytoplasmic end of transmembrane 3. However, the site also displays quenching by 5-doxyl stearic acid in the pre-complex and high-affinity complex (12% and 18% respectively). Similarly the site 139 is also quenched by 5-doxyl stearic acid in the pre-complex (14%). This result is surprising, as in the crystal structure these sites are located

far from the membrane interior, and neither site displays the wavelength shifts indicative of localization in a hydrophobic environment. The observed quenching by 5-doxyl stearic acid, therefore, is not easily explained. However, it is possible that these loops may lie in a different orientation to that observed in the crystal structure, or that the observed quenching is due to the presence of the negatively charged carboxyl head-group of 5-doxyl stearic acid.

In the ops*/arrestin-1 fusion complex crystal structure (Kang, Zhou et al. 2015), the 160-loop on the arrestin N-domain interacts with the cytoplasmic end of TM6 of the receptor, and this orientation places the 160-loop far from the membrane surface (>15Å). This observation is consistent with biochemical studies employing Tryptophan-induced fluorescence quenching (TrIQ) (Sinha, Jones Brunette et al. 2014) which found that the 160-loop of arrestin-1 came into contact with TM6 of opsin. However, quenching was observed by N-tempoyl palmitamide at site 161 in both the pre-complex and high-affinity complex (21% and 19%, respectively) as well as to a lesser extent at site 159 in the pre-complex and high-affinity complex (5% and 9%, respectively). The fluorophore at site 159 also displayed negative quenching in the presence of 5-doxyl stearic acid, indicating association with the membrane. Electron microscopy (EM) studies of arrestin-2 bound to a GPCR indicated binding modes where the finger loop of arrestin does not engage the receptor helical core (Shukla, Westfield et al. 2014, Thomsen, Plouffe et al. 2016). Although the visualized complexes are at low resolution, they suggest an interaction of the N-domain of arrestin with the receptor, which would place the 160-loop close to the membrane surface. This, along with the quenching data, suggest that these loops can be highly flexible, and adopt orientations bringing them into contact with the membrane surface.

No interaction is observed between arrestin and the membrane in the absence of phosphorylated receptor

In order to determine if the interaction of the C-edge of arrestin with the membrane was dependent on activation of arrestin by receptor attached phosphates, fluorescence quenching experiments were also carried out with ROS membranes containing non-phosphorylated rhodopsin (see figure 3.1.5).

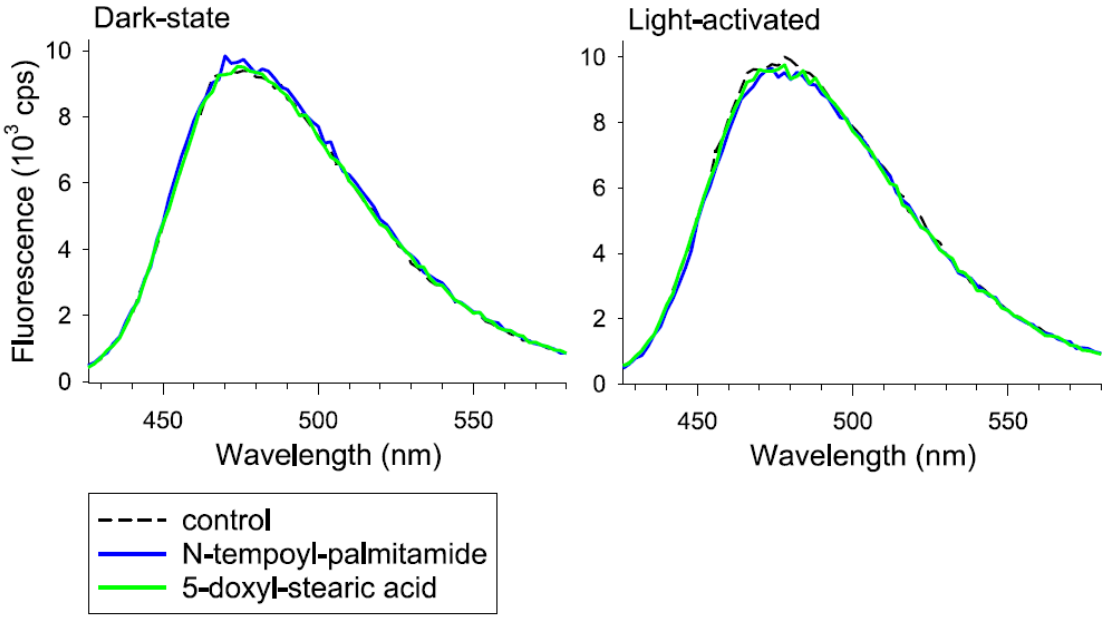

Figure 3.1.5 Fluorescence spectra of arrestin S344B (1 µM) and fatty-acid enriched ROS membranes containing non-phosphorylated rhodopsin (20 µM)

black = arrestin + ROS membranes, blue = arrestin + ROS membranes enriched with tempo palmitate, green = arrestin + ROS membranes enriched with doxyl stearate Figure taken from Lally CCM, Bauer B, Selent J, Sommer ME. (2017) *C-edge Loops of Arrestin Function as a Membrane Anchor* Nature Communications **8:**14258

Arrestin mutant S344B in the presence of a large excess of fatty acid enriched ROS membranes containing non-phosphorylated rhodopsin, showed no quenching by N-tempoyl palmitamide nor 5-doxyl stearic acid, in either dark-state conditions, or after photo-activation. This result indicates that the C-edge of arrestin does not spontaneously insert into the membrane, and that the membrane anchor acts as a functional binding element that is activated only when arrestin is bound to phosphorylated receptor in either the pre-complex or the high-affinity complex.

3.1.3 Molecular dynamics simulations

Fluorescence quenching experiments were complemented by molecular dynamics simulations, which were performed by Dr Jana Selent (University Pompeu Fabra, Barcelona). In these simulations, the isolated C-domain of arrestin was simulated with a lipid bilayer fragment composed of 1-stearoyl-2-docosahexaenoyl-sn-glycero-3-

phosphocholine (SDPC). This approach reduced the system size so that longer simulations could be carried out.

Unbiased simulations with the C-domain of basal arrestin (pdb 1CF1, α-conformer) found no interaction of arrestin with the membrane, and upon application of an energetic bias a deformation of the membrane was observed. In this conformation, the polar residues on the C-edge of arrestin (S344 and E341) were exposed, whereas the hydrophobic residues (L342 and L339) were buried within the β-sheets of the C-domain. Therefore, the repulsion between the C-edge and the membrane restricted membrane insertion. This finding correlates well with the fluorescence data which showed no membrane association of arrestin in the presence of ROS membranes containing non-phosphorylated rhodopsin.

However, during one simulation, there was a spontaneous rearrangement of the 344-loop, to a conformation similar to that observed in the crystal structure of p44 (Kim, Hofmann et al. 2013). p44 is a pre-active splice variant of arrestin-1, lacking the regulatory C-tail, and is able to bind non-phosphorylated (Rh*) with a micromolar affinity (as determined by the Kd) as well as phosphorylated receptor, regardless of activation state, with high affinity (Schröder, Pulvermüller et al. 2002) (See Introduction section 1.3.2). In p44, the hydrophobic residues on the 344-loop (L342 and L339) are exposed. Therefore, further simulations were carried out using the C-domain of p44 (PDB: 4J2Q, chain B), and in this conformation membrane insertion occurred in 1 simulation out of 10, which is a statistically significant result.

3.1.4 Comparison of fluorescence quenching data with molecular dynamics data

Comparison of fluorescence quenching data with the molecular dynamics simulations showed that the orientation and conformation of the C-edge loops in the simulation most resembled the quenching experiments for the light-activated, high-affinity complex (see figure 3.1.6). In the molecular dynamics simulations, the hydrophobic residues L338, L339, L342, as well as F197 and M198, were embedded in the membrane, and polar residues including S344, S336 and E341 made transient contacts with the phospholipid layer of the membrane. In order to better compare the molecular dynamics and fluorescence data, the distance of the Cα of selected residues to either the phosphate layer of the membrane, or the carbon at position 5 on the acyl chain (C5), were calculated from the simulation. These distances approximate the position of N-tempoyl palmitamide and

5-doxyl stearic acid respectively. Overall the quenching efficiencies and simulated distances are very similar to each other. However, some differences are observed. In particular site 344 is predicted to be further away from both the phosphate layer and from C5 in the simulation data as compared to fluorescence quenching experiments. These differences can be explained by the fact that molecular dynamics data are derived from the isolated C-domain simulated in the absence of receptor, which allows more freedom of movement as compared to full-length arrestin in complex with the receptor. Furthermore, simulation-derived distances were calculated from the Cα of each residue, whereas fluorescence data was derived from a monobromobimane fluorophore attached to a cysteine residue many angstroms away from Cα. However, even with these limitations there is a strong correlation between the simulations and the fluorescence quenching profile derived for the high-affinity complex.

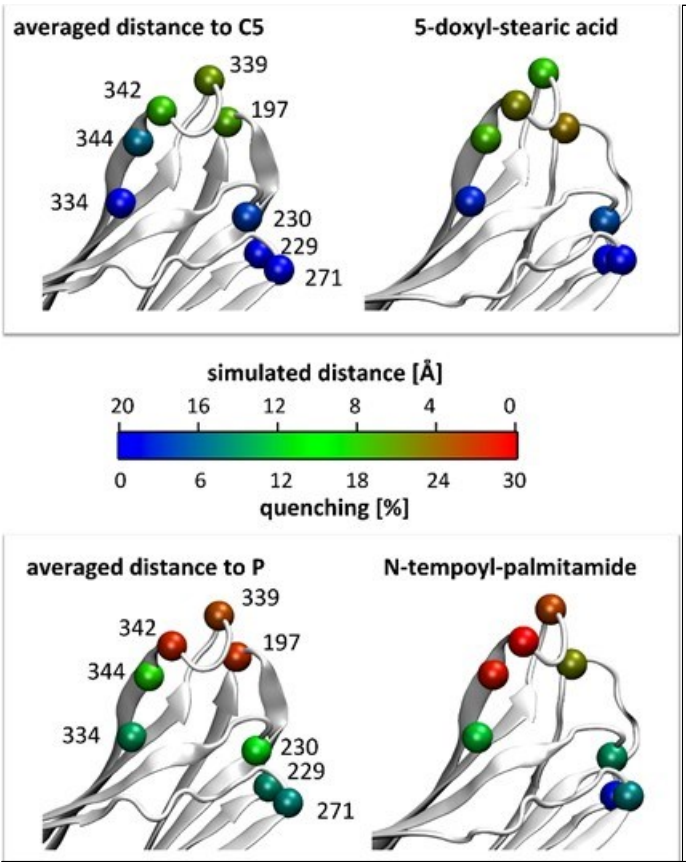

Figure 3.1.6 Comparison of fluorescence data with molecular dynamics simulations

Left: *Cα atoms of residues on arrestin are shown as spheres, coloured according to distance (0-20 Å) from Carbon-5 on the acyl chain (approximate position of the 5-doxyl stearic acid spin-label), and to the phosphate head-group layer of the membrane (approximate distance of the N-tempoyl palmitamide head-group).*
Right: *Cα atoms of residues on arrestin labelled with monobromobimane are shown as spheres, coloured according to quenching efficiency (0–30 %) by 5-doxyl stearic acid and N-tempoyl palmitamide, when bound in the high-affinity complex to Rh*P.*

Figure prepared by Jana Selent, Pompeu Universiry, Barcelona, and taken from Lally CCM, Bauer B, Selent J, Sommer ME. (2017) *C-edge Loops of Arrestin Function as a Membrane Anchor* Nature Communications **8:**14258

3.1.5 Comparison of the molecular dynamics and fluorescence quenching data with the ops*/arrestin-1 fusion complex

One frame from the simulation was selected based on the best fit to the arrestin C-domain and hypothetical membrane plane (which was determined using computational methods) of the ops*/arrestin-1 fusion complex (Kang, Zhou et al. 2015). An overlay of the selected frame and the crystal structure is shown in Fig. 3.1.7. As the 344-loop was unresolved in the crystal structure, this overlay effectively fills in structural details missing in the structure. This overlaid model shows that in this orientation residues L342, L339, S344 and F197 could all make contact with the phosphate layer of the membrane, which fits well with the fluorescence quenching efficiencies by N-tempoyl palmitamide obtained after light-activation, of 31%, 27%, 30% and 23% respectively. These residues were also located in close proximity to the C5 atom, which correlates well with quenching by 5-doxyl stearic acid after light-activation by 22%, 18%, 19% and 23% respectively. This comparison indicates that the Ops*/arrestin-1 fusion complex crystal structure most likely resembles the high-affinity complex, and that the C-edge loops of arrestin adopt a conformation similar to that seen in the p44 structure.

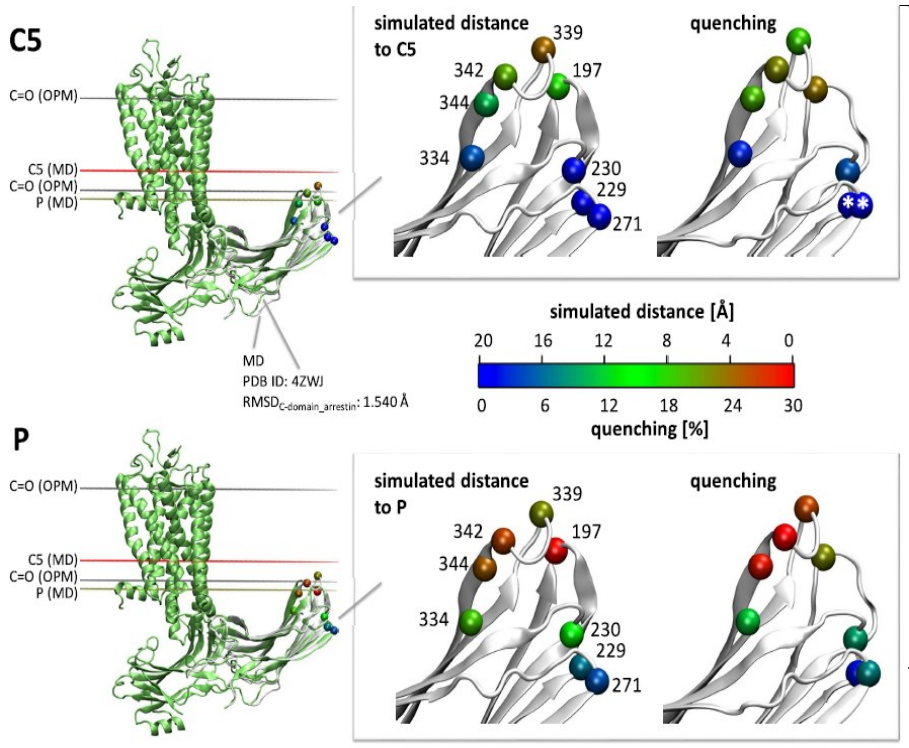

Figure prepared by Jana Selent, Pompeu Universiry, Barcelona, and taken from Lally CCM, Bauer B, Selent J, Sommer ME. (2017) *C-edge Loops of Arrestin Function as a Membrane Anchor* Nature Communicatio ns **8:**14258

Figure 3.1.7 Comparison of molecular dynamics simulations and fluorescence quenching data with the Ops*/arrestin-1 complex

Left: *superposition of the Ops*/arrestin-1 fusion complex crystal structure* ***(green, PDB code = 4ZWJ),*** *with a C-domain conformation selected from MD simulation (grey). The membrane layers were modelled by Jana Selent using computational tools….*

Right: *Distance maps derived from MD and fluorescence experiments. Sites on the C-edge are represented by spheres at the Cα atoms. For the MD derived distances, proximity to the phospholipid bilayer (lower panel) or to Carbon 5 on the acyl chain (upper panel) are shown using the colour scheme (red being close contact and blue being 20Å away), as seen during the simulations. For the fluorescence quenching derived distances, red corresponds to a high level of quenching (up to 30%) and blue to low levels of quenching, by N-tempoyl palmitamide on the membrane surface (lower panel) and 5-doxyl stearic acid in the membrane interior (upper panel). White asterisks correspond to negative quenching values (see main text for details).*

3.1.6 Conformation of the C-edge loops of arrestin in the pre-complex and high-affinity complex.

Comparison of molecular dynamics simulations employing the isolated C-domain of p44 with fluorescence quenching data shows that the orientation of the C-edge loops in the simulations resembles that of the high-affinity complex. However, fluorescence data suggest that the C-edge has a different orientation and conformation in the pre-complex. In the pre-complex, sites 342 and 339 are more deeply inserted into the membrane than in the high-affinity complex, and the 197-loop does not engage the membrane at all. Based on these findings, it is possible the C-edge adopts a conformation similar to that seen in one of the crystallographic tetramers of basal arrestin. In the "open" conformation (molecules A and C in PDB structure 1CF1), the hydrophobic residues on the 344-loop are exposed, the polar residues buried, and the 197-loop is not orientated for interaction with the membrane (see figure 3.1.7). Therefore, based on the fluorescence and molecular dynamics data, it can be proposed that the conformation of the C-edge in the high-affinity complex is similar to the conformation of p44, and in the pre-complex is similar to the "open" basal conformation of arrestin.

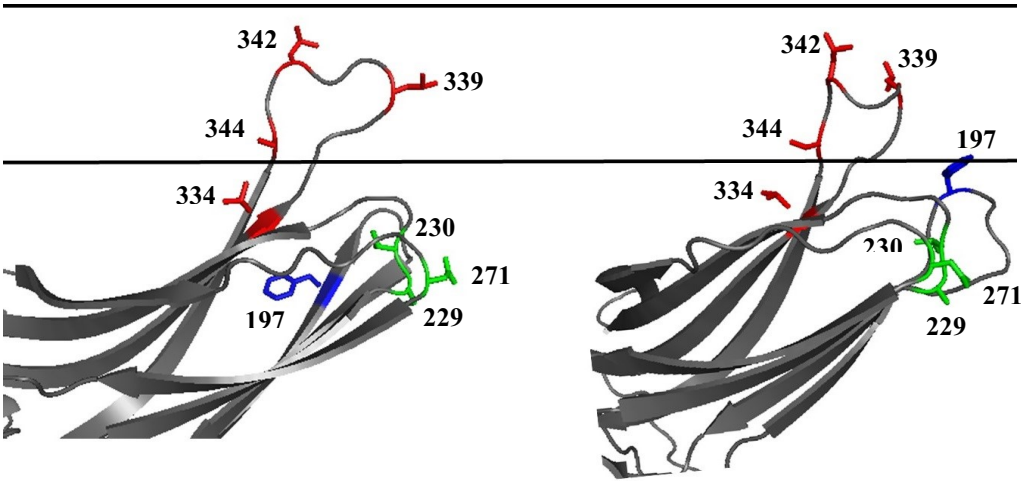

Figure 3.1.8 Orientation of the C-domain of basal arrestin and p44 with the membrane

Left: *basal arrestin, PDB 1CF1, α conformer, C-edge loops* ***Right:*** *p44 arrestin PDB 4ZJW, chain b, C-edge loops. Side chains of the arrestin sites that were labelled with monobromobimane*

are shown. Red = residues on the 344-loop: T334, S344, L342, L339, blue = F197 on the 197-loop, green = residues on the lower C-edge loops: N271, S229, T230.

3.1.7 Conclusions

The seminal finding of this work is that the C-edge of arrestin serves as a membrane anchor and is an important binding element in the arrestin-receptor complex. The fluorescence experiments, carried out with arrestin mutants showed a clear association between the C-edge of arrestin with the membrane. As the results from the fluorescence quenching experiments correlated strongly with the molecular dynamics simulations, it signifies that the interaction also occurs with wild type arrestin. Furthermore, as some fluorescently labelled sites on the N-domain of arrestin showed no interaction with the membrane, and no interaction was observed between arrestin and the membrane in the absence of the receptor, it is clear that membrane association is not simply an artefact of the presence of the fluorophore on arrestin.

Notably, the membrane anchor is engaged differently between the pre-complex and the high-affinity complex. In the pre-complex only the 344-loop interacts with the membrane, with the hydrophobic residues penetrating the hydrophobic layer. This would correspond to a C-edge conformation similar to that observed in the “open” crystallographic conformer of basal-state arrestin. In the high-affinity complex there is a change in orientation in the 344-loop, with residues adjacent to the hydrophobic patch also able to penetrate the membrane interior, as well as the 197-loop. This resembles the interaction observed by simulating interaction of the C-edge of p44 with the membrane. Hence, the membrane anchor likely resembles the C-edge of p44 in the high-affinity complex.

Mutation of residues on the C-edge of arrestin to alanine have been previously shown to correspond to reduced binding to Rh*P (Ostermaier, Peterhans et al. 2014). As the membrane anchor of arrestin is not deployed in the absence of the receptor, it acts as a specific binding element, possibly functioning to orientate arrestin in the correct conformation for fast binding to the receptor. Therefore, these results have identified a further functional binding element on arrestin, and the relevance of this will be further discussed in the Discussion, Chapter 4.

Supplementary Information

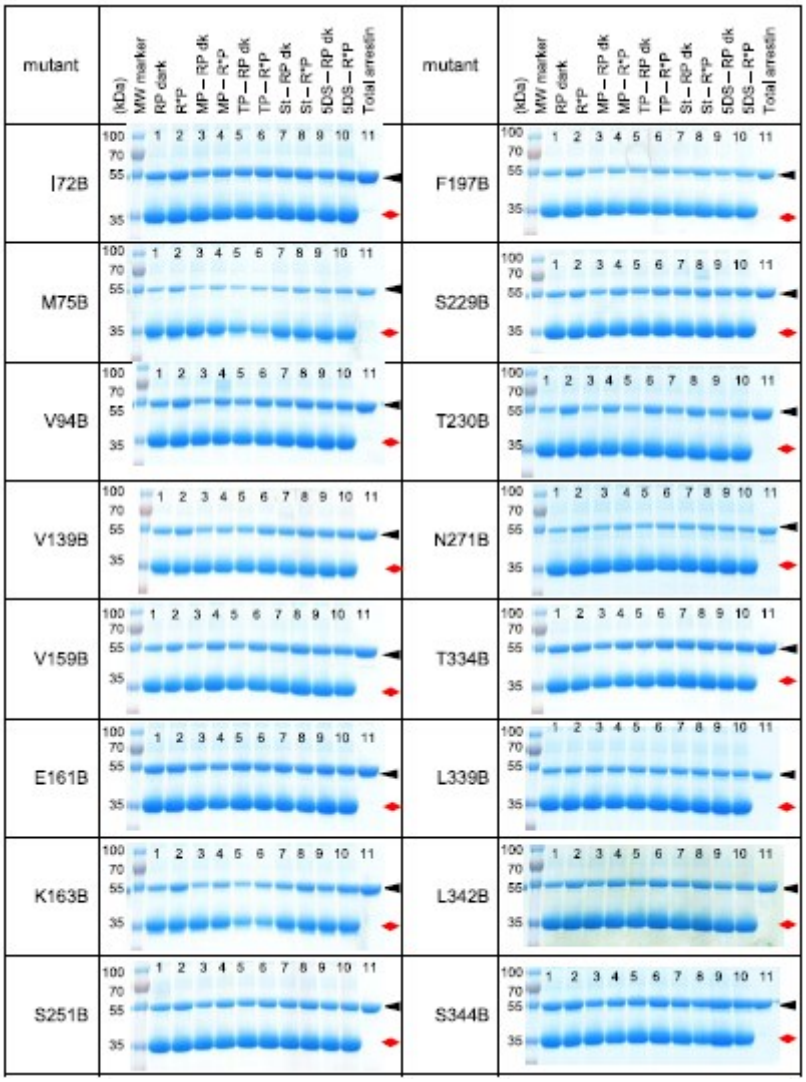

Supplementary Figure 3.1.1 Centrifugal pull down assay of arrestin binding to ROS membranes

Binding of 1μM arrestin to 4μM rhodopsin, in the dark and light, and with membranes enriched with: MP = methyl palmitate, TP = tempo palmitate, St = stearic acid, 5DS = 5-doxyl stearic acid. The black arrows indicate the position of arrestin on the gels, and the red arrows indicate the position of rhodopsin.

Figure taken from Lally CCM, Bauer B, Selent J, Sommer ME. (2017) *C-edge Loops of Arrestin Function as a Membrane Anchor* Nature Communications **8:**14258

Supplementary table 3.1.1 ***Fluorescence properties of bimane-labelled arrestin mutants in the presence of enriched ROS-P membranes.*** Fluorescence intensities are normalized to the fluorescence of 1 μM unbound arrestin (see *Methods* for more details). Mean ± standard error is reported. Numbers in brackets indicate number of independent measurements. Quenching efficiencies are reported as a percentage. Negative wavelength shifts indicate shifts to lower emission wavelength values.

Dark-state pre-complex

	Mutant	Ethanol (control)	Methyl palmitate	N-tempoyl-palmitamide	% Quenched	Stearic acid	5-doxyl-stearic acid	% Quenched	Wavelength shift (nm)
N-domain, finger loop	I72B	0.94 ± 0.16 (2)	0.87 ± 0.12 (2)	0.85 ± 0.10 (2)	**2.3**	0.90 ± 0.15 (2)	0.94 ± 0.16 (2)	**-4.4**	**-5**
	M75B	0.89 ± 0.08 (2)	0.86 ± 0.04 (2)	0.95 ± 0 (2)	**-10.5**	0.86 ± 0 (2)	0.82 ± 0.01 (2)	**4.6**	
N-domain	V94B	1.05 ± 0 (2)	1.02 ± 0 (2)	1.08 ± 0.03 (2)	**-5.9**	1.13 ± 0.03 (2)	1.09 ± 0.04 (2)	**3.5**	
N-domain, middle loop	V139B	0.86 ± 0.02 (2)	0.87 ± 0.05 (2)	0.87 ± 0 (2)	**0**	0.84 ± 0 (2)	0.72 ± 0.02 (2)	**14.3**	
N-domain, 160 loop	V159B	1.08 ± 0.05 (3)	1.15 ± 0.03 (3)	1.09 ± 0.10 (3)	**5.2**	1.04 ± 0.10 (3)	1.19 ± 0.02 (3)	**-14.4**	
	E161B	1.3 ± 0.05 (2)	1.4 ± 0.2 (2)	1.1 ± 0.13 (2)	**21.4**	1.3 ± 0.25 (2)	1.25 ± 0.12 (2)	**3.8**	
	K163B	0.92 ± 0.10 (2)	0.98 ± 0.06 (2)	0.94 ± 0.11 (2)	**4.1**	0.90 ± 0.09 (2)	0.87 ± 0.05 (2)	**3.3**	
C-domain, 197 loop	F197B	0.89 ± 0.03 (2)	0.94 ± 0 (2)	0.88 ± 0.06 (2)	**6.4**	0.88 ± 0.05 (2)	0.81 ± 0.07 (2)	**7.9**	
C-domain, 229 loop	S229B	1.16 ± 0.04 (2)	1.02 ± 0.05 (2)	1.10 ± 0 (2)	**-7.8**	1.03 ± 0.01 (2)	0.95 ± 0.03 (2)	**7.8**	
	T230B	1.05 ± 0.17 (3)	1.08 ± 0.14 (3)	1.01 ± 0.15 (3)	**6.5**	0.96 ± 0.17 (3)	0.95 ± 0.16 (3)	**1.0**	
C-domain, C loop	S251B	2.15 ± 0.5 (3)	1.83 ± 0.31 (3)	1.46 ± 0.10 (3)	**20.2**	1.79 ± 0.22 (3)	1.58 ± 0.09 (3)	**11.7**	**-3**
C-domain	N271B	1.04 ± 0.03 (3)	1.06 ± 0.04 (3)	0.98 ± 0.05 (3)	**7.5**	0.89 ± 0.11 (3)	1.05 ± 0.14 (3)	**-18.0**	
C-domain, 344 loop	T334B	0.70 ± 0.02 (3)	0.64 ± 0 (3)	0.56 ± 0 (3)	**12.5**	0.58 ± 0.08 (3)	0.66 ± 0.05 (3)	**-13.8**	
	L339B	0.99 ± 0.02 (2)	1.22 ± 0.09 (2)	1.17 ± 0.07 (2)	**4.1**	0.93 ± 0 (2)	0.79 ± 0.04 (2)	**15.0**	**-5**
	L342B	1.01 ± 0.2 (2)	1.13 ± 0.26 (2)	1.01 ± 0.23 (2)	**10.6**	0.98 ± 0.21 (2)	0.69 ± 0.08 (2)	**29.6**	**-8**
	S344B	0.5 ± 0.07 (2)	0.58 ± 0.12 (2)	0.48 ± 0.05 (2)	**17.2**	0.46 ± 0.02 (2)	0.51 ± 0.04 (2)	**-10.9**	**-3**

Light-activated high-affinity complex									
	Mutant	Ethanol (control)	Methyl palmitate	N-tempoyl-palmitamide	% Quenched	Stearic acid	5-doxyl-stearic acid	% Quenched	Wavelength shift (nm)
N-domain, finger loop	I72B	1.66 ± 0.13 (2)	1.69 ± 0.07 (2)	1.52 ± 0.12 (2)	10.1	1.77 ± 0.21 (2)	1.86 ± 0.24 (2)	-5.1	-27
	M75B	0.93 ± 0.07 (2)	0.95 ± 0.02 (2)	0.97 ± 0.03 (2)	-2.1	0.97 ± 0.02 (2)	0.95 ± 0.05 (2)	2.1	-6
N-domain	V94B	1.08 ± 0 (2)	1.05 ± 0 (2)	1.12 ± 0.04 (2)	-6.7	1.23 ± 0.02 (2)	1.18 ± 0.04 (2)	4.1	
N-domain, middle loop	V139B	1.29 ± 0.02 (2)	1.15 ± 0.02 (2)	1.12 ± 0.01 (2)	2.6	1.23 ± 0 (2)	1.18 ± 0.02 (2)	4.1	
N-domain, 160 loop	V159B	1.19 ± 0.06 (3)	1.30 ± 0.04 (3)	1.18 ± 0.11 (3)	9.2	1.19 ± 0.11 (3)	1.38 ± 0.05 (3)	-16.0	
	E161B	1.3 ± 0.08 (2)	1.42 ± 0.15 (2)	1.15 ± 0.14 (2)	19.0	1.31 ± 0.26 (2)	1.31 ± 0.12 (2)	0	
	K163B	0.95 ± 0.10 (2)	1.01 ± 0.05 (2)	0.94 ± 0.11 (2)	6.9	0.97 ± 0.09 (2)	0.96 ± 0.05 (2)	1.0	
C-domain, 197 loop	F197B	1.07 ± 0.04 (2)	1.13 ± 0.02 (2)	0.87 ± 0.08 (2)	23.0	1.11 ± 0.07 (2)	0.85 ± 0.11 (2)	23.4	-11
C-domain, 229 loop	S229B	1.28 ± 0.03 (2)	1.20 ± 0.03 (2)	1.19 ± 0.02 (2)	0.83	1.18 ± 0.05 (2)	1.25 ± 0.06 (2)	-5.9	
	T230B	1.07 ± 0.14 (3)	1.06 ± 0.10 (3)	0.96 ± 0.14 (3)	9.4	1.03 ± 0.14 (3)	0.98 ± 0.15 (3)	4.8	-3
C-domain, C loop	S251B	2.8 ± 0.5 (3)	2.48 ± 0.29 (3)	1.90 ± 0.16 (3)	23.4	2.39 ± 0.2 (3)	1.95 ± 0.07 (3)	18.4	-5
C-domain	N271B	1.01 ± 0.03 (3)	1.03 ± 0 (3)	0.95 ± 0.06 (3)	7.8	0.98 ± 0.13 (3)	1.13 ± 0.11 (3)	-15.3	
C-domain, 344 loop	T334B	0.95 ± 0.04 (3)	1.05 ± 0.06 (3)	0.92 ± 0 (3)	12.4	0.95 ± 0.04 (3)	0.93 ± 0.04 (3)	2.1	
	L339B	1.11 ± 0.11 (2)	1.37 ± 0.08 (2)	1.0 ± 0.03 (2)	27.0	1.16 ± 0.11 (2)	0.95 ± 0.08 (2)	18.1	-10
	L342B	1.01 ± 0.23 (2)	1.06 ± 0.21 (2)	0.73 ± 0.16 (2)	31.1	1.03 ± 0.25 (2)	0.80 ± 0.12 (2)	22.3	-10
	S344B	0.78 ± 0.04 (2)	0.84 ± 0.02 (2)	0.59 ± 0 (2)	29.8	0.78 ± 0.08 (2)	0.63 ± 0.05 (2)	19.2	-10

3.2 Conformation of arrestin in the pre-complex as compared to the high-affinity complex

3.2.1 Introduction

Arrestin binding to light-activated phosphorylated rhodopsin (Rh*P) occurs in a two-step process. First arrestin interacts with the phosphorylated receptor C-terminus in a primarily electrostatic interaction termed the pre-complex, which orientates the two proteins for subsequent fast transition to the high-affinity complex (Schröder, Pulvermüller et al. 2002). To date, there is little information in the literature regarding the structure of the pre-complex. However, several studies have shown that the C-tail becomes more susceptible to proteolysis upon interaction with receptor phosphates, indicating that it may be displaced. This effect has also been observed to occur in the presence of the polyanionic molecules heparin and IP6, indicating that a negative charge may be sufficient for C-tail release. Moreover truncation of the C-tail of arrestin results in a loss of specificity of the interaction, and results in a higher binding affinity to Rh* and RhP as well as to Rh*P, suggesting that the C-tail acts as an auto-inhibitory element on arrestin, and is displaced upon recognition of either the phosphorylation or activation state of the receptor, so that arrestin can transition to the high-affinity complex (Palczewski, Buczylko et al. 1991, Palczewski, Pulvermüller et al. 1991, Palczewski, Pulvermüller et al. 1991, Gurevich, Chen et al. 1994, Zhuang, Vishnivetskiy et al. 2010).

Crystal structures of active arrestin in complex with a GPCR phosphopeptide (Shukla, Manglik et al. 2013), as well as the truncated p44 arrestin variant which lacks the C-tail (Kim, Hofmann et al. 2013), provided insights into the conformational changes occurring in arrestin upon C-tail displacement. The C-tail makes several contacts within the N-domain of arrestin, and upon displacement this results in disruption of elements which stabilise the basal state of arrestin, in particular the polar core and three element interaction. In addition, movement of the gate loop and the central crest loops, and a 21° interdomain rotation are observed (Kim, Hofmann et al. 2013, Shukla, Manglik et al. 2013) (see introduction section 1.3). Displacement of the C-tail has also been observed to increase the flexibility of the finger loop, which is located at the arrestin-receptor interface, and binds within the active receptor crevice (Hanson, Dawson et al. 2008).

3.2.2 Conformation of arrestin in the presence of IP6

The experiments presented in this section aim to investigate the conformational changes occurring in arrestin in both the pre-complex and the high-affinity complex using intramolecular quenching, which allows for monitoring of the movement and orientation of different sites on arrestin. The initial experiments focussed on determining the extent of C-tail displacement upon arrestin interaction with the polyanionic molecule IP6, which has previously been shown to bind arrestin and acts as a mimic for the phosphorylated receptor C-terminus (Palczewski, Pulvermüller et al. 1991) (Zhuang, Vishnivetskiy et al. 2010). Several double-arrestin mutants were prepared with one site mutated to a cysteine and the other site to a tryptophan in an arrestin construct lacking native cysteines and tryptophans. The fluorophore monobromobimane was then covalently-attached to the cysteine residue. This approach is based on the ability of tryptophan residues to quench the fluorescence of a fluorophore in close proximity. The C-tail of arrestin remains unresolved in crystal structures, and so its location in the arrestin structure is not known. However, the C-tail contains many acidic residues, and therefore it is possible that it resides within the concave surface of the N-domain, which contains a cluster of basic residues. In order to test this hypothesis sites 72 and 169 on the N-domain were chosen for labelling with monobromobimane, as these are well-characterised and do not interfere with arrestin binding when labelled. These sites, as well as the estimated location of the tryptophan-substituted sites along the arrestin C-tail are shown in figure 3.2.1.

Along with experiments which monitored C-tail displacement, the effect of IP6 on the orientation of the finger loop and gate loop was also investigated using previously established mutants containing tryptophan-monobromobimane pairs (Sommer, Farrens et al. 2007, Kim, Hofmann et al. 2013) (see figure 3.2.1). In order to probe displacement of the gate loop, the arrestin mutant with monobromobimane attached at site 299, and a tryptophan substitution at site 173 (I299B/L173W) was employed. In the basal state of arrestin site 299 and 173 are far apart, and therefore no quenching of fluorescence is observed, but upon arrestin activation the gate loop moves towards the N-domain, thereby bringing the sites into close enough proximity for quenching to occur (Kim, Hofmann et al. 2013). In order to probe for changes occurring in the finger loop, the arrestin mutant K298B/I72W was employed (Sommer, Farrens et al. 2007). The finger loop is the main interaction site in the arrestin-receptor interface, and it adopts an extended conformation to bind into the open crevice of the active receptor (Szczepek, Beyriere et al. 2014, Kang,

Zhou et al. 2015). In the basal state of arrestin the finger loop is folded down, making contact with the N-domain of arrestin (Hirsch, Schubert et al. 1999). However, displacement of the arrestin C-tail has been shown to result in increased flexibility in the finger loop (Hanson, Dawson et al. 2008), and therefore C-tail displacement could correspond to a relief of quenching observed with this arrestin mutant. As phenylalanine is a similar size to tryptophan but does not act as a fluorescence quencher, the arrestin mutants K298B/I72F and I72B/I299F were also measured to serve as a control.

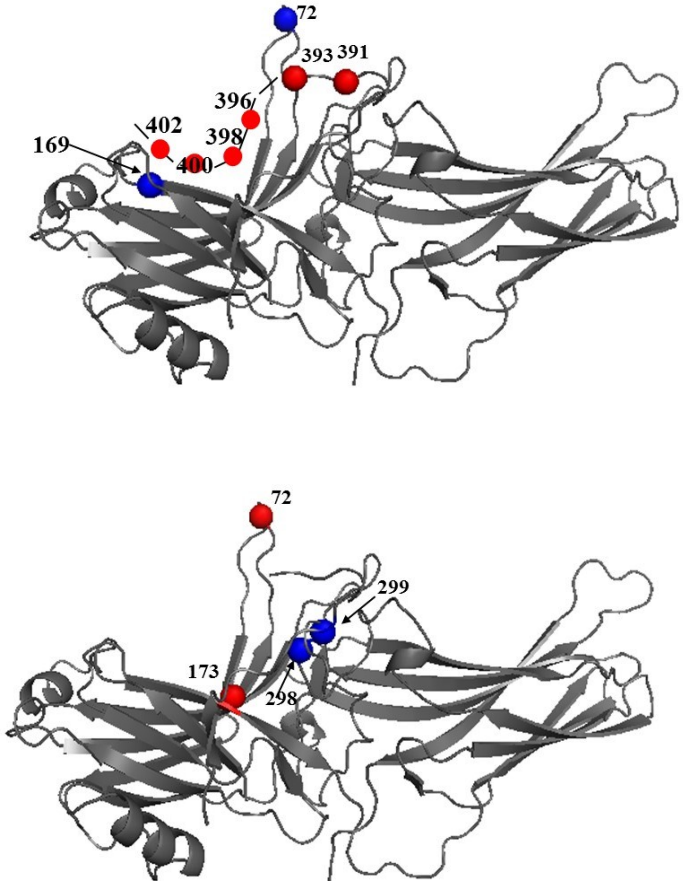

Figure 3.2.1 arrestin-1 shown with sites labelled with a fluorophore or mutated to tryptophan
Sites on arrestin labelled with either the fluorophore monobromobimane (Cα atoms shown as blue spheres), or substituted to Tryptophan (Cα atoms shown as red spheres). ***Top:*** *Arrestin mutants employed to monitor displacement of the C-tail. Sites 72 and 169 on the N domain were labelled with monobromobimane, and 6 sites on the C tail (Y391W, E393W, T296W, Q398W, A400W and M402W were individually mutated to Tryptophan.* ***Bottom:*** *Arrestin mutants employed to measure movement of the gate loop (I299B/L173W), and the finger loop (K298B/I72W)*

Quantum yield measurements: the C-tail is in close proximity to the fluorophore-labelled sites on the N-domain, in the basal state of arrestin

Quantum yield, which is a measure of the proportion of photons emitted as compared to the number of photons absorbed by a fluorophore (see section 2.1 for more details) was measured for each of the arrestin mutants (supplementary table 3.2.1). These values provided the initial indication that the distal C-tail was in close proximity to the fluorophores at sites 169 and 72 in the basal state of arrestin, as the quantum yield of the

fluorophore at these sites was lower in all arrestin mutants containing tryptophan substitutions on the C-tail. In particular, substitution of sites on the most distal portion of the C-tail (T296W, Q398W, A400W and M402W) had the largest effect on the quantum yield of the fluorophore at site 72, and similarly substitutions A400W and M402W decreased the quantum yield of the fluorophore at site 169.

As expected, the fluorophore-tryptophan pair K298B/I72W reported a decrease in quantum yield as compared to the phenylalanine control, indicative that the finger loop is sufficiently close to the interdomain interface for quenching to occur in unbound arrestin. The fluorophore-tryptophan pair I299B/L173W reported no significant decrease in quantum yield as compared to the phenylalanine control, which is consistent with the distance between these sites in the unbound arrestin conformation.

Fluorescence lifetime measurements and quenching analysis

Fluorescence lifetimes were determined for each of the arrestin mutants both in the unbound state in low salt conditions, and in the presence of IP6 (see supplementary tables 3.2.2, and 3.2.3, respectively). The lifetimes were analysed using FluoFit software (from Picoquant GmbH), which plotted the log of intensity decay (log I (t)) against time (t) using reconvoluted curve fitting algorithms, and calculated the lifetimes using χ^2 analysis to determine the best fit (see figure 3.2.2). The IRF (see section 2.2.10), is shown in red. As there were three lifetimes derived from the fit, the amplitude weighted lifetime was used as the average fluorescent lifetime for each of the mutants (see methods chapter, section 2.2.10).

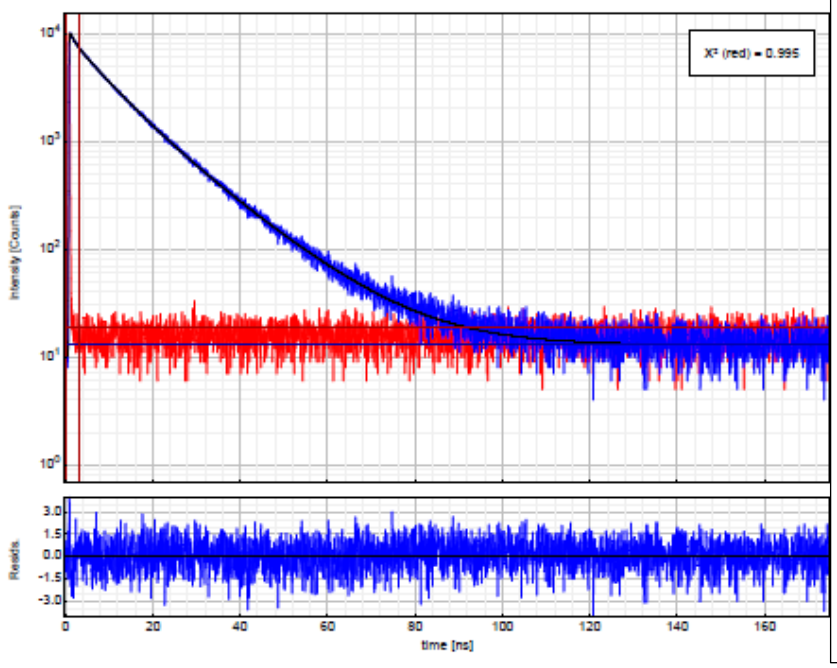

Figure 3.2.2 Example reconvolution curve showing the decay in fluorescence intensity over time

Top: *The IRF is shown in red, and the reconvolution decay curve is shown in blue. The fit yielded three fluorescence lifetimes, with a χ^2 of 0.995, indicating a strong fit.*
Bottom: *Plot of the residuals of the fit.*

The quantum yield and the amplitude weighted lifetime mesaured for each of the arrestin mutants was used to analyse the type of quenching occuring using the equations described in the methods chapter, section 2.2.10. The quenching analysis is shown in figure 3.2.3. For each mutant the relative proportions of unquenched, dynamically quenched and statically quenched fluorphores could be determined. The analysis provided more information about the proximity and flexibility of the loops containing the fluorophore and the trytophan quencher (see section 2.1 for more details on quenching).

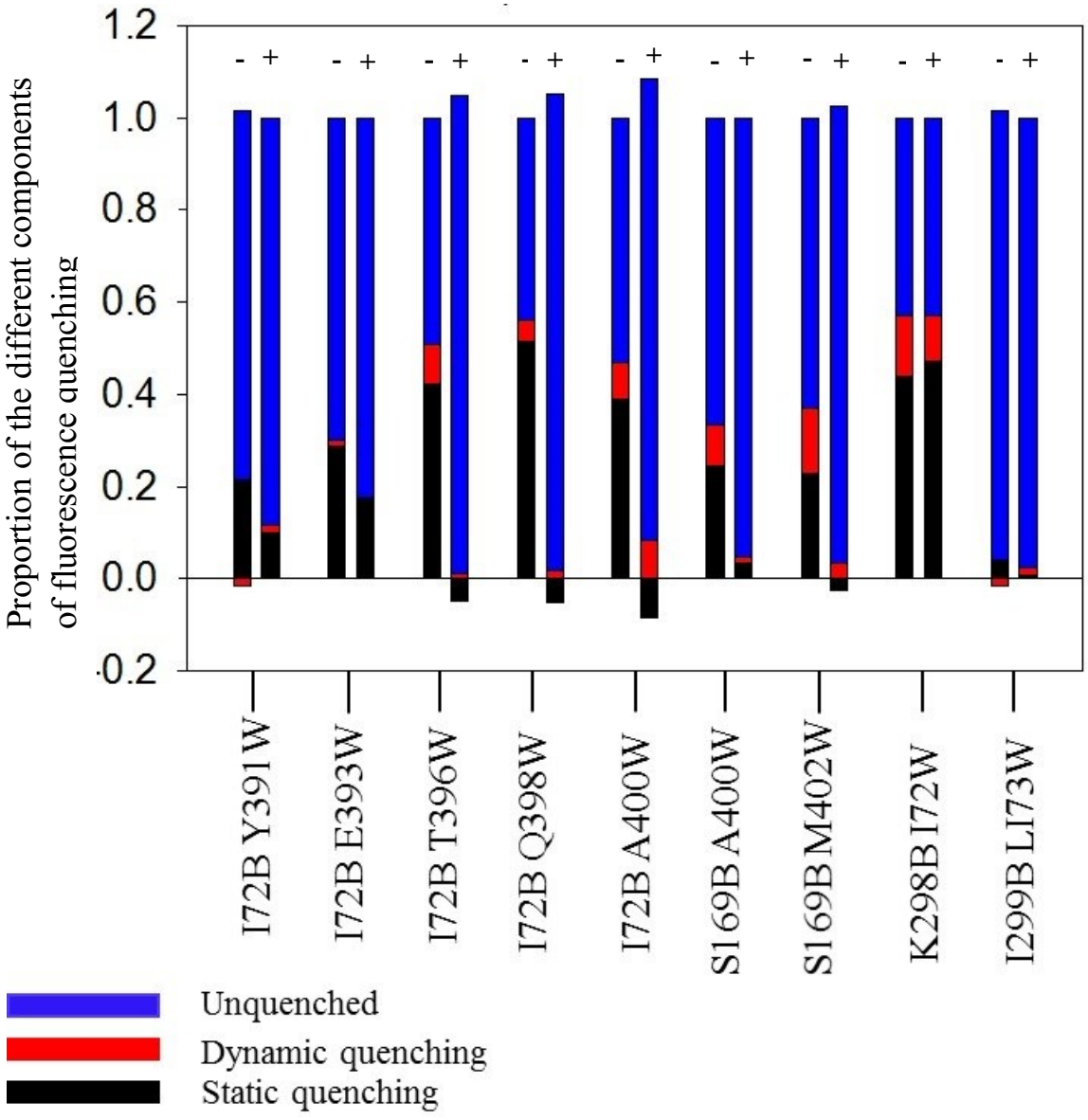

Figure 3.2.3: **Quenching profile of each of the arrestin mutants in the presence and absence of IP6**

Quenching was determined for each of the mutants in the presence (+) and absence (-) of 2.5mM IP6 in 50mM Hepes pH 7 buffer. The fraction of each quenching component was calculated (see methods 2.2.10). ***Blue*** *= unquenched fluorophores,* ***Red*** *= dynamic quenching and* ***Black*** *= static quenching.*

Only the distal portion of the C-tail is displaced in the presence of IP6

Fluorescence quenching was calculated in the presence and absence of IP6 (see figure 3.2.3 and table 3.2.1). In the absence of IP6 quenching of the monobromobimane fluorophore was observed by tryptophan residues at all points tested along the C-tail, with the most quenching observed with mutants I72B/T396W, I72B/Q398W and I72B/A400W, as well as S169B/A400W and S169B/M402W. Most of the quenching observed was static quenching, although the mutant S169B/M402W reported similar levels of static and dynamic quenching. The presence of IP6 yielded very interesting results. For mutants I72B/Y391W and I72B/E393W there was a very small reduction in the quenching efficiency. However, at sites I72B/T396W, I72B/Q398W I72B/A400W, S169B/A400W and S169B/M402W the quenching was almost completely disrupted. This difference in quenching profile indicates that release of the C-tail in the presence of a negatively charged species displaces only the terminal portion of the C-tail, with sites 391 and 393 remaining in contact with the N-domain.

The gate loop and finger loop are unaffected by IP6

Very little quenching was observed with the arrestin mutant I299B/L173W in the presence of IP6 indicating that IP6 does not induce any movement of the gate loop. The arrestin mutant K298B/I72W reported a similar level of quenching in both the presence and absence of IP6, indicating that the finger-loop is in a folded down conformation (see figure 3.2.3 and table 3.2.1).

Overall these quenching results indicate that the presence of IP6 does displace the C-tail, but importantly, only the distal portion. The proximal portion of the C-tail remains unchanged by the presence of IP6. As this proximal region of the C-tail comprises part of the gate loop, and forms part of the polar core and three-element interaction (See Introduction chapter, section 1.3), activation of arrestin only occurs when this portion is displaced. This correlates well with the quenching reported for the gate loop and finger loop, which indicates that displacement of the distal C-tail in the presence of IP6 does not induce movement within these regions on arrestin.

Table 3.2.1 Percentage of unquenched, statically quenched and dynamically quenched fluorophores calculated for each of the arrestin mutants in low salt buffer and in the presence of 2.5mM IP6.

	% Non-quenched		% static quenching		% dynamic quenching	
Mutant	**No salt**	**+IP6**	**No salt**	**+IP6**	**No salt**	**+IP6**
I72B Y391W	80	88	22	10	-2	2
I72B E393W	70	82	29	17	1	0
I72B T396W	49	104	42	-5	9	1
I72B Q398W	44	104	52	-5	4	2
I72B A400W	53	100	39	-8	8	8
S169B A400W	67	95	25	4	9	1
S169B M402W	63	99	23	-3	14	4
K298B I72W	43	43	44	47	13	10
I299B L173W	97	97	4	0	-1	2

3.2.3 Conformation of arrestin in complex with phosphorylated opsin.

Opsin arises in the rod cell when all-*trans*-retinal moves out of the binding pocket of active rhodopsin (Rh*). Arrestin remains bound to phosphorylated Opsin (OpsP) until regeneration with 11-*cis*-retinal reforms RhP. The conformation of phosphorylated opsin exists in an equilibrium between OpsP, which has a conformation similar to inactive rhodopsin, and Ops*P, which has a similar conformation to Rh*P. Under physiological conditions this equilibrium favours OpsP, with very low amounts of Ops*P present in the rod cell. However, it has previously been shown that the equilibrium is pH dependent: more Ops*P is present at lower pHs and more OpsP is present at higher pHs (Vogel and Siebert 2001) (see figure 3.2.4). As Opsin contains no retinal (which as an absorptive molecule can interfere with the fluorescence signal), fluorescence experiments measuring

arrestin binding to Opsin at different pHs serve as a useful tool to monitor the conformation of arrestin in the pre-complex and the high-affinity complex.

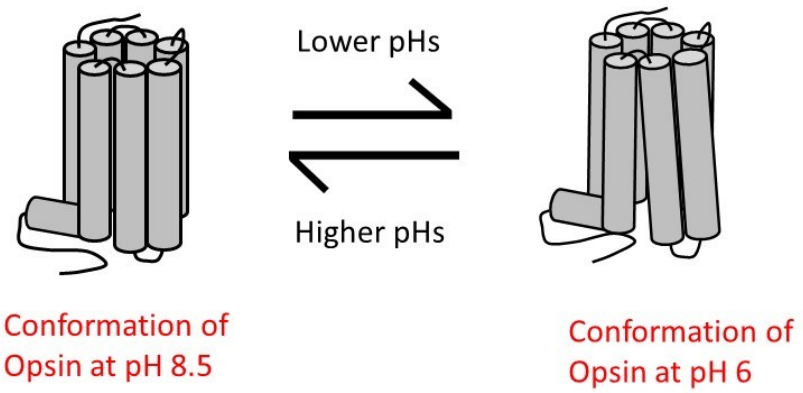

Figure 3.2.4 Schematic of the conformational equilibrium of opsin
At higher pHs the inactive conformation of opsin is favoured, whereas the active conformation is favoured at higher pHs.

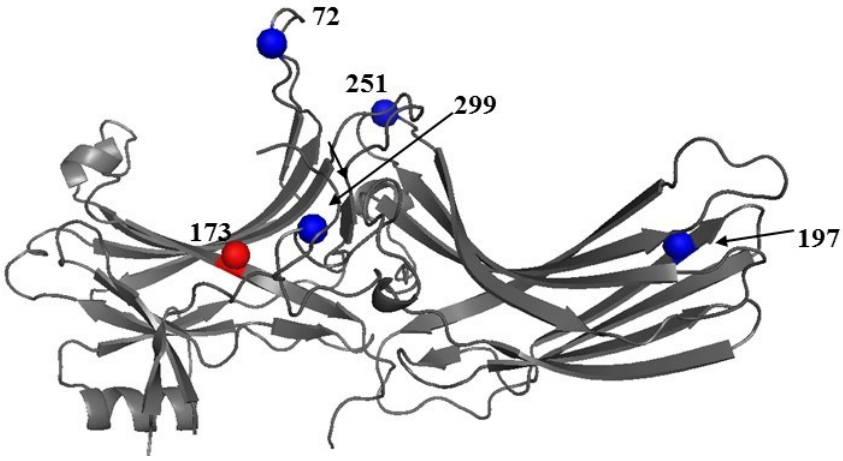

Figure 3.2.5 Sites on arrestin-1 labelled with a fluorophore or substituted to tryptophan
The Cα atoms of sites on arrestin labelled with a fluorophore are shown as blue spheres, and substituted to tryptophan are shown as red spheres)

In order to investigate the conformation of arrestin in the pre-complex as compared to the high-affinity complex, the fluorescence of labelled arrestin mutants was measured in the presence of phosphorylated opsin at three different pHs: pH 6 (with the active opsin conformation favoured), pH 7 (with a mixture of active and inactive opsin conformations) and pH 8 (with the inactive conformation favoured). The arrestin mutants employed were I72NBD, which is sensitive to the activation state of the receptor, F197NBD, which reports on membrane anchoring in the high-affinity complex only, I299B/L173W, which monitors movement of the gate loop, and S251B, which reports on interdomain rotation upon arrestin activation.

The fluorescence changes occurring at fluorophores on the finger loop and the 197-loop demonstrated that arrestin binding to opsin at pH 8 resembles the pre-complex, and at pH 6 resembles the high-affinity complex.

The fluorescence at site 72 on the finger loop reports an increase and blue-shift in fluorescence intensity upon formation of the high-affinity complex, due the site being embedded within the active receptor crevice. The fluorescence spectra in the presence of opsin (figure 3.2.6) show a fluorescence intensity at pH 6 comparable to that observed with Rh*P, indicating that the finger loop binds within the active helical core of active opsin as well as Rh*P. At pH 7 the fluorescence intensity upon binding opsin is lower, and at pH 8 the fluorescence intensity is only slightly higher than unbound arrestin. Pull-down assays showed comparable arrestin binding to the receptor in all conditions, which confirm that the fluorescence changes are as a result of the finger loop engaging the active receptor at pH 6, but not at pH 8.

The fluorophore at site 197 reports an increase in fluorescence intensity when bound to Rh*P as a result of this site penetrating the membrane interior (see section 3.1). The fluorescence at this site similarly changed when bound to phosphorylated opsin at the three different pHs (see figure 3.2.7). When bound to Opsin at pH 6, the fluorescence intensity reported was higher, indicative of the membrane anchoring which occurs at this site in the high-affinity complex. The fluorescence intensity at pH 7 was lower, and when bound to opsin at pH 8 there was only a small fluorescence increase as compared to unbound arrestin, which is indicative of the orientation of this site in the pre-complex, where no membrane association occurs (see section 3.1).

Arrestin is only activated in the presence of the helical crevice of the active receptor

The fluorescence changes in arrestin mutants monitoring movement of the gate loop and interdomain rotation, provided information about the conformation of arrestin when bound in the pre-complex to inactive opsin at pH 8, and in the high-affinity complex to active opsin at pH 6.

The fluorescence intensity of the arrestin mutant I299B/L173W is sensitive to movement of the gate loop. In the basal state of arrestin the gate loop comprises part of the polar core and the two sites are far apart. Upon arrestin activation, the polar core is disrupted, and movement of the gate loop brings the sites into close enough proximity for quenching

to occur, resulting in a decrease in fluorescence intensity. The fluorescence spectra shown for this mutant (figure 3.2.6) shows that the decrease in fluorescence intensity as compared to unbound arrestin, is similar when bound to opsin at pH 6 and Rh*P, indicating arrestin is in an active conformation. The fluorescence intensity when bound to opsin at pH 7 and pH 8 is higher, although pull-down assays show that arrestin is bound to opsin in all conditions. This indicated that arrestin bound to opsin in the absence of the active helical core, remains in a basal conformation with the polar core intact.

The arrestin mutant S251B reports on the interdomain rotation that occurs upon arrestin activation. In the basal conformation of arrestin the fluorophore at site 251 is quenched by a neighbouring tyrosine (Y61) residue, with both sites comprising part of the YKS(N)D(A) hydrogen bond network, which binds the base of the finger loop to the C-loop and stabilises the interdomain interface. Upon arrestin activation this hydrogen bond network is disrupted, which results in an interdomain rotation of the two domains relative to each other. The two sites are no longer in close enough proximity for quenching to occur, which corresponds to an observed increase in fluorescence at a fluorophore placed at site 251 (Kim, Hofmann et al. 2013). The fluorescence at site 251 when bound to opsin at the three different pHs is shown in figure 3.2.7. At pH 6, in the presence of the active receptor helical core, there is a large increase in fluorescence as compared to unbound arrestin, indicative of the interdomain rotation which occurs with arrestin activation. However, when bound to opsin at pH 8, there is a smaller increase in fluorescence, indicating that arrestin bound to the inactive receptor in the pre-complex is in a basal conformation, with respect to interdomain rotation.

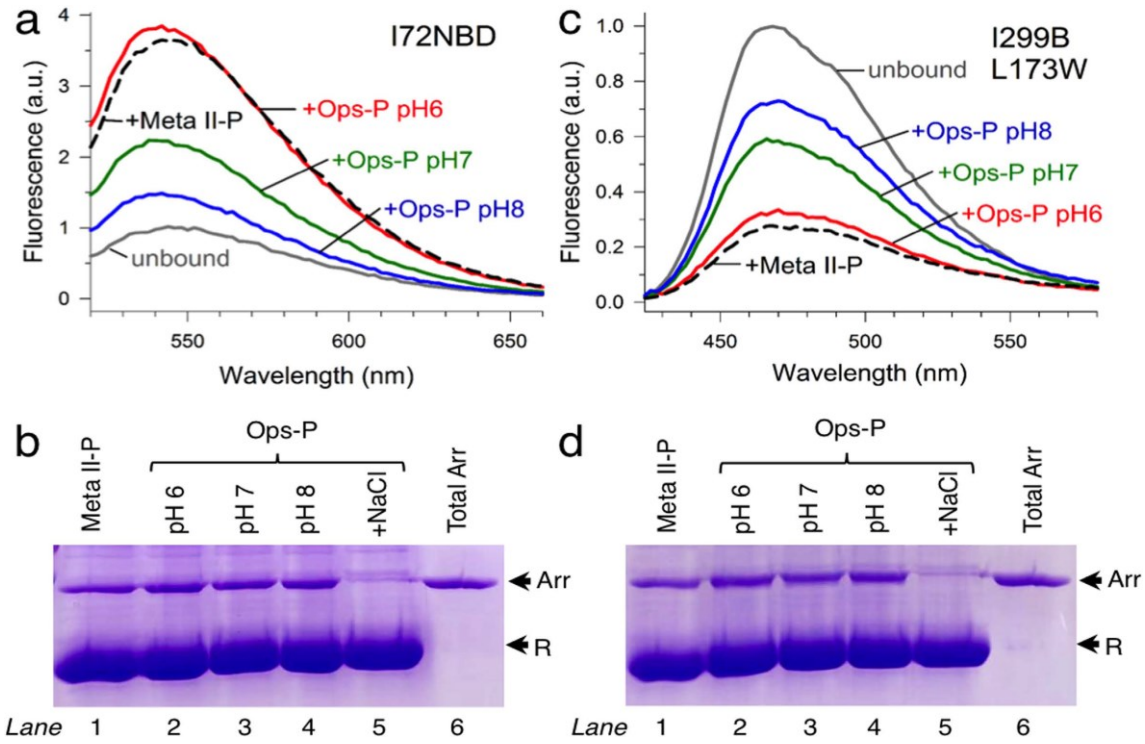

Figure 3.2.6 Steady-state fluorescence spectra of arrestin mutants bound to Rh*P and OpsP at different pHs.

Top: *fluorescence spectra of 2μM arrestin mutants* ***a)*** *I72NBD and* ***c)*** *I299B/L173W.* ***grey*** *= unbound arrestin,* ***black dashed line*** *= arrestin bound to Rh*P,* ***red*** *= arrestin bound to OpsP at pH 6,* ***green*** *= arrestin bound to OpsP at pH 7,* ***blue*** *= arrestin bound to OpsP at pH 8.*

Bottom: *SDS gels showing the amount of arrestin bound using the pull-down assay, for arrestin mutants* ***b)*** *I72NBD and* ***d)*** *I299B/L173W.* ***Lane 1*** *= arrestin binding to Rh*P,* ***lane 2*** *= arrestin binding to opsin at pH 6,* ***lane 3*** *= arrestin binding to opsin at pH 7,* ***lane 4*** *= arrestin binding to opsin at pH 8,* ***lane 5*** *= negative control showing no arrestin is bound to Rh*P in the presence of 5M NaCl,* ***lane 6*** *= positive control showing the amount of arrestin present in each of the samples.*

Figure published in "Functional map of arrestin binding to phosphorylated opsin, with and without agonist" Peterhans C., Lally C.C.M., Ostermaier M.K., Sommer M.E., Standfuss J. Scientific Reports ***6:****28686.*

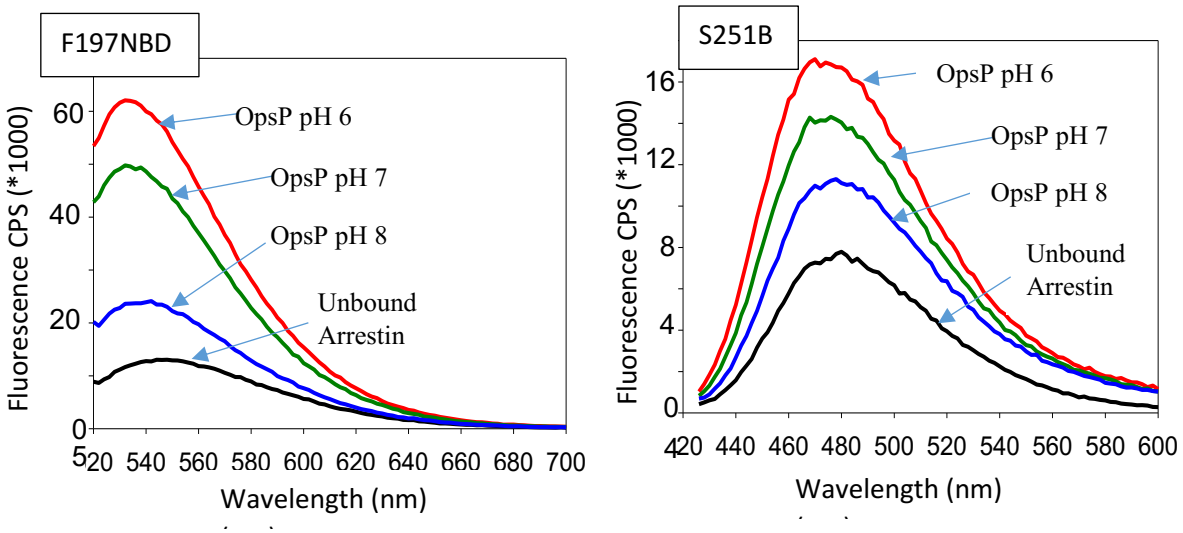

Figure 3.2.7 Steady-state fluorescence spectra of arrestin mutants bound to OpsP at different pHs
Fluorescence spectra of 2μM labelled arrestin mutants ***left****: F197NBD and* ***right:*** *S251B.* ***black****: unbound arrestin. 2μM Arrestin bound to 6μM OpsP was measured at* ***red:*** *pH 6,* ***green:*** *pH 7,* ***blue:*** *pH 8*

3.2.4 Conclusions

Overall the quenching results show information about the conformation of arrestin when bound to IP6, as well as to the phosphorylated receptor C-terminus, in both the presence and absence of the active helical core of the receptor.

Arrestin remains in a basal conformation in the pre-complex

In the pre-complex arrestin is bound to the inactive phosphorylated receptor, through interaction with the receptor phosphates. It had previously been proposed that receptor phosphates, or a negatively charged species such as IP6 or heparin, could displace the auto-inhibitory arrestin C-tail. However, the results presented in this section demonstrate that only the distal portion of the C-tail is displaced in the absence of an active receptor species. IP6 was found to displace the C-tail as far as site 396, but site 393 remained in contact with the arrestin N-domain. As this proximal portion of the C-tail remained in contact with the N-domain of arrestin, the gate loop and finger loop did not undergo any movement in the presence of IP6. Similarly the presence of OpsP at pH 8 which favours the inactive form of the receptor did not induce any activating conformational changes in most of the arrestin population: The gate loop remained in its basal conformation, the C-edge membrane anchor was not engaged, and there was no interdomain rotation observed.

Therefore, it can be deduced that in the pre-complex interaction with the phosphorylated receptor C-terminus, arrestin likely remains in a basal conformation with just the terminal 8-11 C-tail residues displaced.

Arrestin adopts an active conformation in the presence of the active receptor

In the presence of OpsP at pH6, most of the opsin is in an active conformation (Ops*P), and this is correlated to changes in the conformation of arrestin: the finger-loop is embedded within the active helical core of the receptor, there is movement of the gate loop, interdomain rotation, and engagement of the C-edge membrane anchor. All of these structural changes are observed in the active conformation of arrestin when bound in the high-affinity complex (Kang, Zhou et al. 2015), and in the p44 crystal structure (Kim, Hofmann et al. 2013). Therefore, it is likely that interaction with the active receptor is required for full displacement of the arrestin C-tail, which allows for the subsequent interdomain rotation, and an active arrestin conformation.

Supplementary Information

Supplementary Table 3.2.1 *Fluorescence properties of monobromobimane-labelled arrestin mutants*

Mutant	Absorbance λ_{max} (nm)	Emission λ_{max} (nm)	Estimated ϕ, low salt	Estimated ϕ, With IP6	Average $\langle\tau\rangle$ (ns)
I72B	390	480	0.20	0.17	8.51
I72B Y391W	390	480	0.16	0.15	8.69
I72B E393W	392	480	0.14	0.14	8.37
I72B T396W	394	480	0.098	0.176	7.21
I72B Q398W	394	480	0.088	0.176	7.75
I72B A400W	392	480	0.106	0.17	7.39
S169B	385	480	0.27	0.284	10.35
S169B A400W	387	480	0.18	0.27	9.15
S169B M402W	387	480	0.17	0.28	8.44
K298B I72F	390	480	0.2	0.21	9.24
K298B I72W	395	480	0.094	0.09	7.08
I299B L173F	389	468	0.39	0.39	13.98
I299B L173W	389	468	0.38	0.38	14.18

λ_{max}, wavelength of maximal absorbance or emission

ϕ, quantum yield, measured in isotonic buffer (50 mM HEPES pH 7, 130 mM NaCl). Quantum yield in low salt buffer and 2.5mM IP6 were determined through titration curves of NaCl and IP6, respectively (see methods section 2.2.10).

$\langle\tau\rangle = \alpha_1\tau_1 + \alpha_2\tau_2 + \alpha_3\tau_3$, the amplitude weighted average fluorescence lifetime. The average amplitude weighted fluorescence lifetime was calculated from three different repeats for each mutant (see supplementary table 3.2.2).

Supplementary table 3.2.2 Fluorescence lifetime data under **low-salt** conditions								
	Fractional amplitude of positive decay components							
Mutant	α_1	τ_1 (ns)	α_2	τ_2 (ns)	α_3	τ_3 (ns)	Amplitude-weighted average lifetime (ns)	χ^2
I72B	*0.20*	0.56	*0.31*	5.74	*0.50*	13.14	8.4004	0.991
	0.16	0.9	*0.48*	7.3	*0.36*	14.22	8.783	1.035
	0.02	0.84	*0.45*	7.19	*0.36*	13.95	8.3479	0.878
I72B Y391W	*0.15*	1.19	*0.35*	6.11	*0.50*	13.25	8.924	1.022
	0.18	1.52	*0.52*	8.31	*0.29*	15.31	9.106	0.966
	0.23	0.63	*0.45*	7.28	*0.32*	14.45	8.0368	0.910
I72B E393W	*0.16*	0.87	*0.34*	5.97	*0.50*	13.67	9.0429	1.034
	0.21	0.85	*0.49*	7.04	*0.30*	14.39	7.973	1.061
	0.23	0.66	*0.46*	7.32	*0.31*	14.72	8.1022	0.919
I72B T396W	*0.24*	0.77	*0.37*	5.22	*0.39*	12.57	7.0024	1.112
	0.25	1.75	*0.55*	7.83	*0.20*	15.27	7.759	0.938
	0.27	0.74	*0.45*	6.47	*0.28*	13.52	6.8684	0.892
I72B Q398W	*0.21*	0.84	*0.39*	5.46	*0.39*	13.21	7.4994	0.995
	0.24	1.46	*0.53*	7.67	*0.23*	15.67	8.037	0.943
	0.24	1.08	*0.49*	7.10	*0.27*	14.74	7.7017	1.004
I72B A400W	*0.20*	1.14	*0.50*	6.71	*0.30*	14.18	7.877	0.957
	0.24	0.77	*0.46*	6.43	*0.31*	13.55	7.2546	0.960
	0.25	0.75	*0.45*	6.40	*0.30*	13.3	7.0287	0.947
S169B	*0.09*	1.81	*0.52*	9.30	*0.39*	16.84	11.566	1.005
	0.19	0.55	*0.39*	8.16	*0.42*	16.18	10.0410	0.951
	0.22	0.46	*0.40*	8.26	*0.38*	15.9	9.4466	0.951
S169B A400W	*0.18*	1..76	*0.49*	8.6	*0.33*	16.3	9.932	0.937
	0.25	0.58	*0.39*	7.10	*0.37*	15.43	8.5622	0.972
	0.21	0.67	*0.43*	7.43	*0.36*	15.6	8.9510	0.930

S169B M402W	*0.19*	1.20	*0.47*	7.52	*0.35*	15.29	9.037	0.953
	0.28	0.50	*0.38*	6.88	*0.34*	15.13	7.9268	0.966
	0.24	0.61	*0.41*	7.05	*0.35*	15.15	8.3529	0.979
K298B I72F	*0.17*	0.81	*0.40*	5.94	*0.43*	15.47	9.1756	0.980
	0.18	1.22	*0.54*	8.09	*0.28*	18.02	9.685	1.004
	0.22	0.76	*0.50*	7.54	*0.28*	17.47	8.8735	0.961
K298B I72W	*0.23*	0.91	*0.41*	5.57	*0.36*	13.41	7.2700	1.019
	0.22	1.07	*0.52*	6.60	*0.26*	14.77	7.508	0.944
	0.29	0.56	*0.45*	5.89	*0.26*	14.06	6.4667	1.005
I299B L173F	*0.24*	1.06	*0.59*	14.38	*0.17*	27.15	13.298	1.263
	0.17	2.75	*0.43*	11.26	*0.41*	22.36	14.330	0.950
	0.18	1.18	*0.38*	10.99	*0.44*	22.39	14.309	1.016
I299B L173W	*0.20*	2.44	*0.63*	15.00	*0.17*	28.41	14.818	1.118
	0.24	1.60	*0.36*	9.38	*0.40*	21.77	12.503	0.986
	0.16	1.84	*0.40*	12.04	*0.4*	22.89	15.228	1.051

τ = lifetime
α = proportion of fluorophores with lifetime, τ
χ^2 = statistical robustness of the fit
Repeats are shown for each mutant

Supplementary table 3.2.3 Fluorescence lifetime data in the presence of 2.5mM **IP6**								
	Fractional amplitude of positive decay components							
Mutant	α_1	τ_1 (ns)	α_2	τ_2 (ns)	α_3	τ_3 (ns)	Amplitude-weighted average lifetime (ns)	χ^2
I72B	*0.12*	0.75	*0.29*	4.94	*0.59*	12.05	8.621	1.033
	0.15	1.76	*0.55*	8.25	*0.30*	14.96	9.309	1.013
	0.22	0.54	*0.37*	6.32	*0.41*	12.53	7.5756	0.911
I72B Y391W	*0.18*	0.54	*0.31*	5.01	*0.51*	12.24	7.942	1.045
	0.16	1.41	*0.52*	8.01	*0.32*	14.18	8.935	0.941
	0.21	0.76	*0.46*	7.46	*0.33*	13.62	8.1313	0.942
I72B E393W	*0.16*	1.02	*0.34*	6.66	*0.51*	13.00	8.9957	1.028
	0.17	1.28	*0.49*	7.38	*0.34*	13.45	8.431	0.962
	0.22	0.61	*0.44*	7.39	*0.34*	13.65	7.9911	0.968
I72B T396W	*0.14*	0.72	*0.31*	5.43	*0.55*	12.03	8.3894	0.984
	0.16	1.20	*0.52*	7.59	*0.32*	13.71	8.505	0.922
	0.21	1.52	*0.61*	8.75	*0.18*	14.91	8.3333	1.005
I72B Q398W	*0.16*	0.78	*0.31*	5.59	*0.53*	12.28	8.3841	1.012
	0.16	1.33	*0.53*	7.93	*0.31*	14.19	8.844	0.959
	0.22	0.63	*0.42*	7.01	*0.36*	13.26	7.8745	0.946
I72B A400W	*0.18*	1.70	*0.49*	7.93	*0.32*	13.67	8.669	0.993
	0.23	0.56	*0.36*	6.28	*0.41*	12.52	7.5438	0.905
	0.24	0.57	*0.37*	6.33	*0.39*	12.31	7.3190	0.959
S169B	*0.10*	1.79	*0.43*	9.34	*0.47*	17.13	11.802	1.024
	0.16	0.69	*0.39*	8.63	*0.45*	16.8	11.085	1.066
	0.17	0.58	*0.38*	8.49	*0.45*	16.3	10.6248	0.913
S169B A400W	*0.10*	1.80	*0.49*	10.03	*0.41*	17.49	12.225	0.992
	0.20	0.46	*0.34*	7.91	*0.46*	16.37	10.333	0.909
	0.18	0.55	*0.37*	8.35	*0.46*	16.23	10.5536	0.972

S169B M402W	*0.10*	1.82	*0.44*	9.32	*0.46*	16.97	12.0893	1.010
	0.19	0.56	*0.36*	8.33	*0.45*	16.45	10.558	0.939
	0.24	0.4	*0.35*	8.27	*0.41*	16.27	9.6990	0.928
K298B I72F	*0.15*	1.75	*0.56*	8.63	*0.29*	17.60	10.252	0.944
	0.19	0.84	*0.51*	7.79	*0.29*	16.89	9.113	0.958
K298B I72W	*0.21*	1.55	*0.48*	7.63	*0.31*	15.35	8.771	0.877
	0.28	0.50	*0.40*	6.08	*0.31*	14.0	6.9842	0.998
I299B L173F	*0.15*	1.92	*0.38*	9.77	*0.48*	21.9	14.392	0.973
	0.14	1.53	*0.39*	11.50	*0.47*	22.45	15.271	1.016
I299B L173W	*0.18*	2.46	*0.34*	10.07	*0.47*	21.58	14.105	0.955
	0.16	1.13	*0.33*	11.12	*0.51*	21.9	15.040	1.044

τ = lifetime
α = proportion of fluorophores with lifetime, τ
χ^2 = statistical robustness of the fit
Repeats are shown for each mutant

3.3 Different binding stoichiometries of the arrestin-rhodopsin complex

3.3.1 Introduction

Research in the literature has reported different stoichiometries for the arrestin-rhodopsin complex, with evidence for both one-to-one and a one-to-two interactions being reported.

Evidence for a one-to-one interaction has been obtained through biochemical binding assays between arrestin and rhodopsin monomers reconstituted into nanodiscs (Bayburt, Vishnivetskiy et al. 2011). These assays observed a comparable binding affinity to that of arrestin bound to rhodopsin in native disc membranes. Although these assays do not occlude the possibility of a higher stoichiometry, they nonetheless confirmed that a one-to-one interaction was functional. Furthermore, experiments monitoring binding of arrestin by the Extra-Meta-II assay (see methods chapter, section 2.2.4), found that stabilisation of the active Meta-II (Rh*P) form of rhodopsin by arrestin was found to saturate at a one-to-one stoichiometry (Schleicher, Kühn et al. 1989, Pulvermüller, Maretzki et al. 1997). The recently published crystal structure of the Ops*/arrestin-1 complex (Kang, Zhou et al. 2015) also supports a one-to-one interaction, as the structure obtained was of one arrestin bound to one Ops*.

The proposal for a one-to-two interaction of arrestin-rhodopsin initially arose based on the dimensions of the two proteins. Arrestin has a diameter almost double that of rhodopsin, and therefore it was speculated that each of the domains on arrestin could interact with a receptor molecule (Modzelewska, Filipek et al. 2006). Evidence for a one-to-two interaction have arisen from titration analyses using biophysical methods to measure arrestin binding to rhodopsin, which have identified possible factors which influence the stoichiometry, described below.

1. **Photo-activation density of rhodopsin**

   Arrestin binding to rhodopsin in native disc membranes containing differing percentages of light-activated receptors was measured using different biophysical methods (Sommer, Hofmann et al. 2011). The stoichiometry of the interaction was found to be dependent on the photo-activation density. At low photo-activation densities titration analysis indicated a stoichiometry of one-to-one, whereas at high photo-activation densities the measured stoichiometry saturated at one arrestin for every two Rh*P. The authors speculated two possible

explanations for the change in interaction stoichiometry. Firstly, it could arise from lack of space on the membrane. In native ROS membranes there is a high concentration of rhodopsin molecules, and therefore at high photo-activation density steric hindrance could result in arrestin being unable to bind to every active receptor. This explanation fits well with *in vivo* data measuring the translocation of arrestin to the rod outer segment (ROS) in transgenic mice (Hanson, Gurevich et al. 2007). This study found that when rhodopsin was expressed at a higher level, the ratio of arrestin to rhodopsin was lower than when less rhodopsin was expressed. The second explanation provided was that the one-to-two interaction resulted from each of the two domains of arrestin being able to interact with a receptor molecule. A follow up study looking into this possibility (Sommer, Hofmann et al. 2012) monitored the fluorescence changes occurring at a site on the finger loop, as well as the 344-loop, upon arrestin binding to either the phosphorylated light-activated receptor (Rh*P), or the phosphorylated aporeceptor (OpsP). The fluorescence changes reported that the finger loop was only engaged in the presence of the active receptor (Rh*P). The fluorescence changes occurring at the site on the 344-loop, on the other hand, correlated to the amount of arrestin bound, irrespective of the receptor state (Rh*P or OpsP). A model was therefore proposed whereby the finger loop interacted with Rh*P in a high-affinity interaction with the active receptor crevice, whereas the 344-loop could bind either a neighbouring receptor (which would give rise to a one-to-two stoichiometry) or the membrane (which would give rise to a one-to-one stoichiometry).

2. **Phosphorylation level of rhodopsin**

Titration analyses from centrifugal pull-down assays described above measuring arrestin binding to Rh*P at full photo-activation density, initially reported a stoichiometry of one-to-two (Sommer, Hofmann et al. 2011) as compared to a stoichiometry of one arrestin molecule to 1.4 rhodopsin molecules in the subsequent study (Sommer, Hofmann et al. 2012), indicating a mixture of one-to-one and one-to-two stoichiometries in the sample. The difference in binding stoichiometry reported in the two studies was attributed to the phosphorylation level of rhodopsin used in the studies. The sample preparation protocol to yield phosphorylated rhodopsin (see methods chapter, section 2.2.2), had been optimised for the second study, thereby resulting in a higher phosphorylation

level. Therefore, this suggested a correlation between arrestin interaction with the phosphorylated C-terminus and the final binding stoichiometry.

3. **Formation of the pre-complex**

   The interaction of arrestin with the phosphorylated receptor C-terminus is termed the pre-complex, which is thought to be the initial binding step, before transitioning of arrestin into the high-affinity complex with Rh*P (Schröder, Pulvermüller et al. 2002).. The C-terminus of rhodopsin contains seven phosphorylation sites, even though it has been shown that just three are required for high-affinity binding to Rh*P (Vishnivetskiy, Raman et al. 2007). However, it is conceivable that higher levels of phosphorylation of the receptor C-terminus affect formation of the pre-complex. The results presented in this section investigate the effect of pre-complex formation on the final binding stoichiometry of the high-affinity complex. As the pre-complex is a primarily electrostatic interaction, its stability is adversely affected by salt. Therefore, by modulating the salt concentration and carrying out binding titration assays, the correlation between pre-complex formation and the stoichiometry of the light-activated high-affinity complex could be investigated.

3.3.2 Salt sensitivity of arrestin binding to RhP and Rh*P

Pull down assays which monitor the amount of arrestin bound to the receptor were carried out with fluorescently-labelled arrestin at different concentrations of NaCl. Initial binding experiments were carried out with arrestin labelled with the fluorophore N,N'-Dimethyl-N-(Iodoacetyl)-N'-(7-Nitrobenz-2-Oxa-1,3-Diazol-4-yl=Ethylenediamine (NBD) at site 366 (A366NBD). This site is on the backside of arrestin, away from the arrestin-receptor binding interface, and therefore reports the amount of arrestin bound to rhodopsin under different conditions.

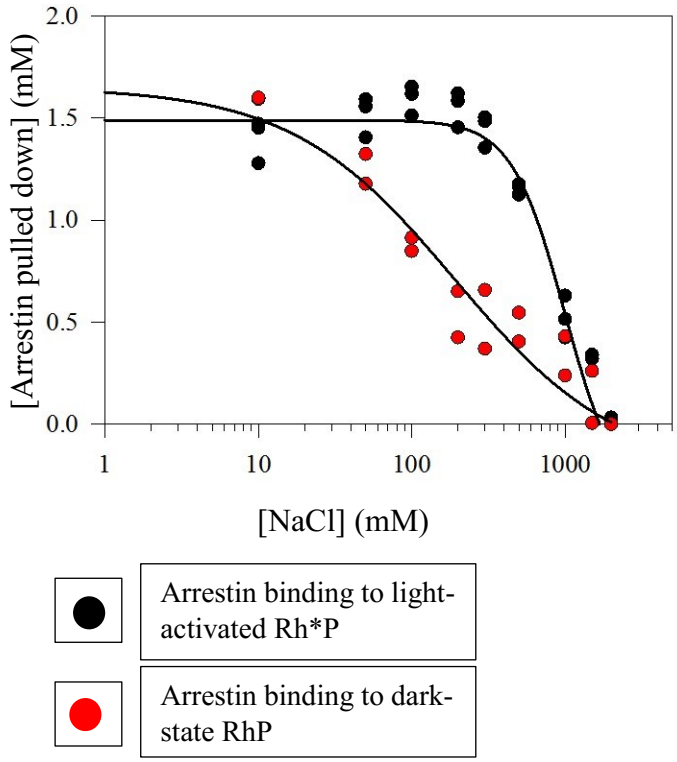

Figure 3.3.1 Salt sensitivity curve for the arrestin - receptor complex, with dark state (red) and light-activated (black) rhodopsin. A centrifugal pull down assay with 2µM arrestin A366NBD and 8µM receptor was carried out at different salt concentrations, and the amount of arrestin pulled down was determined by UV-vis-spectrometry. The high-affinity complex is more resistant to salt than the pre-complex.

The binding assays shown in figure 3.3.1 showed that almost all of the arrestin present in the sample was fully bound to rhodopsin in both the pre-complex and the high-affinity complex in the absence of NaCl. The high-affinity complex was less salt sensitive, with an IC50 value of 997mM NaCl, as compared to the pre-complex which had an IC50 value of 191mM NaCl. The NaCl titrations allowed for conditions to be chosen to monitor arrestin binding to rhodopsin in conditions which favour or abrogate the pre-complex. Measurements were carried out with either no NaCl added, in which case the amount of arrestin bound to RhP and Rh*P were comparable, as well as with 300mM NaCl added, in which case the high-affinity complex is unaffected, whereas there is little binding in the pre-complex.

3.3.3 Effect of pre-complex formation on the final stoichiometry of the high-affinity complex

Both receptor and arrestin titrations were carried out (figure 3.3.2), as they provide different information about binding. The receptor titration reported that all of the arrestin was functional and able to bind the receptor, as all of the arrestin present in the sample was able to be pulled down by an excess of receptor. The arrestin titration provides a clear insight into the stoichiometry of the interaction, as it reports the maximal amount of

arrestin that can bind to a given amount of rhodopsin. Arrestin titrations are also less prone to measurement error due to scattering by membranes. The Kd of arrestin binding and stoichiometry of the interaction calculated for each of the arrestin titrations and receptor titrations (binding to RhP and Rh*P in low salt and 300mM NaCl conditions) are shown in table 3.3.1.

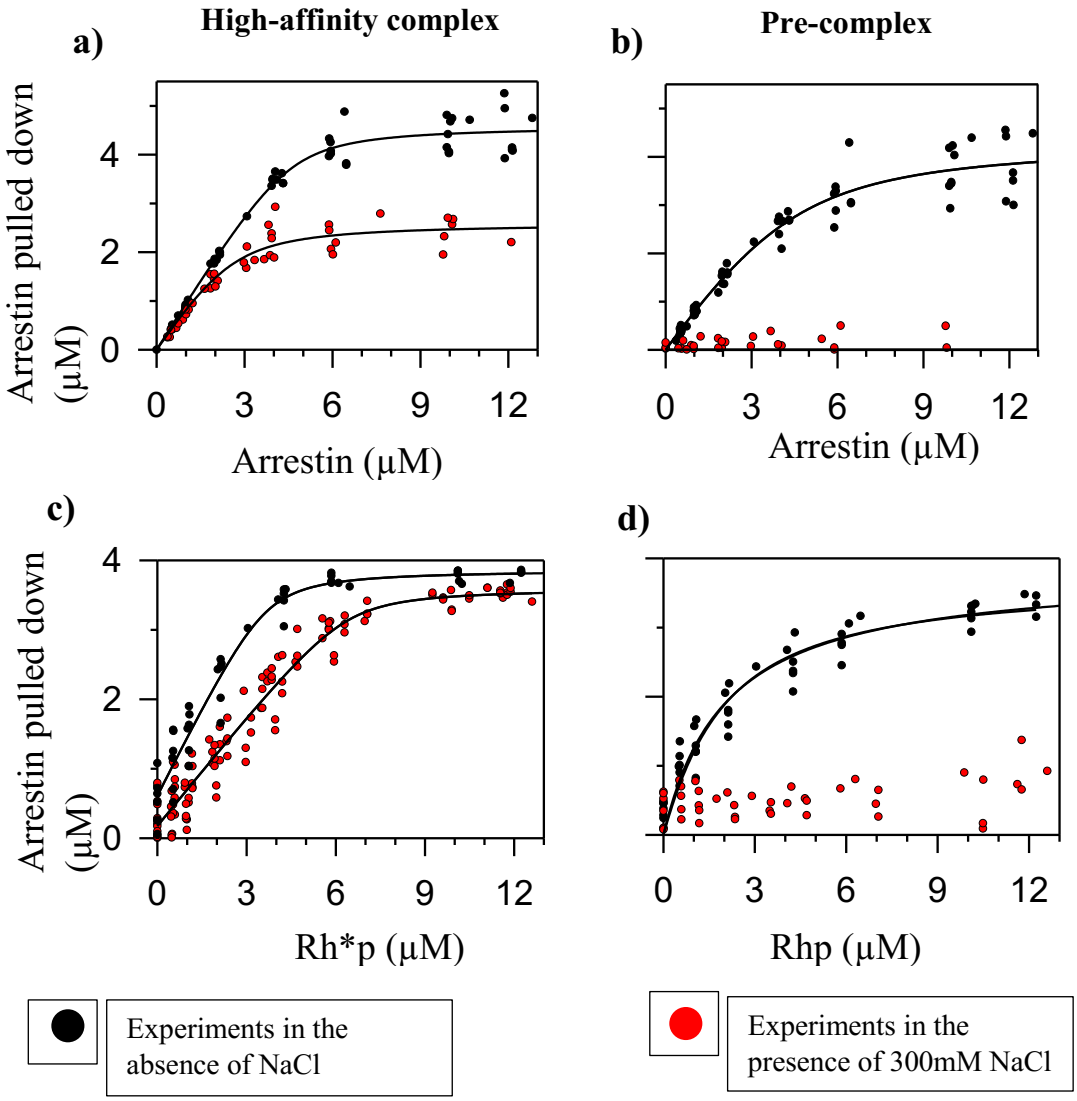

Figure 3.3.2 Centrifugal pull down assays in the dark (pre-complex) and after light-activation (high-affinity complex) in conditions favouring and abrogating formation of the pre-complex

Top: *Arrestin titrations against 4μM Receptor. Arrestin binding was measured by centrifugal pull-down using the labelled arrestin mutant A366NBD, where the concentration of arrestin remaining in the supernatant was determined by UV-vis spectroscopy in the presence of low salt (black) or 300mM NaCl (red). graph* ***a*** *is after photo-activation, and graph* ***b*** *measures binding in the dark.*

Bottom: *Receptor titration against 4μM of the labelled arrestin mutant A366NBD, also using the centrifugal pull down assay with low salt (black) or with 300mM NaCl (red). graph* ***c*** *is after photo-activation, and graph* ***d*** *is in the dark. Points represent multiple experiments.*

Table 3.3.1 *Kd values and binding stoichiometry of A366NBD arrestin bound to dark-state RhP and light-activated Rh*P in low salt conditions, and in the presence of 300mM NaCl*

		Dark RhP, low salt	**Dark RhP, 300mM NaCl**	**Light-activated Rh*P, low salt**	**Light-activated Rh*P, 300mM NaCl**
Arrestin titration	*Apparent Kd (μM)*	0.993	n.d.	0.206	0.4
	Stoichiometry	1 : 0.9	n.d.	1 : 0.9	1 : 1.5
Receptor titration	*Apparent Kd (μM)*	0.796	n.d	0.203	0.4
	Stoichiometry	1 : 1.4	n.d	1 : 1.1	1 : 1.7

The Kd values calculated in low salt conditions for arrestin binding to Rh*P report values of 206nM and 203nM for the arrestin and receptor titrations respectively, and arrestin binding to RhP reported a Kd of 993nM and 796nM for the arrestin titrations and receptor titrations, respectively. These values are similar to the values reported previously using the centrifugal pull-down method (Sommer, Hofmann et al. 2011). The stoichiometry of the interaction, as determined from the arrestin titration curves was shown to be sensitive to the formation of the pre-complex, as explained below.

In the absence of NaCl each arrestin binds one rhodopsin molecule

The stoichiometry of the interaction as determined by the arrestin titrations in the absence of salt is 1 arrestin to 0.9 receptor, for both the pre-complex and the high-affinity complex (graphs a and b, black circles). All arrestin present in the sample was bound to the ROS membranes in the dark in the absence of NaCl, (graph d, black circles) which indicates all of the arrestin was pre-complexed in an electrostatic interaction with the phosphorylated receptor C-terminus. Upon light-activation, the arrestin transitions to the high-affinity complex with the receptor. As the stoichiometry is unchanged, it suggests that arrestin binds the same receptor in the high-affinity complex that it was pre-complexed to in the dark.

In the presence of 300mM NaCl the final binding stoichiometry shifts

In the presence of 300mM NaCl, a different effect emerges. It is clear from the data that the addition of salt abrogates formation of the pre-complex, as no binding of arrestin occurs to dark state RhP in the presence of 300mM NaCl (graphs b and d, red circles). This confirms that 300mM NaCl is sufficient to abrogate this interaction, but still allows

for the high-affinity interaction between arrestin and Rh*P, as all of the arrestin was able to be pulled down in with an excess of receptor (graph c, red circles). However, the stoichiometry of the high-affinity complex in the presence of 300mM NaCl is different to that observed in no salt conditions, saturating at a binding stoichiometry of one arrestin to 1.5 receptor molecules (determined by the arrestin titrations), which indicates a mixture of one-to-one and one-to-two stoichiometries in the sample (see table 3.3.1). Therefore, pre-complex formation influences the final binding stoichiometry of the high-affinity complex.

3.3.4 Fluorescence changes occurring at sites on arrestin in conditions favouring different binding stoichiometries

In order to further probe the binding of arrestin to rhodopsin in the both the dark state pre-complex and the high-affinity complex, fluorescence changes at different sites on arrestin were monitored, as a function of receptor concentration, at the two different salt conditions (low salt, and 300mM NaCl) in the dark and after light-activation. As a control the actual amount of arrestin bound to the membranes was determined by centrifugal pull-down analysis. The arrestin mutants employed were I72NBD (probe located on the finger loop) and S344NBD (probe located on the 344-loop on the C-edge). These sites demonstrate an increase in fluorescence upon high-affinity binding to Rh*P (Sommer, Hofmann et al. 2012), and are accompanied by wavelength shifts in the emission spectra, indicative of movement of the fluorophore into a more hydrophobic environment (see section 2.1). At site 72 this is as a result of interaction with the active receptor crevice (Sommer, Smith et al. 2005, Hanson, Francis et al. 2006, Szczepek, Beyriere et al. 2014) and at site 344 this is due to association with the membrane (see section 3.1).

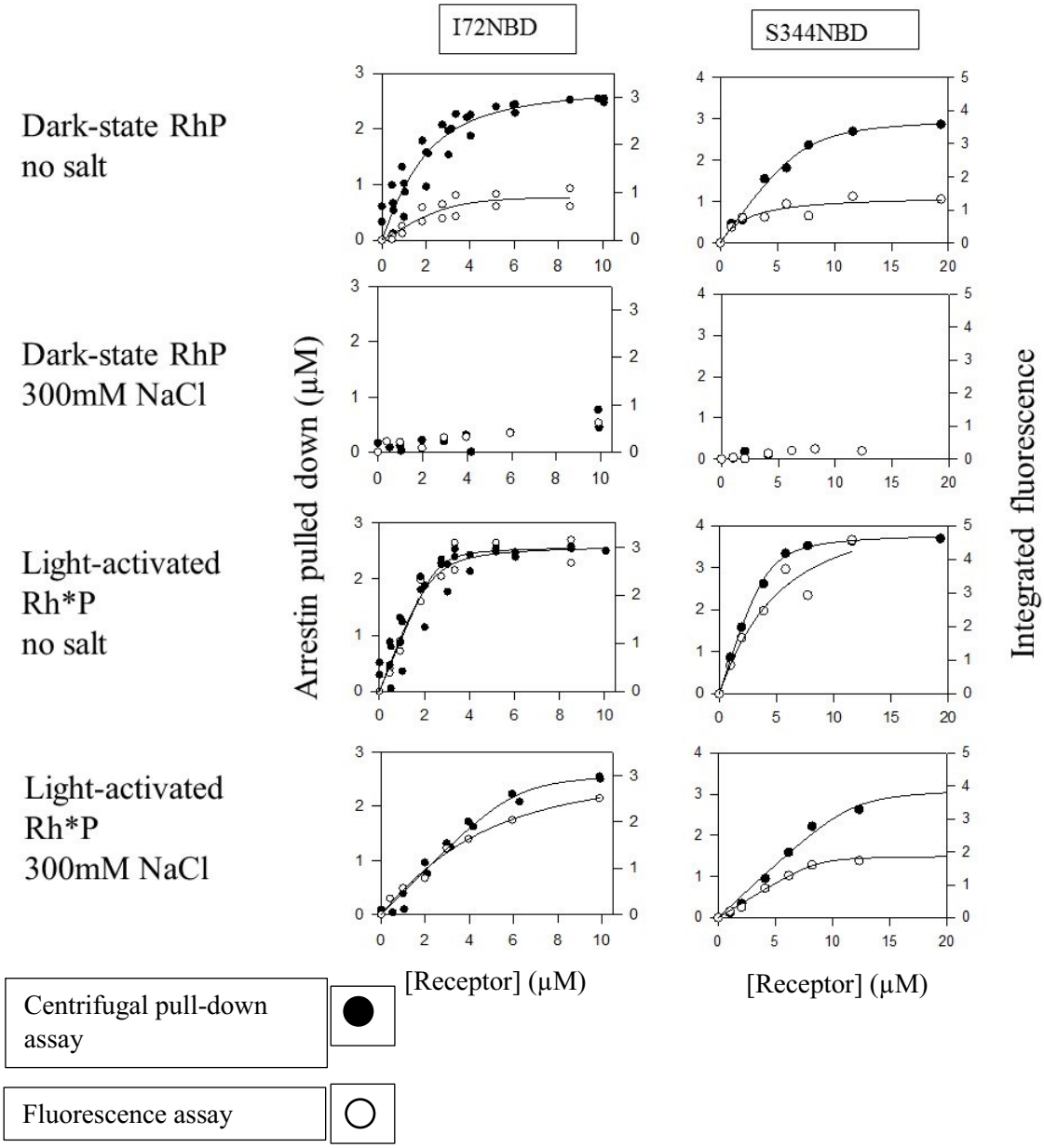

Figure 3.3.3 Centrifugal pull down assays, (black circles), in combination with fluorescence measurements (white circles), *with 4μM of two different arrestin mutants: I72NBD and S344NBD. Receptor titrations were carried out in order to see how the fluorescence changes at each of the sites as compared to the total amount of arrestin bound to the receptor in 4 different conditions: dark state binding to RhP in low salt, dark state binding to RhP with 300mM NaCl, light-activated binding to Rho*P in low salt, light-activated binding to Rh*P with 300mM NaCl.*

By combining the fluorescence data with the binding data from the centrifugal pull-down experiments information about engagement of the different sites on arrestin can be obtained. In the presence of 300mM NaCl binding of the mutants to dark state RhP was abrogated, and there was no change in fluorescence, indicating that no pre-complex interaction was occurring. The fluorophore at site 72 showed minimal fluorescence

change when bound to RhP in the pre-complex in the absence of NaCl, even though arrestin was bound. Conversely after light-activation the fluorescence increase reported the amount of arrestin bound, in both low salt conditions and with 300mM NaCl. This is consistent with this site binding in the crevice of the active receptor. The fluorophore at site 344 similarly only showed a small fluorescence increase when bound in the pre-complex to RhP in the absence of NaCl, but reports the amount of arrestin bound in the high-affinity complex to Rh*P in the absence of NaCl. This site has been shown to associate with the membrane in both the pre-complex and the high-affinity complex (see section 3.1). However, the depth of membrane association is different. In the high-affinity complex it penetrates the membrane interior, which is consistent with a fluorescence increase due to a hydrophobic environment. In the pre-complex, however, it is located at the membrane surface, which correlates with a lower fluorescence intensity (see section 3.2.3). When bound to Rh*P in the high-affinity complex in the presence of 300mM NaCl, the fluorescence signal saturates at a lower receptor concentration, as compared to arrestin binding. This indicates that this site is in a different environment when arrestin is bound in a one-to-one or a one-to-two stoichiometry.

3.3.5 Can the 344-loop contact a second receptor?

The 344-loop of the C-edge of arrestin was shown to act as a membrane anchor in both the pre-complex and the high-affinity complex (see section 3.1). However, the model proposed by Sommer et al. (Sommer, Hofmann et al. 2012), suggested that when arrestin was bound to rhodopsin in a one-to-two stoichiometry, this loop could interact with a second receptor. In order to investigate this hypothesis further, fluorescence quenching experiments using spin-labelled fatty acids were carried out, as described in section 3.1, in the presence of 300mM NaCl, which favours a binding stoichiometry of between one-to-one and one-to-two.

Briefly, the experiment followed the fluorescence of fluorescently-labelled arrestin in the presence of rod outer segment (ROS) membranes containing rhodopsin, that were enriched with spin-labelled fatty acids which insert spontaneously into the membrane and are able to quench fluorescence. The fatty acid N-tempoyl-palmitamide reported on association with the membrane surface, and the fatty acid 5-doxyl-stearic acid reported on association within the membrane interior. Experiments were carried out with dark state (RhP) and light-activated (Rh*P) phosphorylated rhodopsin.

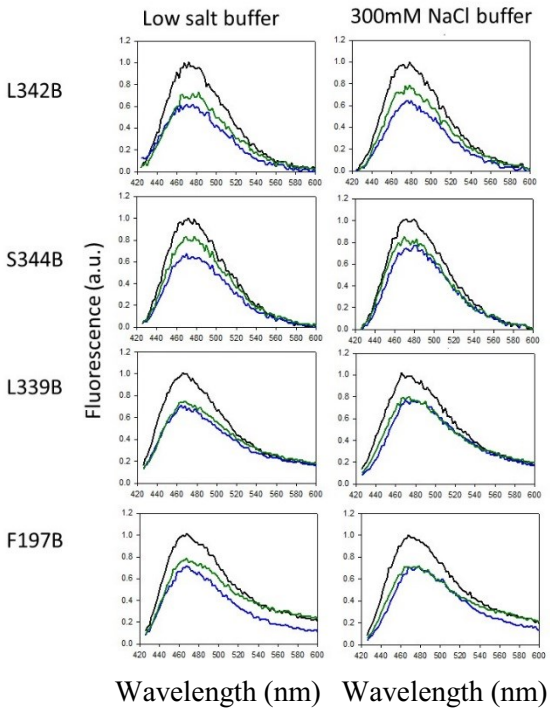

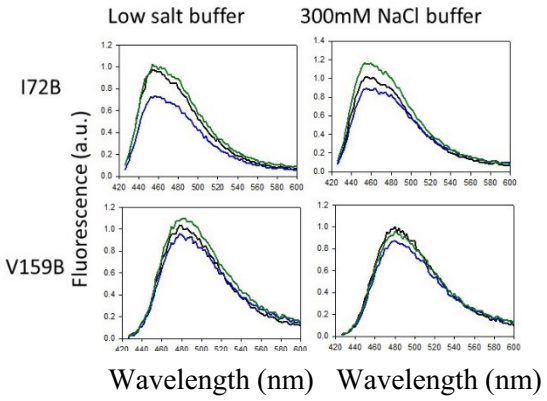

Figure 3.3.4 Steady-state fluorescence spectra of fluorescently-labelled arrestin mutants in low salt buffer and buffer with 300mM NaCl, bound to Rh*P

Black= 1μM arrestin + 4μM ROS, green = 1μM arrestin + 4μM ROS enriched with N-tempoyl palmitamide, blue = 1μM arrestin + 4μM ROS enriched with 5-doxyl stearic acid

The C-edge of arrestin interacts with the membrane in the presence of 300mM NaCl

Very little quenching was observed in the dark state, due to the low amount of arrestin binding to dark state phosphorylated rhodopsin (RhP) in the presence of 300mM NaCl. However, after light-induced arrestin binding, quenching was observed at all sites on the 344-loop (L342B, S344B and L339B) and 197-loop (F197B), by both N-tempoyl palmitamide and 5-doxyl stearic acid, indicative of arrestin interacting with the membrane (see figure 3.3.4). Moreover, the quenching pattern was similar to that observed at sites on these loops in buffer containing low salt. This demonstrates that the 344-loop and the 197-loop both penetrate the membrane, and are accessible to quenchers at the membrane surface and in the hydrophobic interior in conditions favouring a one-to-one stoichiometry as well as conditions in which a one-to-two binding stoichiometry occurs.

Fluorophores attached to sites on the N-domain of arrestin (I72B and V159B), also showed a similar quenching pattern in the presence of 300mM NaCl as compared to low salt buffer, with quenching of the fluorophore at site 72 observed by N-tempoyl palmitamide at the membrane surface. Site 159 serves as a negative control as it showed very little quenching by either N-tempoyl-palmitamide or 5-doxyl stearic acid, in both

low salt or 300mM NaCl buffers. This demonstrates that the quenching observed on the C-edge loops in the presence of 300mM NaCl is due to specific penetration of the membrane by these loops, when arrestin is bound to Rh*P.

3.3.6 Conclusions

Experiments presented in this section indicate that one-to-one and one-to-two binding stoichiometries of arrestin-to-Rh*P are both possible in native rod outer segment membranes. The clear observation of one-to-one binding indicates that space on the ROS membrane is not limited with respect to arrestin binding. Furthermore, there is a correlation between the stoichiometry of the high-affinity complex and the formation of the pre-complex. The stoichiometry of the high-affinity complex shifts to a mixture of one-to-one and one-to-two, in concentrations of salt which abrogate formation of the pre-complex.

The fluorophore at site 72 always reports the amount of arrestin bound in the high-affinity complex, but not in the pre-complex, indicative of engagement with the active receptor crevice. Similarly, the fluorophore at site 344 reported an increase in fluorescence when bound in the high affinity complex as compared to the pre-complex, which correlates to movement of this site into the hydrophobic membrane interior in the high affinity complex. However, the fluorescence at this site was sensitive to the stoichiometry of the interaction. The model proposed by Sommer et al. 2012 suggested that in the one-to-two binding stoichiometry the 344-loop could contact a neighbouring receptor. However, fluorescence quenching experiments using spin-labelled fatty acids presented in this section report membrane anchoring of this loop in the presence of 300mM NaCl, which favours a higher stoichiometry. As this loop serves as a membrane anchor in conditions with both one-to-one and one-to-two arrestin binding stoichiometries, it does not play a role in interacting with the second receptor. It remains unclear why the fluorescence of the fluorophore at site 344 does not report on the amount of arrestin bound in the presence of 300mM NaCl, even though the loop is associating within the membrane interior. One possible explanation is that the fluorescence is being quenched by a component in the membrane, for example the phospho-head groups of the phospholipids, and that this effect is increased in the presence of salt. Another possibility is that either the angle or the flexibility of the loop is different in the presence of 300mM NaCl as compared to in the absence of salt, and so even though the loop remains accessible to the quencher groups on the fatty acids, the fluorescence signal is reduced.

A model can therefore be proposed to explain the effect of pre-complex formation upon the final arrestin-rhodopsin stoichiometry in the high-affinity complex. When arrestin is pre-complexed to RhP in the dark, it transitions into the high-affinity complex upon light-activation, remaining bound to the same receptor. However, in conditions that abrogate the pre-complex, arrestin is free in solution. Upon light-activation, it binds Rh*P in the high-affinity complex but is able to contact a second receptor, in an irreversible interaction, thereby blocking interaction of the second receptor with another arrestin molecule. As the C-edge of arrestin always functions as a membrane anchor, irrespective of the binding stoichiometry, this secondary interaction site must be with another region on arrestin. Other possible candidates are either the N-edge of arrestin, or the arrestin C-tail. Both of these ideas will be discussed further in the discussion chapter, in section 4.

4. Discussion

This dissertation presents results regarding arrestin-rhodopsin interactions, in particular the structural and functional characterization of the different binding modes of arrestin. These binding modes are dependent on the phosphorylation and activation state of the receptor, and represent intermediate states on the path to binding to the receptor in a high-affinity complex. Arrestin is initially able to interact with the phosphorylated receptor in a primarily electrostatic interaction, termed the pre-complex. This pre-complex involves interaction of the phosphorylated receptor C-terminus with basic residues within the N-domain of arrestin, and is a low affinity and dynamic complex. After formation of the pre-complex, the interaction between arrestin and rhodopsin transitions into a high-affinity complex. Arrestin undergoes several conformational changes, involving displacement of the C-tail, and an interdomain rotation, resulting in re-orientation of the flexible binding loops, which allows for tight binding to the crevice of the active receptor.

$$RhP + Arr \rightleftharpoons [Rh^*P \sim Arr]_{pre\text{-}complex} \rightleftharpoons [R^*P - Arr]_{high\text{-}affinity\ complex}$$

Scheme 4.1 *Scheme of arrestin binding to rhodopsin. The first step is a pre-complex interaction, which primes arrestin for transition to tight binding to the receptor in a high-affinity complex.*

This work utilised site directed fluorescence in order to monitor the conformational changes occurring in arrestin when bound to rhodopsin. A previously unidentified interaction of arrestin with the membrane was determined, and the orientation of this functional binding element, along with the monitoring of the movement of flexible loops on arrestin as it binds different forms of the receptor, have provided insights into the structure of the pre-complex as compared to the high-affinity complex. This section will discuss the interpretation of these results and their functional implications for arrestin-1 and other members of the arrestin family.

4.1 Membrane anchoring by arrestin

The interaction observed between the C-edge of arrestin and the membrane, led to the characterization of a previously unidentified binding element on arrestin. Interestingly this C-edge membrane anchor is sensitive to the activation state of the receptor, and was

deployed differently in the pre-complex as compared to the high-affinity complex. In the pre-complex the membrane anchor involves just the 344-loop, and is orientated such that the hydrophobic residues penetrate the membrane interior. In the high-affinity complex, the orientation of the 344-loop changes. Residues adjacent to the hydrophobic patch penetrate the membrane, and additionally the 197-loop embeds within the membrane. Mutation of residues on the 344-loop and 197-loop to alanine, have previously been shown to reduce binding of arrestin to light-activated phosphorylated rhodopsin (Rh*P) (Ostermaier, Peterhans et al. 2014), and there was no association with the membrane observed in the absence of receptor, suggesting that engagement of these loops with the membrane is a functionally relevant interaction. The function of the membrane anchor most likely serves to stabilize the arrestin-rhodopsin interaction, and in particular orientates arrestin in the pre-complex to facilitate fast transition to the high-affinity complex. Interestingly, both G proteins and GRKs, have also been seen to engage the membrane. In the rod cell, transducin, PDE and GRK1 all contain lipid modifications which anchor them to the ROS membrane. Therefore, the theme of membrane anchoring among GPCR-binding proteins is a frequent one.

The mechanism of membrane anchoring by the C-edge of arrestin possibly involves interaction with acidic phospholipids. It has previously been determined that arrestin binding to Rh*P solubilised in detergent is significantly reduced. However, addition of acidic phospholipids restored binding to a level comparable to that observed with native ROS membranes (Sommer, Smith et al. 2006). Furthermore, upon light-activation acidic phospholipids in the ROS membrane have been shown to flip to the outer membrane (Hessel, Muller et al. 2001). The surface of the β-sheet on the C-domain of arrestin contains a cluster of basic residues (K232, K235, K236, K238, K257, K267, K332 and K330). Therefore it can be speculated that the increased negative charge on the membrane surface induced by rhodopsin activation could initially act to electrostatically attract the C-domain of arrestin to the membrane.

In terms of the evolution of arrestin, membrane interaction is a common theme. The arrestin clan is made up of the alpha family, the visual/beta family, and the Vsp26 family. The alpha arrestins and the Vps26 proteins are more evolutionarily distant, and therefore have little sequence similarity with rod arrestin. However, the alpha arrestins are membrane-associated proteins with roles in endocytic trafficking, and the Vps26 family, which have a similar fold to the visual/beta arrestins, form part of a rotamer complex involved in protein trafficking. Even though these members of the arrestin clan are able

to associate with the membrane, it is likely that the mechanism of membrane anchoring is different from that observed with the hydrophobic 344-loop of arrestin-1. Some alpha arrestins in fungi, for example, have been found to contain a C2 membrane binding subunit, which binds the membrane through an intermediate Ca^{2+} ion (Aubry and Klein 2013).

Among the visual/beta arrestin family, there is a higher homology, in terms of sequence and structure. The 344-loop identified as the main membrane anchor in arrestin-1, is conserved in both the visual arrestins, as well as the long variant of arrestin-2 (β-arrestin-1). The β-arrestins have other functions apart from deactivation of GPCR signalling, such as protein scaffolding, and clathrin binding which mediates endocytosis. It is possible these processes could be facilitated by the presence of a membrane anchor. The 344-loop of the long variant of arrestin-2 has been observed by x-ray crystallography to bind clathrin (Kang, Kern et al. 2009, Kern, Kang et al. 2009). This is not the primary clathrin binding site, which is located in the region linking the C-tail to the C-domain, but mutagenesis studies showed that it is nonetheless functional. In this structure the conformation of the 344-loop is similar to that observed in the p44 structure of arrestin, indicating that this conformation facilitates clathrin association to arrestin-2 in a similar way as membrane association of arrestin-1. Even though association with the membrane and clathrin binding are mutually exclusive processes, it is conceivable that the additional role of a clathrin binding loop as a membrane anchor could be conducive to endocytosis. The short variant of arrestin-2, and arrestin-3 both lack the 344-loop (Zhan, Gimenez et al. 2011). However, both splice variants of arrestin-2 have been shown to interact in a similar way with β2-adrenergic and M2-muscarinic cholinergic receptors (Gurevich, Dion et al. 1995), suggesting that the presence of the 344-loop is not necessary for GPCR binding. It is possible that the 197-loop, which is conserved among all arrestins, and was observed to penetrate the membrane in the high-affinity complex, is sufficient for membrane anchoring in the absence of the 344-loop.

4.2 Structure of the pre-complex

The pre-complex represents an intermediate binding step in the arrestin Rh*P interaction, involving a primarily electrostatic interaction with the phosphorylated receptor C-terminus. The conformation of arrestin in the pre-complex is not well characterised in the literature. This dissertation provided some more insights into the structural features of

arrestin interaction with receptor phosphates, as well as identifying a secondary interaction site, with the membrane. It had previously been proposed that the C-tail was displaced upon binding to receptor phosphates or polyanions like heparin or IP6 (Palczewski, Buczylko et al. 1991, Palczewski, Pulvermüller et al. 1991, Palczewski, Pulvermüller et al. 1991). The results presented in this dissertation, however, which monitored conformational changes at sites on arrestin when bound to IP6 or phosphorylated opsin (OpsP), found that in the absence of the active receptor conformation, only the distal portion of the C-tail was displaced. The proximal C-tail makes several contacts with the N-domain of arrestin, including the polar core and three element interaction, which stabilise arrestin in a basal conformation. As this was not displaced by IP6, it indicated that the structure of arrestin in the pre-complex resembles the basal conformation. Further experiments which monitored the position of the gate loop of arrestin supported this proposal. In the active arrestin structure disruption of the polar core results in a significant movement of the gate loop towards the N-domain (Kim, Hofmann et al. 2013). However, arrestin interaction with neither IP6 nor OpsP was observed to induce this effect. Similarly no interdomain rotation was observed in the absence of the active receptor. Recent studies which mutated every site on arrestin individually to alanine, and measured binding to Rh*P (Ostermaier, Peterhans et al. 2014) and OpsP (Peterhans, Lally et al. 2016), found differences in the proposed arrestin phospho-sensing sites. The region of arrestin observed to interact with phosphate groups in the crystal structure of arrestin-2 in complex with a phosphopeptide derived from the vasopressin receptor (Shukla, Manglik et al. 2013) is a cluster of positively charged residues within the N-domain, which are exposed in the active arrestin conformation. Mutation of these residues to alanine was found to decrease binding to Rh*P but not to OpsP. Arrestin binding to OpsP, however, was decreased by mutation of positively charged residues lining the cup of the N-domain (Peterhans, Lally et al. 2016). As these residues are exposed in the basal structure of arrestin, it is possible that this is the site of interaction of arrestin with the receptor C-terminus in the pre-complex.

The secondary interaction site of arrestin in the pre-complex, which was identified in this dissertation, was membrane anchoring by the arrestin C-edge. In the “open” conformation of the crystal structure of basal arrestin-1 (pdb: 1CF1, conformers a and c), the 344-loop adopts an extended conformation which exposes the hydrophobic side chains. Membrane insertion of this loop conformation would be consistent with results from fluorescence quenching experiments, which suggested relative deep insertion of the hydrophobic

residues on the 344-loop. Similarly, the lack of interdomain rotation and orientation of the 197-loop in the basal arrestin-1 structure would be expected to prevent interaction of this loop with the membrane, which is consistent with fluorescence experiments. Hence, the "open" conformation of basal arrestin-1 correlates well to the orientation of the membrane anchor observed experimentally, and is further evidence that arrestin remains in a basal conformation when bound in the pre-complex.

4.3 Function of the pre-complex

The pre-complex acts as a dynamic interaction between arrestin and the phosphorylated receptor which primes arrestin for tight binding in the high-affinity complex. In the pre-complex arrestin is brought into close contact with the receptor, which allows both proteins to sense the other's conformational equilibrium. This facilitates for a fast transition to the high-affinity complex, in which the active conformation of both arrestin and rhodopsin are stabilised.

After release of all-*trans*-retinal from the receptor, opsin exists in a conformational equilibrium between Ops (with a conformation similar to that of the inactive receptor), and Ops* (with a conformation similar to that of the active receptor). At physiological conditions, the inactive Ops conformation is favoured (Vogel and Siebert 2001), but arrestin has been shown to stabilise the active Ops* conformation. All-*trans*-retinal is only able to re-enter the binding pocket of the active Ops* conformation (Schafer, Fay et al. 2016), and experiments following re-uptake of ATR by opsin found that the percentage of OpsP that could bind ATR was increased in the presence of arrestin (50%, compared to just 10% in the absence of arrestin) (Sommer, Hofmann et al. 2012). These studies indicate that arrestin binding is able to stabilise the otherwise transitory active conformation in the receptor. As arrestin binds Ops* with high affinity, this stabilisation of Ops* does not result in further signalling as transducin remains occluded from the binding site. However, the retinal binding pocket is accessible in the arrestin-bound Ops* conformation, to allow for re-entry by ATR. This has physiological implications as ATR is toxic to the rod cell. Therefore, under bright light conditions, when a large concentration of ATR is released from Rh*P, the ability of arrestin to stabilise the Ops* conformation, allowing for ATR re-uptake, acts as a protective mechanism (Sommer, Hofmann et al. 2014).

As both arrestin and the receptor are able to sample different conformations in a structural equilibrium, it is likely that the structure of the pre-complex displays some heterogeneity. As the interaction occurs at two sites, it is possible that different orientations exist where both sites are not engaged simultaneously. A recent EM structure of the arrestin-receptor complex visualized two different orientations of arrestin binding to the receptor (Shukla, Westfield et al. 2014). In the first orientation arrestin was interacting with the helical core of the receptor, and is likely to represent the high-affinity complex. However, in the second structure, arrestin was "hanging off" from the receptor, at a 90° angle to the membrane. The structure obtained was a visualisation of the complex in a detergent micelle, and so no membrane was present. It is therefore possible that this represents an orientation of arrestin in the pre-complex, bound only by the interaction between the N-domain of arrestin and the phosphorylated receptor C-terminus. Heterogeneity in engagement of both interaction sites in the pre-complex could also explain recent FTIR experiments, which monitored the kinetics of transition of arrestin from the pre-complex to the high-affinity complex. In this study, two rate constants were measured: a fast and a slow component (Beyriere, Sommer et al. 2015). It is possible that the fast component measured represents arrestin pre-complexed with both interaction sites engaged. In the absence of one of the two interactions, arrestin would be bound in a more flexible orientation, similar to that observed in the EM structure described above (Shukla, Westfield et al. 2014), which could result in the slow component observed.

Apart from facilitating fast binding upon receptor activation, the pre-complex could have other functions, particularly in other GPCR systems. Recently an EM structure of a "supercomplex" was visualized (Thomsen, Plouffe et al. 2016) which showed a GPCR in complex with both β-arrestin and a G protein, which allows for continued signalling from GPCRs internalized in endosomes. In the structure the G protein was bound to the helical core of the receptor, with arrestin bound adjacent to the G protein. Arrestin was not engaged by the receptor binding crevice, and interestingly the C-edge of arrestin was positioned in such a way as to suggest interaction with the membrane. It is therefore possible that the structure represents an orientation similar to that of the pre-complex. This interaction would therefore have further implications beyond fast GPCR signal shut-off, and may be implicated in arrestin-mediated signalling.

4.4 The high-affinity complex

Site directed fluorescence measurements carried out in this dissertation, which monitored the position of different sites on arrestin when bound to Rh*P or Ops*P provided information about the conformational changes occurring in arrestin when bound in the high-affinity complex as compared to the pre-complex. Interaction with the phosphorylated, active receptor results in the release of the distal and proximal portions of the arrestin C-tail. Full C-tail displacement results in the fully active conformation of arrestin, in which the polar core is broken due to gate loop movement, the finger loop is freed for receptor interaction, and the domains of arrestin are rotated against one another, as shown in chapter 3.2. These conformational hallmarks of arrestin activation are seen in the crystal structures of p44, arrestin-2 bound to a phosphopeptide analogue of the phosphorylated receptor C-terminus, and the Ops*/arrestin-1 fusion complex (Kim, Hofmann et al. 2013, Shukla, Manglik et al. 2013, Kang, Zhou et al. 2015).

A change in the orientation of the membrane anchor was also observed during transition from the pre-complex to the high-affinity complex. The C-edge conformation and orientation suggested by fluorescence experiments correlated well with molecular dynamics simulations of the C-edge of p44 with the membrane (see chapter 3.1). In this conformation the hydrophobic residues that were observed to penetrate the membrane in the pre-complex insert more shallowly with the membrane, and the residues adjacent to the hydrophobic cluster are also seen to interact with the membrane interior. The 197-loop, which does not associate with the membrane in the pre-complex, penetrates the membrane interior in the high-affinity complex. Overlay of the simulated C-edge of p44 with the crystal structure of the Ops*/arrestin-1 fusion complex in the hypothetical membrane plane (Kang, Zhou et al. 2015), found that the orientation of arrestin in the crystal structure is consistent with that predicted by the simulations and the fluorescence experiments for the high-affinity complex.

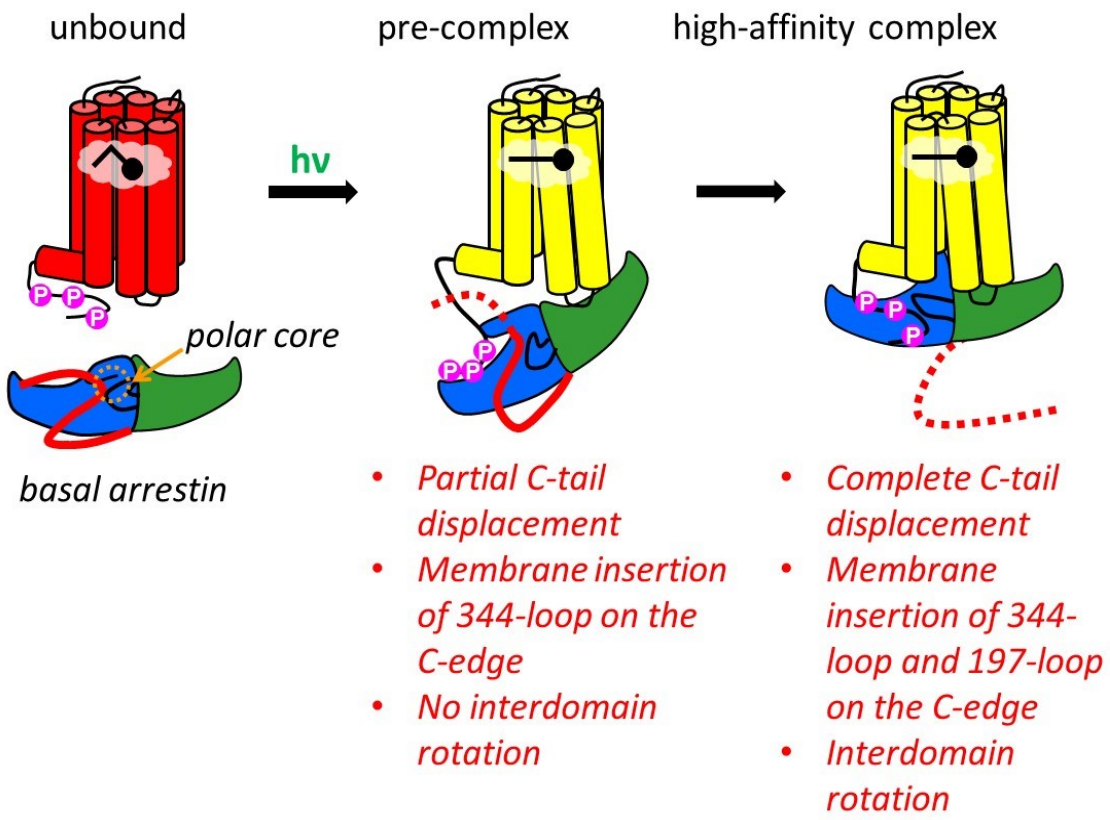

Figure 4.1 Model of arrestin binding to rhodopsin

The N-domain of arrestin is shown in blue, and the C-domain is shown in green. In the basal state of arrestin the C-tail (shown in red) makes several contacts with the N-domain, and the finger loop is folded down. In the pre-complex interaction the distal part of the C-tail is displaced (shown in red, dashed line) but the proximal portion remains in contact with the N-domain (red, solid line). The phosphorylated receptor C-terminus interacts with the concave surface of the N-domain (denoted by purple spheres with the letter p), and the 344-loop of the C-edge is penetrating the membrane. After light-activation the receptor adopts an active conformation, and the high-affinity complex forms. In this conformation, the C-tail is completely displaced, the polar core is disrupted, the finger loop is extended and binds into the open receptor crevice, and there is an interdomain rotation. The C-edge penetrates the membrane through both the 344- and 197-loops, and the receptor phosphates bind within the N-domain. Figure adapted from Martha Sommer, poster.

The stoichiometry of the high-affinity complex was observed to be dependent on formation of the pre-complex; robust pre-complex formation favoured a one-to-one arrestin-to-Rh*P binding stoichiometry, while dissolution of the pre-complex with moderate salt concentrations favoured a mixture of one-to-one and one-to-two binding stoichiometries (see chapter 3.3). The membrane anchor was shown to be engaged in both the one-to-one and one-to-two complex, which rules out the previously proposed

hypothesis that the 344-loop on arrestin could contact a second receptor (Sommer, Hofmann et al. 2012). The exact nature of the one-to-two arrestin-rhodopsin complex therefore, remains unclear. Fluorescence studies with the finger loop on arrestin, indicate that this loop is always embedded within the receptor crevice in both the one-to-one and one-to-two complex. It is possible that in the one-to-two complex, the neighbouring receptor is contacted by the N-domain of arrestin. The 160-loop in particular contains many negatively charged residues, which could be involved in an electrostatic interaction with the positively charged cytoplasmic surface of the receptor. In the crystal structure of the Ops*–arrestin-1 fusion complex, the 160-loop folds back to contact the cytoplasmic portion of helix 6 of the receptor (Kang, Zhou et al. 2015). However, the fluorescence quenching experiments presented in this dissertation suggest the 160-loop can interact with the membrane surface (see chapter 3.1). As the 160-loop is flexible it can likely adopt many different conformations, which could allow it to access a second receptor. Another possible interaction site is the displaced arrestin C-tail. This also has a cluster of negatively charged residues, which could be form an electrostatic interaction with the surface of the second receptor. Importantly these interactions need not bind deep into the receptor binding crevice in the same manner as the finger loop in order to be sufficient to block further binding of arrestin. Many studies have proposed that GPCRs are able to form dimers or higher oligomers. Rhodopsin was initially crystallised as a dimer, and atomic force microscopy has shown that higher-order oligomers are also likely to occur in the rod cell (Fotiadis, Liang et al. 2003, Liang, Fotiadis et al. 2003). It has been proposed that the organisation of GPCRs into asymmetric oligomeric clusters, allows for the receptor to be stabilised in distinct conformations, resulting in differential modulation of ligand binding (Maurice, Kamal et al. 2011). It is also conceivable that binding of interaction partners, such as arrestin, to the receptor could induce or stabilise oligomer formation. When arrestin is not already pre-complexed, it would then be able to contact the second receptor, either through interaction of the 160-loop, the C-tail, or a further binding element, to occlude any further arrestin binding. In contrast, when arrestin is pre-complexed in the dark, transition to the high-affinity complex occurs fast, with each arrestin binding to the active receptor crevice, before any interaction with a second receptor can occur.

4.5 Conclusions and future directions

This dissertation reports site directed fluorescence experiments that have furthered our knowledge of arrestin-rhodopsin interactions. In particular, a new functional binding element of arrestin, the C-edge membrane anchor, was identified. The C-edge membrane anchor is activated for membrane engagement only in the presence of phosphorylated receptor and is engaged differently when arrestin is bound in the pre-complex as compared to the high-affinity complex.

The distinct conformation of arrestin in the pre-complex as compared to the high-affinity complex was investigated further. In the pre-complex arrestin was found to adopt an orientation similar to that seen in the "open" conformer in the basal crystal structure, with just the distal portion of the C-tail displaced. In this pre-complex there are two interaction sites: an electrostatic interaction between the receptor phosphates and the concave surface of the N-domain, as well as the 344-loop on the C-edge of arrestin with the membrane. Upon light-activation, the conformation of arrestin changes as it transitions to the high-affinity complex. In this complex arrestin has a conformation similar to that observed in the p44 crystal structure. The C-tail is displaced, the polar core and three element interaction are disrupted, which results in changes within the central crest loops and a 21° rotation. This complex involves interactions between the receptor phosphates and the positively-charged cleft, which is exposed within the N-domain in the active arrestin structure, the finger loop and the central crest loops of arrestin interact with the helical core of the receptor, and the 344-loop and 197-loop on the C-edge of arrestin penetrate the membrane.

In addition, the effect of the pre-complex on the final binding stoichiometry of the high-affinity complex was investigated. Conditions that abrogated the pre-complex were found to result in a higher stoichiometry of arrestin-rhodopsin interaction, whereas in conditions allowing for pre-complex formation the stoichiometry suggested that each arrestin interacted with one rhodopsin molecule.

The results presented in this dissertation provide further insights into the arrestin-rhodopsin complex, which have implications not just within the visual system, but across the entire GPCR family. In humans, mutations in arrestin result in a form of night-blindness, called Oguchi disease, caused by a delay in dark adaptation (Lamb and Pugh 2004). Even though the experiments presented in this dissertation were carried out with bovine arrestin and bovine rhodopsin, they both share a high homology to their human

counterparts. As such the insights gained in this dissertation into arrestin binding to rhodopsin in the pre-complex and the high-affinity complex, can be applied for studying this disease in humans. Importantly, further characterisation of the arrestin-rhodopsin complex also has implications with other GPCR systems. In particular, the interaction between arrestin and the membrane is likely to occur for all four arrestin members of the visual/beta arrestin family. Arrestin-2 and arrestin-3 (β-arrestin-1 and β-arrestin-2) interact with hundreds of different GPCRs, and are involved not only with G protein-mediated signal shut-off, but also facilitate receptor internalisation, and mediate their own signalling pathways (Xiao et al. 2007; Lohse and Hoffmann 2015; Reiter et al. 2012). Therefore, the discovery of an additional binding element between visual arrestin-1 and the membrane, opens a new area of research not only into the role this interaction plays in arrestin binding to GPCRs, but also in carrying out its additional cellular functions.

There are a number of details about the arrestin-receptor interaction, which remain to be investigated in the future. This includes the implications of the membrane anchor in different GPCR systems, and its possible role in clathrin binding or scaffolding of proteins to the membrane. Studies using BRET would be useful for monitoring the interactions occurring with the arrestin membrane anchor. Similarly, studies investigating the effect of arrestin binding to the receptor in the absence of the 344-loop (as in the case of arresitn-3 and the short splice variant of arrestin-2) would be interesting in further elucidating the functional implications of membrane anchoring in the pre-complex interaction. The effects of membrane composition on the arrestin-membrane interaction would also be useful for determining the mechanism of binding.

Further investigation into the structure of the pre-complex, and in particular the conformational flexibility and heterogeneity of this interaction, using techniques such as double-electron-electron resonance (DEER) or Fourier transform infra-red spectroscopy (FTIR) could be utilised to provide more inights into this interaction. Further investigation into the implications of pre-complex formation in other GPCR systems, such as simultaneous arrestin and G protein mediated signalling would also be an interesting area of research.

More research is also required in order to probe the nature of the one-to-two stoichiometry observed in this dissertation. Experiments with p44, which lacks the C-tail, or with fluorescence probes on the 160-loop on the arrestin N-domain in combination with quenching groups introduced into the rhodopsin binding pocket, would be initial

experiments that could be carried out in order to identify if these arrestin elements are involved with contacting a second receptor. Further experiments should also be carried out to investigate if G-protein binding is effectively inhibited when arrestin is bound to two receptors.

In conclusion, this dissertation has addressed many questions about the arrestin-rhodopsin complex, and the conformation of different binding modes of interaction. The findings presented in this dissertation also have other implications in different GPCR-systems, which can be further investigated.

References

Arshavsky, V. Y., T. D. Lamb and E. N. Pugh, Jr. (2002). "G proteins and phototransduction." Annu Rev Physiol **64**: 153-187.

Aubry, L. and G. Klein (2013). "True arrestins and arrestin-fold proteins: a structure-based appraisal." Prog Mol Biol Transl Sci **118**: 21-56.

Bayburt, T. H., S. A. Vishnivetskiy, M. A. McLean, T. Morizumi, C. C. Huang, J. J. Tesmer, O. P. Ernst, S. G. Sligar and V. V. Gurevich (2011). "Monomeric rhodopsin is sufficient for normal rhodopsin kinase (GRK1) phosphorylation and arrestin-1 binding." J Biol Chem **286**(2): 1420-1428.

Beyriere, F., M. E. Sommer, M. Szczepek, F. J. Bartl, K. P. Hofmann, M. Heck and E. Ritter (2015). "Formation and decay of the arrestin-rhodopsin complex in native disc membranes." J Biol Chem.

Brann, M. R. and L. V. Cohen (1987). "Diurnal expression of transducin mRNA and translocation of transducin in rods of rat retina." Science **235**(4788): 585-587.

Broekhuyse, R. M., E. F. Tolhuizen, A. P. Janssen and H. J. Winkens (1985). "Light induced shift and binding of S-antigen in retinal rods." Curr Eye Res **4**(5): 613-618.

Daemen, F. J. (1973). "Vertebrate rod outer segment membranes." Biochim Biophys Acta **300**(3): 255-288.

Eaton, D. F. (1988). "International union of pure and applied chemistry organic chemistry division commission on photochemistry: Reference materials for fluorescence measurement." Journal of Photochemistry and Photobiology **2**(4): 523-531.

Fotiadis, D., Y. Liang, S. Filipek, D. A. Saperstein, A. Engel and K. Palczewski (2003). "Atomic-force microscopy: Rhodopsin dimers in native disc membranes." Nature **421**(6919): 127-128.

Granzin, J., U. Wilden, H. W. Choe, J. Labahn, B. Krafft and G. Buldt (1998). "X-ray crystal structure of arrestin from bovine rod outer segments." Nature **391**(6670): 918-921.

Gunkel, M., J. Schoneberg, W. Alkhaldi, S. Irsen, F. Noe, U. B. Kaupp and A. Al-Amoudi (2015). "Higher-Order Architecture of Rhodopsin in Intact Photoreceptors and Its Implication for Phototransduction Kinetics." Structure.

Gurevich, V. V. and J. L. Benovic (1993). "Visual arrestin interaction with rhodopsin. Sequential multisite binding ensures strict selectivity toward light-activated phosphorylated rhodopsin." J Biol Chem **268**(16): 11628-11638.

Gurevich, V. V. and J. L. Benovic (1995). "Visual arrestin binding to rhodopsin. Diverse functional roles of positively charged residues within the phosphorylation-recognition region of arrestin." J Biol Chem **270**(11): 6010-6016.

Gurevich, V. V. and J. L. Benovic (1997). "Mechanism of phosphorylation-recognition by visual arrestin and the transition of arrestin into a high affinity binding state." Mol Pharmacol **51**(1): 161-169.

Gurevich, V. V., C. Y. Chen, C. M. Kim and J. L. Benovic (1994). "Visual arrestin binding to rhodopsin. Intramolecular interaction between the basic N terminus and acidic C terminus of arrestin may regulate binding selectivity." J Biol Chem **269**(12): 8721-8727.

Gurevich, V. V., S. B. Dion, J. J. Onorato, J. Ptasienski, C. M. Kim, R. Sterne-Marr, M. M. Hosey and J. L. Benovic (1995). "Arrestin interactions with G protein-coupled receptors. Direct binding studies of wild type and mutant arrestins with rhodopsin, beta 2-adrenergic, and m2 muscarinic cholinergic receptors." J Biol Chem **270**(2): 720-731.

Gurevich, V. V. and E. V. Gurevich (2004). "The molecular acrobatics of arrestin activation." Trends Pharmacol Sci **25**(2): 105-111.

Hanson, S. M., E. S. Dawson, D. J. Francis, N. Van Eps, C. S. Klug, W. L. Hubbell, J. Meiler and V. V. Gurevich (2008). "A model for the solution structure of the rod arrestin tetramer." Structure **16**(6): 924-934.

Hanson, S. M., D. J. Francis, S. A. Vishnivetskiy, E. A. Kolobova, W. L. Hubbell, C. S. Klug and V. V. Gurevich (2006). "Differential interaction of spin-labeled arrestin with inactive and active phosphorhodopsin." Proc Natl Acad Sci U S A **103**(13): 4900-4905.

Hanson, S. M., E. V. Gurevich, S. A. Vishnivetskiy, M. R. Ahmed, X. Song and V. V. Gurevich (2007). "Each rhodopsin molecule binds its own arrestin." Proc Natl Acad Sci U S A **104**(9): 3125-3128.

Hanson, S. M., N. Van Eps, D. J. Francis, C. Altenbach, S. A. Vishnivetskiy, V. Y. Arshavsky, C. S. Klug, W. L. Hubbell and V. V. Gurevich (2007). "Structure and function of the visual arrestin oligomer." EMBO J **26**(6): 1726-1736.

Hessel, E., P. Muller, A. Herrmann and K. P. Hofmann (2001). "Light-induced reorganization of phospholipids in rod disc membranes." J Biol Chem **276**(4): 2538-2543.

Hirsch, J. A., C. Schubert, V. V. Gurevich and P. B. Sigler (1999). "The 2.8 A crystal structure of visual arrestin: a model for arrestin's regulation." Cell **97**(2): 257-269.

Hofmann, K. P., P. Scheerer, P. W. Hildebrand, H. W. Choe, J. H. Park, M. Heck and O. P. Ernst (2009). "A G protein-coupled receptor at work: the rhodopsin model." Trends Biochem Sci **34**(11): 540-552.

Hofmann, K. P., C. M. Spahn, R. Heinrich and U. Heinemann (2006). "Building functional modules from molecular interactions." Trends Biochem Sci **31**(9): 497-508.

Imamoto, Y., C. Tamura, H. Kamikubo and M. Kataoka (2003). "Concentration-dependent tetramerization of bovine visual arrestin." Biophys J **85**(2): 1186-1195.

Jastrzebska, B., T. Orban, M. Golczak, A. Engel and K. Palczewski (2013). "Asymmetry of the rhodopsin dimer in complex with transducin." FASEB J.

Kang, D. S., R. C. Kern, M. A. Puthenveedu, M. von Zastrow, J. C. Williams and J. L. Benovic (2009). "Structure of an arrestin2-clathrin complex reveals a novel clathrin binding domain that modulates receptor trafficking." J Biol Chem **284**(43): 29860-29872.

Kang, Y., X. E. Zhou, X. Gao, Y. He, W. Liu, A. Ishchenko, A. Barty, T. A. White, O. Yefanov, G. W. Han, Q. Xu, P. W. de Waal, J. Ke, M. H. Tan, C. Zhang, A. Moeller, G. M. West, B. D. Pascal, N. Van Eps, L. N. Caro, S. A. Vishnivetskiy, R. J. Lee, K. M. Suino-Powell, X. Gu, K. Pal, J. Ma, X. Zhi, S. Boutet, G. J. Williams, M. Messerschmidt, C. Gati, N. A. Zatsepin, D. Wang, D. James, S. Basu, S. Roy-Chowdhury, C. E. Conrad, J. Coe, H. Liu, S. Lisova, C. Kupitz, I. Grotjohann, R. Fromme, Y. Jiang, M. Tan, H. Yang, J. Li, M. Wang, Z. Zheng, D. Li, N. Howe, Y. Zhao, J. Standfuss, K. Diederichs, Y. Dong, C. S. Potter, B. Carragher, M. Caffrey, H. Jiang, H. N. Chapman, J. C. Spence, P. Fromme, U. Weierstall, O. P. Ernst, V. Katritch, V. V. Gurevich, P. R. Griffin, W. L. Hubbell, R. C. Stevens, V. Cherezov, K. Melcher and H. E. Xu (2015). "Crystal structure of rhodopsin bound to arrestin by femtosecond X-ray laser." Nature **523**(7562): 561-567.

Kern, R. C., D. S. Kang and J. L. Benovic (2009). "Arrestin2/clathrin interaction is regulated by key N- and C-terminal regions in arrestin2." Biochemistry **48**(30): 7190-7200.

Kim, M., S. A. Vishnivetskiy, N. Van Eps, N. S. Alexander, W. M. Cleghorn, X. Zhan, S. M. Hanson, T. Morizumi, O. P. Ernst, J. Meiler, V. V. Gurevich and W. L. Hubbell (2012). "Conformation of receptor-bound visual arrestin." Proc Natl Acad Sci U S A **109**(45): 18407-18412.

Kim, Y. J., K. P. Hofmann, O. P. Ernst, P. Scheerer, H. W. Choe and M. E. Sommer (2013). "Crystal structure of pre-activated arrestin p44." Nature **497**(7447): 142-146.

Kiser, P. D., M. Golczak, A. Maeda and K. Palczewski (2012). "Key enzymes of the retinoid (visual) cycle in vertebrate retina." Biochim Biophys Acta **1821**(1): 137-151.

Kiser, P. D., M. Golczak and K. Palczewski (2014). "Chemistry of the Retinoid (Visual) Cycle." Chemical reviews **114**(1): 194-232.

Krupnick, J. G., V. V. Gurevich and J. L. Benovic (1997). "Mechanism of quenching of phototransduction. Binding competition between arrestin and transducin for phosphorhodopsin." J Biol Chem **272**(29): 18125-18131.

Krupnick, J. G., V. V. Gurevich, T. Schepers, H. E. Hamm and J. L. Benovic (1994). "Arrestin-rhodopsin interaction. Multi-site binding delineated by peptide inhibition." J Biol Chem **269**(5): 3226-3232.

Kühn, H. (1978). "Light-regulated binding of rhodopsin kinase and other proteins to cattle photoreceptor membranes." Biochemistry **17**(21): 4389-4395.

Kühn, H. (1980). "Light- and GTP-regulated interaction of GTPase and other proteins with bovine photoreceptor membranes." Nature **283**(5747): 587-589.

kühn, H. (1980). "Light-induced, reversible binding of proteins to bovine photoreceptor membranes. Influence of nucleotides." Neurochem Int **1**: 269-285.

Kuhn, H., S. W. Hall and U. Wilden (1984). "Light-induced binding of 48-kDa protein to photoreceptor membranes is highly enhanced by phosphorylation of rhodopsin." FEBS Lett **176**(2): 473-478.

Lakowicz, J. R. (2010). Principles of Fluorescence spectroscopy, springer science and business media, LLC. **4th edition**.

Lamb, T. D. and E. N. Pugh, Jr. (2004). "Dark adaptation and the retinoid cycle of vision." Prog Retin Eye Res **23**(3): 307-380.

Lee, K. A., M. Nawrot, G. G. Garwin, J. C. Saari and J. B. Hurley (2010). "Relationships among visual cycle retinoids, rhodopsin phosphorylation, and phototransduction in mouse eyes during light and dark adaptation." Biochemistry **49**(11): 2454-2463.

Lefkowitz, R. (2004). "Historical review: A brief history and personal retrospective of seven-transmembrane receptors." Trends in Pharmacological Sciences **25**(8): 413-422.

Leskov, I. B., V. A. Klenchin, J. W. Handy, G. G. Whitlock, V. I. Govardovskii, M. D. Bownds, T. D. Lamb, E. N. Pugh, Jr. and V. Y. Arshavsky (2000). "The gain of rod phototransduction: reconciliation of biochemical and electrophysiological measurements." Neuron **27**(3): 525-537.

Liang, Y., D. Fotiadis, S. Filipek, D. A. Saperstein, K. Palczewski and A. Engel (2003). "Organization of the G protein-coupled receptors rhodopsin and opsin in native membranes." J Biol Chem **278**(24): 21655-21662.

Lohse, M. J. and C. Hoffmann (2014). "Arrestin interactions with g protein-coupled receptors." Handb Exp Pharmacol **219**: 15-56.

Lohse, M. J. and K. P. Hofmann (2015). "Spatial and Temporal Aspects of Signaling by G-Protein-Coupled Receptors." Mol Pharmacol **88**(3): 572-578.

Mansoor, S. E., M. A. Dewitt and D. L. Farrens (2010). "Distance mapping in proteins using fluorescence spectroscopy: the tryptophan-induced quenching (TrIQ) method." Biochemistry **49**(45): 9722-9731.

Maurice, P., M. Kamal and R. Jockers (2011). "Asymmetry of GPCR oligomers supports their functional relevance." Trends Pharmacol Sci **32**(9): 514-520.

McBee, J. K., K. Palczewski, W. Baehr and D. R. Pepperberg (2001). "Confronting complexity: the interlink of phototransduction and retinoid metabolism in the vertebrate retina." Prog Retin Eye Res **20**(4): 469-529.

Mendez, A., M. E. Burns, A. Roca, J. Lem, L. W. Wu, M. I. Simon, D. A. Baylor and J. Chen (2000). "Rapid and reproducible deactivation of rhodopsin requires multiple phosphorylation sites." Neuron **28**(1): 153-164.

Modzelewska, A., S. Filipek, K. Palczewski and P. S. Park (2006). "Arrestin interaction with rhodopsin: conceptual models." Cell Biochem Biophys **46**(1): 1-15.

Molday, R. S. (1998). "Photoreceptor membrane proteins, phototransduction, and retinal degenerative diseases. The Friedenwald Lecture." Invest Ophthalmol Vis Sci **39**(13): 2493-2513.

Nygaard, R., T. M. Frimurer, B. Holst, M. M. Rosenkilde and T. W. Schwartz (2009). "Ligand binding and micro-switches in 7TM receptor structures." Trends in Pharmacological Sciences **30**(5).

Ostermaier, M. K., C. Peterhans, R. Jaussi, X. Deupi and J. Standfuss (2014). "Functional map of arrestin-1 at single amino acid resolution." Proc Natl Acad Sci U S A.

Palczewski, K., J. Buczylko, N. R. Imami, J. H. McDowell and P. A. Hargrave (1991). "Role of the carboxyl-terminal region of arrestin in binding to phosphorylated rhodopsin." J Biol Chem **266**(23): 15334-15339.

Palczewski, K., P. A. Hargrave, J. H. McDowell and T. S. Ingebritsen (1989). "The catalytic subunit of phosphatase 2A dephosphorylates phosphoopsin." Biochemistry **28**(2): 415-419.

Palczewski, K., T. Kumasaka, T. Hori, C. A. Behnke, H. Motoshima, B. A. Fox, I. Le Trong, D. C. Teller, T. Okada, R. E. Stenkamp, M. Yamamoto and M. Miyano (2000). "Crystal structure of rhodopsin: A G protein-coupled receptor." Science **289**(5480): 739-745.

Palczewski, K., A. Pulvermüller, J. Buczylko, C. Gutmann and K. P. Hofmann (1991). "Binding of inositol phosphates to arrestin." FEBS Lett **295**(1-3): 195-199.

Palczewski, K., A. Pulvermüller, J. Buczylko and K. P. Hofmann (1991). "Phosphorylated rhodopsin and heparin induce similar conformational changes in arrestin." J Biol Chem **266**(28): 18649-18654.

Park, J. H., P. Scheerer, K. P. Hofmann, H. W. Choe and O. P. Ernst (2008). "Crystal structure of the ligand-free G-protein-coupled receptor opsin." Nature **454**(7201): 183-187.

Parkes, J. H. and P. A. Liebman (1984). "Temperature and pH dependence of the metarhodopsin I-metarhodopsin II kinetics and equilibria in bovine rod disk membrane suspensions." Biochemistry **23**(21): 5054-5061.

Peterhans, C., C. C. Lally, M. K. Ostermaier, M. E. Sommer and J. Standfuss (2016). "Functional map of arrestin binding to phosphorylated opsin, with and without agonist." Sci Rep **6**: 28686.

Philp, N. J., W. Chang and K. Long (1987). "Light-stimulated protein movement in rod photoreceptor cells of the rat retina." FEBS Lett **225**(1-2): 127-132.

Piechnick, R., E. Ritter, P. W. Hildebrand, O. P. Ernst, P. Scheerer, K. P. Hofmann and M. Heck (2012). "Effect of channel mutations on the uptake and release of the retinal ligand in opsin." Proc Natl Acad Sci U S A **109**(14): 5247-5252.

Pierce, K. L., Premont RT, Lefkowitz RJ (2002). "Seven-transmembrane receptors." Nat Rev Mol Cell Biol **3**(9): 639-650.

Pulvermüller, A., D. Maretzki, M. Rudnicka-Nawrot, W. C. Smith, K. Palczewski and K. P. Hofmann (1997). "Functional differences in the interaction of arrestin and its splice variant, p44, with rhodopsin." Biochemistry **36**(30): 9253-9260.

Raman, D., S. Osawa, V. V. Gurevich and E. R. Weiss (2003). "The interaction with the cytoplasmic loops of rhodopsin plays a crucial role in arrestin activation and binding." J Neurochem **84**(5): 1040-1050.

Raman, D., S. Osawa and E. R. Weiss (1999). "Binding of arrestin to cytoplasmic loop mutants of bovine rhodopsin." Biochemistry **38**(16): 5117-5123.

Reiter, E., S. Ahn, A. K. Shukla and R. J. Lefkowitz (2012). "Molecular mechanism of beta-arrestin-biased agonism at seven-transmembrane receptors." Annu Rev Pharmacol Toxicol **52**: 179-197.

Schafer, C. T., J. F. Fay, J. M. Janz and D. L. Farrens (2016). "Decay of an active GPCR: Conformational dynamics govern agonist rebinding and persistence of an active, yet empty, receptor state." Proc Natl Acad Sci U S A.

Scheerer, P., J. H. Park, P. W. Hildebrand, Y. J. Kim, N. Krauss, H. W. Choe, K. P. Hofmann and O. P. Ernst (2008). "Crystal structure of opsin in its G-protein-interacting conformation." Nature **455**(7212): 497-502.

Schleicher, A., H. Kühn and K. P. Hofmann (1989). "Kinetics, binding constant, and activation energy of the 48-kDa protein-rhodopsin complex by extra-metarhodopsin II." Biochemistry **28**(4): 1770-1775.

Schröder, K., A. Pulvermüller and K. P. Hofmann (2002). "Arrestin and its splice variant Arr1-370A (p44). Mechanism and biological role of their interaction with rhodopsin." J Biol Chem **277**(46): 43987-43996.

Shi, W., C. D. Sports, D. Raman, S. Shirakawa, S. Osawa and E. R. Weiss (1998). "Rhodopsin arginine-135 mutants are phosphorylated by rhodopsin kinase and bind arrestin in the absence of 11-cis-retinal." Biochemistry **37**(14): 4869-4874.

Shukla, A. K., A. Manglik, A. C. Kruse, K. Xiao, R. I. Reis, W. C. Tseng, D. P. Staus, D. Hilger, S. Uysal, L. Y. Huang, M. Paduch, P. Tripathi-Shukla, A. Koide, S. Koide,

W. I. Weis, A. A. Kossiakoff, B. K. Kobilka and R. J. Lefkowitz (2013). "Structure of active beta-arrestin-1 bound to a G-protein-coupled receptor phosphopeptide." Nature **497**(7447): 137-141.

Shukla, A. K., G. H. Westfield, K. Xiao, R. I. Reis, L. Y. Huang, P. Tripathi-Shukla, J. Qian, S. Li, A. Blanc, A. N. Oleskie, A. M. Dosey, M. Su, C. R. Liang, L. L. Gu, J. M. Shan, X. Chen, R. Hanna, M. Choi, X. J. Yao, B. U. Klink, A. W. Kahsai, S. S. Sidhu, S. Koide, P. A. Penczek, A. A. Kossiakoff, V. L. Woods, Jr., B. K. Kobilka, G. Skiniotis and R. J. Lefkowitz (2014). "Visualization of arrestin recruitment by a G-protein-coupled receptor." Nature **512**(7513): 218-222.

Sillen, A. and Y. Engelborghs (1998). "The correct use of "average" fluorescence parameters " Photochem Photobiol **67**(5): 475-486.

Sinha, A., A. M. Jones Brunette, J. F. Fay, C. T. Schafer and D. L. Farrens (2014). "Rhodopsin TM6 Can Interact with Two Separate and Distinct Sites on Arrestin: Evidence for Structural Plasticity and Multiple Docking Modes in Arrestin-Rhodopsin Binding." Biochemistry **53**(20): 3294-3307.

Smith, W. C., A. H. Milam, D. Dugger, A. Arendt, P. A. Hargrave and K. Palczewski (1994). "A splice variant of arrestin. Molecular cloning and localization in bovine retina." J Biol Chem **269**(22): 15407-15410.

Sommer, M. E., D. L. Farrens, J. H. McDowell, L. A. Weber and W. C. Smith (2007). "Dynamics of arrestin-rhodopsin interactions: loop movement is involved in arrestin activation and receptor binding." J Biol Chem **282**(35): 25560-25568.

Sommer, M. E., K. P. Hofmann and M. Heck (2011). "Arrestin-rhodopsin binding stoichiometry in isolated rod outer segment membranes depends on the percentage of activated receptors." J Biol Chem **286**(9): 7359-7369.

Sommer, M. E., K. P. Hofmann and M. Heck (2012). "Distinct loops in arrestin differentially regulate ligand binding within the GPCR opsin." Nat Commun **3**: 995.

Sommer, M. E., K. P. Hofmann and M. Heck (2014). "Not just signal shutoff: the protective role of arrestin-1 in rod cells." Handb Exp Pharmacol **219**: 101-116.

Sommer, M. E., W. C. Smith and D. L. Farrens (2005). "Dynamics of arrestin-rhodopsin interactions: arrestin and retinal release are directly linked events." J Biol Chem **280**(8): 6861-6871.

Sommer, M. E., W. C. Smith and D. L. Farrens (2006). "Dynamics of arrestin-rhodopsin interactions: acidic phospholipids enable binding of arrestin to purified rhodopsin in detergent." J Biol Chem **281**(14): 9407-9417.

Szczepek, M., F. Beyriere, K. P. Hofmann, M. Elgeti, R. Kazmin, A. Rose, F. J. Bartl, D. von Stetten, M. Heck, M. E. Sommer, P. W. Hildebrand and P. Scheerer (2014). "Crystal structure of a common GPCR-binding interface for G protein and arrestin." Nat Commun **5**: 4801.

Thomsen, A. R., B. Plouffe, T. J. Cahill, 3rd, A. K. Shukla, J. T. Tarrasch, A. M. Dosey, A. W. Kahsai, R. T. Strachan, B. Pani, J. P. Mahoney, L. Huang, B. Breton, F. M. Heydenreich, R. K. Sunahara, G. Skiniotis, M. Bouvier and R. J. Lefkowitz (2016). "GPCR-G Protein-beta-Arrestin Super-Complex Mediates Sustained G Protein Signaling." Cell **166**(4): 907-919.

Vishnivetskiy, S. A., J. A. Hirsch, M. G. Velez, Y. V. Gurevich and V. V. Gurevich (2002). "Transition of arrestin into the active receptor-binding state requires an extended interdomain hinge." J Biol Chem **277**(46): 43961-43967.

Vishnivetskiy, S. A., C. L. Paz, C. Schubert, J. A. Hirsch, P. B. Sigler and V. V. Gurevich (1999). "How does arrestin respond to the phosphorylated state of rhodopsin?" J Biol Chem **274**(17): 11451-11454.

Vishnivetskiy, S. A., D. Raman, J. Wei, M. J. Kennedy, J. B. Hurley and V. V. Gurevich (2007). "Regulation of arrestin binding by rhodopsin phosphorylation level." J Biol Chem **282**(44): 32075-32083.

Vishnivetskiy, S. A., C. Schubert, G. C. Climaco, Y. V. Gurevich, M. G. Velez and V. V. Gurevich (2000). "An additional phosphate-binding element in arrestin molecule. Implications for the mechanism of arrestin activation." J Biol Chem **275**(52): 41049-41057.

Vogel, R. and F. Siebert (2001). "Conformations of the active and inactive states of opsin." J Biol Chem **276**(42): 38487-38493.

Vogel, R., F. Siebert, G. Mathias, P. Tavan, G. Fan and M. Sheves (2003). "Deactivation of rhodopsin in the transition from the signaling state meta II to meta III involves a thermal isomerization of the retinal chromophore C[double bond]D." Biochemistry **42**(33): 9863-9874.

Watts, A., I. D. Volotovski and D. Marsh (1979). "Rhodopsin-lipid associations in bovine rod outer segment membranes. Identification of immobilized lipid by spin-labels." Biochemistry **18**(22): 5006-5013.

Wilden, U., S. W. Hall and H. Kuhn (1986). "Phosphodiesterase activation by photoexcited rhodopsin is quenched when rhodopsin is phosphorylated and binds the intrinsic 48-kDa protein of rod outer segments." Proc Natl Acad Sci U S A **83**(5): 1174-1178.

Xiao, K., D. B. McClatchy, A. K. Shukla, Y. Zhao, M. Chen, S. K. Shenoy, J. R. Yates, 3rd and R. J. Lefkowitz (2007). "Functional specialization of beta-arrestin interactions revealed by proteomic analysis." Proc Natl Acad Sci U S A **104**(29): 12011-12016.

Zhan, X., L. E. Gimenez, V. V. Gurevich and B. W. Spiller (2011). "Crystal structure of arrestin-3 reveals the basis of the difference in receptor binding between two non-visual subtypes." J Mol Biol **406**(3): 467-478.

Zhuang, T., Q. Chen, M. K. Cho, S. A. Vishnivetskiy, T. M. Iverson, V. V. Gurevich and C. R. Sanders (2013). "Involvement of distinct arrestin-1 elements in binding to different functional forms of rhodopsin." Proc Natl Acad Sci U S A **110**(3): 942-947.

Zhuang, T., S. A. Vishnivetskiy, V. V. Gurevich and C. R. Sanders (2010). "Elucidation of inositol hexaphosphate and heparin interaction sites and conformational changes in arrestin-1 by solution nuclear magnetic resonance." Biochemistry **49**(49): 10473-10485.

Declaration of academic integrity

I hereby declare that the present thesis has not been submitted as a part of any other examination procedure and has been independently written. All passages, including those from the internet, which were used directly or in modified form, especially those sources using text, graphs, charts or pictures, are indicated as such. I realize that an infringement of these principles which would amount to either an attempt of deception or deceit will lead to the institution of proceedings against myself.

Ciara Lally Berlin den 02/03/2017